Institute of Thermoelectricity, Academy of Sciences and Ministry of Education and Science of Ukraine

Journal of THERMOELECTRICITY

International Research

Founded in December, 1993

published 6 times a year

No. 2 *2020*

Editorial Board

International Editorial Board

Founders – National Academy of Sciences, Ukraine
Institute of Thermoelectricity of National Academy of Sciences and Ministry of Education and Science of Ukraine

Certificate of state registration № КВ 15496-4068 ПР

Approved for printing by the Academic Council of Institute of Thermoelectricity of the National Academy of Sciences and Ministry of Education and Science, Ukraine

Address of editorial office:
Ukraine, 58002, Chernivtsi, General Post Office, P.O. Box 86.
Phone: +(380-372) 90 31 65.
Fax: +(380-3722) 4 19 17.
E-mail: jt@inst.cv.ua
http://www.jt.inst.cv.ua

Signed for publication 26.05.2020. Format 70×108/16. Offset paper №1. Offset printing.
Printer's sheet 11.5. Publisher's signature 9.2. Circulation 400 copies. Order 5.

Printed from the layout original made by "Journal of Thermoelectricity" editorial board
in the printing house of "Bukrek" publishers,
10, Radischev Str., Chernivtsi, 58000, Ukraine

CONTENTS

* – papers of XVIII International Forum on thermoelectricity

R.V. Kuz

R.V. Kuz *cand. phys. - math. sciences*

Institute of Thermoelectricity of the NAS and MES of Ukraine,
1 Nauky str., Chernivtsi, 58029, Ukraine
e-mail: anatych@gmail.com

THEORY AND DESIGN OF THERMOELECTRIC GENERATORS USING WASTE HEAT ON VEHICLES

The paper presents the results of the analysis of theoretical works concerning the use of thermoelectric generators for vehicles in order to obtain additional electricity and, accordingly, fuel saving. The trends and current state of development of such generators are considered. Bibl. 21.

Key words: thermoelectric generator, internal combustion engine, heat recovery.

Introduction

General characterization of the problem. The use of thermoelectric generators (TEGs) for heat recovery of internal combustion engines to generate electricity over the past three decades remains a subject of increased interest from the automotive industry and specialists in thermoelectricity.

The purpose of the work is to analyze the existing achievements in the design and construction of thermoelectric generators for vehicles and to determine the prospects in the development and design of such generators.

Basic theories of TEG design for vehicles

The number of publications containing information on the theory of design and optimization of thermoelectric generators for vehicles is a small part of the total number of works on thermoelectric generators for vehicles. Below are the main results of theoretical research.

U.S. Department of Energy's National Renewable Energy Laboratory [1, 2]

A study by Hendricks and Lustbader for different classes of trucks. Model assumptions: one-dimensional TEG model is considered; temperature of hot exhaust gases is 700 °C. An attempt is made to optimize the components of the system by taking into account the contact thermal and electrical resistances in the TEG elements. The unit cost of the heat generator depending on its electric power is analyzed. It is shown that it decreases with increasing TEG output power due to the reduction of the unit cost of the heat removal system and in the considered model it tends to the value of $ 10/W.

A.A. Baikov Institute, Russia [3]

A number of theoretical works have been carried out, where the reasons for the inefficiency of a thermoelectric generator (TEG) for an internal combustion engine are analyzed. The conflict of the "engine-TEG" system is considered. Conclusions are made about the zero efficiency of the TEG, in particular, due to the presence of additional back pressure in the system, additional mass and the need for an additional cooling system of TEG. In the model under consideration, the economic efficiency of the TEG is zero due to a decrease in the efficiency of the engine during the installation of the TEG.

Chalmers University of Technology, Sweden [4]

A computer three-dimensional non-stationary model of a thermoelectric generator for a diesel engine is considered. The model calculates in detail the exhaust gas flows in the generator and the heat carrier flows. It is proposed to use this model to optimize the design of heat exchangers, select the optimal thermoelectric materials and determine the impact of the generator on the engine. In this paper, no conclusions are made about the economic efficiency of TEG.

Department of Mechanical Engineering, Stevens Institute of Technology, Hoboken, NJ, USA [5]

The purpose of the work was to determine the influence of the following parameters on the efficiency of TEG: the length of thermoelement legs, the size of heat carrier channels, the ratio of electrical conductivity and thermal conductivity of materials; the Reynolds, Nusselt and Prandtl numbers *Re*, *Nu*, *Pr*; the dimensionless thermoelectric figure of merit of thermoelement materials *ZT*.

Theoretical approximations used. The model is one-dimensional. Heat fluxes along the direction of heat carriers motion were not taken into account, the physical properties of the materials were assumed to be independent of temperature. Heat losses in structural elements, in connections, on transitional thermal resistances were not taken into account. Losses in electrical connections were also disregarded. The mass flow rate of both heat carriers was assumed to be equal.

The model was not confirmed, as it gave a discrepancy between theoretical calculations and experimental measurements by 40-50%.

North China Electric Power University, China [6]

The multi-parameter model includes hot and cold heat exchangers and thermoelectric modules. In fact, the source of heat of exhaust gases and water cooling of the radiator are modeled. Emphasis is placed on the non-uniformity of temperature differences on thermoelectric units along the gas flow.

Conclusions are made about the possibility of reducing the volume of thermoelectric material when optimizing the design of TEG.

Due to significant assumptions and simplifications, the results obtained are not very suitable for the design of generators. The model does not make it possible to draw conclusions about the economic feasibility of the generator.

Department of Mechanical Engineering, University of Maryland, College Park, USA [7]

In the work of Crane and Jackson, the TEG scheme with perpendicular directions of heat carrier flows in the hot air and cold liquid circuits of the heat exchanger is considered. The fluid circuit uses the fluid of the car's engine cooling system.

The purpose of the work was the simultaneous optimization of the geometry of the heat exchanger and thermoelectric modules. The optimization procedure included: theoretical modeling based on well-known theories of convective heat transfer and thermoelectric energy conversion; numerical analysis, experimental verification and final optimization at the level of the whole system at the cost of a unit of electric power.

The following assumptions are used. The planes in the middle of the partitions between adjacent channels are adiabatic boundaries for heat flows. This allowed the analysis of the entire heat exchanger based on the consideration of one channel. Thomson's heat, as in the Betancourt model, is assumed to be negligibly small. The physical properties of materials are temperature independent. Only convective heat exchange of heat carriers with the heat exchanger was taken into account. The energy balance of the TEG

takes into account the power of the fan, air circuit and liquid pump. It was assumed that Bi_2Te_3 material was used in thermoelectric modules.

The main results of the work. The one-dimensional Betancourt model generalized to the case of non-parallel heat carrier flows. The possibility of obtaining a specific power of 40 W / liter of hot water and a maximum cost of 1.1 kW / $ 10000 is demonstrated.

Clarkson University, Potsdam, NY, USA [8].

Karri developed and researched a TEG model that uses the heat of the exhaust gas. The model is based on the use of Hi-Z 20 modules. Hot heat carrier - exhaust gases, cold - water from the car's radiator circuit.

Mathematically, the model is described by a system of four nonlinear equations solved by computer means. The obtained results are quite accurate, but do not provide information on the optimization of TEG. Simulation is reduced to obtaining values that can be more accurately found experimentally. The model does not yield results of economic efficiency of the generator.

Department of Mechanical Engineering Rochester Institute of Technology Rochester, NY, USA [9]

The Betancourt, Karri, Crane and Jackson models were used and refined in Smith's work.

Smith analyzed a more complex sectional TEG circuit. The hot heat carrier flow creates temperature differences in thermoelectric modules of three sections. The model assumes that each section has a different number of modules. Such sectional TEGs have been investigated with Hi-Z and Melcor modules by computer simulation and optimization.

32 combinations of the number of sections (from 1 to 3) and the number of modules in the section are considered. The temperature dependences of the module parameters given by the empirical linear functions of the average module temperature were taken into account.

The simulation results were tested experimentally on a TEG model.

The experiments differed from the results of computer simulations by 30-40%, which reduces the value of such simulations. The cost of the generator in this model is estimated around $ 10 / W.

Institute of Thermoelectricity, Ukraine [10 – 21]

A number of comprehensive studies of thermoelectric generators for vehicles have been carried out, which follow from the description of the physics of a thermoelectric generator and yield the main thing, i.e. information for determining the optimal models of thermoelectric generators

The first calculations were carried out on a TEG model with lumped parameters. It allows you to identify the most general patterns of TEG. This model contains a local heat exchanger of infinite thermal conductivity and an infinite heat transfer coefficient. Under this condition, the gas enters the heat exchanger and leaves it at a temperature equal to that of the heat exchanger. From the heat exchanger the heat is transferred to a thermoelectric converter, the hot temperature of which is equal to the temperature of the gas. This means that the model does not take into account heat loss during its transfer from the heat exchanger to the thermoelectric converter and during heat transfer from the gas to the heat exchanger. In a thermoelectric converter, thermal energy is partially converted into electrical energy, and the rest is transferred to the thermostat. An important conclusion is that the maximum value of the efficiency of the TEG is achieved at a certain optimal value of the temperature of the heat exchanger, which is half the difference between the temperatures of hot gas and cold thermostat. This is the main conclusion that allows

the optimal design of the thermoelectric generator for the car. Based on the exhaust gas temperatures for different types of engines, it is possible to estimate the temperature of the thermoelectric converter. After analyzing the average exhaust temperatures for petrol and diesel engines, it was concluded that the most acceptable temperature for a petrol engine on the hot side of the thermoelectric module is only 300-350 ° C, and for a diesel engine as low as 200-250 °C.

Such results are understandable, since they are a consequence of two competing factors, namely an improvement in the efficiency of modules with a rise in the hot temperature and a decrease in efficiency with an increase in the thermal power passing through the TEG due to a drop in the hot temperature.

The obtained results refute the generally accepted opinion that high-temperature materials should be used in automotive thermoelectric generators, and also limit the list of currently known materials suitable for use in automotive thermoelectric generators.

The next important step is to analyze sectional generators. In this model, the sections sequentially collect heat from the exhaust gas. The sections are optimized for temperature conditions and the specific materials used in the sections. The following important information was obtained from the analysis of such a model: it is reasonable to use no more than three sections; the use of sections can increase the efficiency of TEG by a factor of 1.3 - 1.4. Therefore, the use of sections should be the subject of analysis in each specific case, since a sectional generator is much more complex in design, and, accordingly, more expensive.

The above results refer to the steady-state mode of TEG operation, when the exhaust gas is stable in temperature and thermal power. In fact, in cars in real operating modes, these conditions are not met. Another important result obtained at the Institute of Thermoelectricity is the analysis of the TEG operation in the transient oprerating modes. Computer simulation of real thermal conditions shows that the average power of the generators is approximately 4 times lower in relation to the maximum.

Conclusions

1. The design of automotive thermoelectric generators is in most cases empirical. Design is based on sorting out various options of the model components in order to find the best one. However, such approaches do not reveal the general regularities that describe the TEG, reducing the possibility of finding optimal constructions.
2. All theoretical models for calculating the power of TEGs for vehicles give an error of about 30-40%, which forces us to look for new approaches to the design of such TEGs.
3. The unit cost of TEG for vehicles is still high. Hope for their implementation remains only if they are significantly reduced in price.
4. A comprehensive approach to the design of a thermoelectric generator is needed, which will take into account the interaction of the TEG and the internal combustion engine.

References

1. Hendricks T.J. and Lustbader J.A. (2002). Advanced thermoelectric power system investigations for light-duty and heavy duty applications: Part 1," *in 21st International Conference on Thermoelectrics*, 381-386.
2. Hendricks T.J. (1988). Optimum design parameters in two-stage thermoelectric generators. *Proc. 23rd Intersociety Energy Conversion and Engineering Conference* (Denver, CO), Vol. 1, 339-345.
3. Korzhuev M.A., Svechnikova T.E. (2013). Thermodynamic restrictions for the net power of automotive thermoelectric generators and prospects of their use in transport. *J.Thermoelectricity*, 3.
4. Нцgblom Olle, Andersson Ronnie (2012). CFD modeling of thermoelectric generators in automotive

EGR-coolers. *9th European Conference on Thermoelectrics AIP Conf. Proc.* 1449, 497-500; doi: 10.1063/1.4731602.

5. Bethancourt A., Echigo R., and Yoshida H. (1995). Thermoelectric conversion analysis in a counter-flow heat exchanger. *AIP Conference Proc.*, vol. 316, 299-304.
6. Mewng Jing-Hui, Wang Xiao-Dong, Chen Wei-Hsin (2016). Performance investigation and design optimization of a thermoelectric generator applied in automobile exhaust waste heat recovery. *Energy Conversion and Management*, 120, 71–80.
7. Crane D.T. and Jackson G.S. (2004). Optimization of cross flow heat exchangers for thermoelectric waste heat recovery. *Energy Conversion and Management*, 45, 1565-82.
8. Karri M.M. (2005). Modeling of an automotive exhaust thermoelectric generator. *Mechanical Engineering. vol. Masters of Science Potsdam*. NY: Clarkson University.
9. Kevin D. Smith (2009). An investigation into the viability of heat sources for thermoelectric power generation systems: *Thesis for the Degree of Master of Science in Mechanical Engineering*. Department of Mechanical Engineering Rochester Institute of Technology.
10. Anatychuk L.I., Luste O.J., Kuz R.V. (2011). Theoretical and experimental studies of thermoelectric generator for vehicles.*J.Electronic Materials*, 40(5).
11. Anatychuk L.I. and Kuz R.V. (2011). Computer designing and test results of automotive thermoelectric generator. *Thermoelectrics goes automotive*. (Berlin: Expert Verlag, 2011).
12. Anatychuk L.I. and Kuz R.V. (2012). Materials for vehicular thermoelectric generators. *J. Electronic Materials*, 41 (6).
13. Анатичук L.I., Kuz R.V. Rozver Yu.Yu (2011). Efficiency of thermoelectric recuperators of exhaust gas heat from internal combustion engines. *J.Thermoelectricity*, 4, 78-83.
14. Anatychuk L.I., Kuz R.V., Rozver Yu.Yu. (2012). Thermoelectric generator for petrol engine. *J.Thermoelectricity*, 2, 93-100.
15. Kuz R.V. (2012). Moving vehicle parameters monitorimng system. *J.Thermoelectricity*, 4, 89-94.
16. Anatychuk L.I., Kuz R.V. (2014). Effect of air cooling on the efficiency of thermoelectric generator in a diesel engined car. *J.Thermoelectricity*, 2, 60-67.
17. Anatychuk L.I., Kuz R.V. (2014). Effect of air cooling on the efficiency of thermoelectric generator in a car with a petrol engine. *J.Thermoelectricity*, 3, 87-91.
18. Anatychuk L.I., Kuz R.V. (2014). Effect of air cooling on the efficiency of sectional thermoelectric generator in a car with a diesel engine. *J.Thermoelectricity*, 4, 81-87.
19. Anatychuk L.I., Kuz R.V. (2014). Effect of air cooling on the efficiency of sectional thermoelectric generator for a car with a petrol engine. *J.Thermoelectricity*, 5, 49-54.
20. Anatychuk L.I., Kuz R.V. Materials Today: Proceedings 2 (2015) 871 - 876 (*ECT-2014*), Madrid.
21. Anatychuk L.I., Kuz R.V. (2016). Thermoelectric generator for trucks. *J.Thermoelectricity*, 3, 5-10.

Submitted 01.04.2020

Кузь Р. В. *канд. фіз.-мат. наук*

Інститут термоелектрики НАН і МОН України,
вул. Науки, 1, Чернівці, 58029, Україна,
e-mail: anatych@gmail.com

ТЕОРІЯ ТА ПРОЕКТУВАННЯ ТЕРМОЕЛЕКТРИЧНИХ ГЕНЕРАТОРІВ, ЩО ВИКОРИСТОВУЮТЬ ВІДХОДИ ТЕПЛА НА ТРАНСПОРТНИХ ЗАСОБАХ

У роботі наводяться результати аналізу теоретичних робіт, що стосуються використання термоелектричних генераторів для транспортних засобів з метою отримання додаткової електричної енергії і, відповідно, економії палива. Розглянуто тенденції розвитку і сучасний стан розробки таких генераторів. Бібл. 21.
Ключові слова: термоелектричний генератор, двигун внутрішнього згорання, утилізація тепла.

Кузь Р.В. *канд. физ.-мат. наук*

Институт термоэлектричества НАН и МОН Украины,
ул. Науки, 1, Черновцы, 58029, Украина,
e-mail: anatych@gmail.com

ТЕОРИЯ И ПРОЕКТИРОВАНИЕ ТЕРМОЭЛЕКТРИЧЕСКИХ ГЕНЕРАТОРОВ, ИСПОЛЬЗУЮЩИХ ОТХОДЫ ТЕПЛА НА ТРАНСПОРТНЫХ СРЕДСТВАХ

В работе приводятся результаты анализа теоретических работ, касающихся использования термоэлектрических генераторов для транспортных средств с целью получения дополнительной электрической энергии и, соответственно, экономии топлива. Рассмотрены тенденции развития и современное состояние разработки таких генераторов. Библ. 21.
Ключевые слова: термоэлектрический генератор, двигатель внутреннего сгорания, утилизация тепла.

References

1. Hendricks T.J. and Lustbader J.A. (2002). Advanced thermoelectric power system investigations for light-duty and heavy duty applications: Part 1," *in 21st International Conference on Thermoelectrics*, 381-386.
2. Hendricks T.J. (1988). Optimum design parameters in two-stage thermoelectric generators. *Proc. 23rd Intersociety Energy Conversion and Engineering Conference* (Denver, CO), Vol. 1, 339-345.
3. Korzhuev M.A., Svechnikova T.E. (2013). Thermodynamic restrictions for the net power of automotive thermoelectric generators and prospects of their use in transport. *J.Thermoelectricity*, 3.
4. Нцgblom Olle, Andersson Ronnie (2012). CFD modeling of thermoelectric generators in automotive EGR-coolers. *9th European Conference on Thermoelectrics AIP Conf. Proc.* 1449, 497-500; doi: 10.1063/1.4731602.
5. Bethancourt A., Echigo R., and Yoshida H. (1995). Thermoelectric conversion analysis in a counter-flow heat exchanger. *AIP Conference Proc.*, vol. 316, 299-304.
6. Mewng Jing-Hui, Wang Xiao-Dong, Chen Wei-Hsin (2016). Performance investigation and design optimization of a thermoelectric generator applied in automobile exhaust waste heat recovery. *Energy*

Conversion and Management, 120, 71–80.
7. Crane D.T. and Jackson G.S. (2004). Optimization of cross flow heat exchangers for thermoelectric waste heat recovery. *Energy Conversion and Management*, 45, 1565-82.
8. Karri M.M. (2005). Modeling of an automotive exhaust thermoelectric generator. *Mechanical Engineering. vol. Masters of Science Potsdam*. NY: Clarkson University.
9. Kevin D. Smith (2009). An investigation into the viability of heat sources for thermoelectric power generation systems: *Thesis for the Degree of Master of Science in Mechanical Engineering*. Department of Mechanical Engineering Rochester Institute of Technology.
10. Anatychuk L.I., Luste O.J., Kuz R.V. (2011). Theoretical and experimental studies of thermoelectric generator for vehicles.*J.Electronic Materials*, 40(5).
11. Anatychuk L.I. and Kuz R.V. (2011). Computer designing and test results of automotive thermoelectric generator. *Thermoelectrics goes automotive*. (Berlin: Expert Verlag, 2011).
12. Anatychuk L.I. and Kuz R.V. (2012). Materials for vehicular thermoelectric generators. *J. Electronic Materials*, 41 (6).
13. Анатичук L.I., Kuz R.V. Rozver Yu.Yu (2011). Efficiency of thermoelectric recuperators of exhaust gas heat from internal combustion engines. *J.Thermoelectricity*, 4, 78-83.
14. Anatychuk L.I., Kuz R.V., Rozver Yu.Yu. (2012). Thermoelectric generator for petrol engine. *J.Thermoelectricity*, 2, 93-100.
15. Kuz R.V. (2012). Moving vehicle parameters monitorimng system. *J.Thermoelectricity*, 4, 89-94.
16. Anatychuk L.I., Kuz R.V. (2014). Effect of air cooling on the efficiency of thermoelectric generator in a diesel engined car. *J.Thermoelectricity*, 2, 60-67.
17. Anatychuk L.I., Kuz R.V. (2014). Effect of air cooling on the efficiency of thermoelectric generator in a car with a petrol engine. *J.Thermoelectricity*, 3, 87-91.
18. Anatychuk L.I., Kuz R.V. (2014). Effect of air cooling on the efficiency of sectional thermoelectric generator in a car with a diesel engine. *J.Thermoelectricity*, 4, 81-87.
19. Anatychuk L.I., Kuz R.V. (2014). Effect of air cooling on the efficiency of sectional thermoelectric generator for a car with a petrol engine. *J.Thermoelectricity*, 5, 49-54.
20. Anatychuk L.I., Kuz R.V. Materials Today: Proceedings 2 (2015) 871 - 876 (*ECT-2014*), Madrid.
21. Anatychuk L.I., Kuz R.V. (2016). Thermoelectric generator for trucks. *J.Thermoelectricity*, 3, 5-10.

Submitted 01.04.2020

E.I. Rogacheva, *doc. phys.-math science, professor*
A.N. Doroshenko,
A.Yu. Sipatov, *doc. phys.-math science, professor*

National Technical University "Kharkiv Polytechnic Institute",
2 Kyrpychova St., Kharkiv 61002, Ukraine; *e-mail: rogachova.olena@gmail.com*

ELECTRONIC PHASE TRANSITIONS IN THIN $Bi_{1-X}Sb_X$ FILMS

The purpose of the present work is to study the concentration dependences of thermoelectric (TE) and galvanomagnetic properties of thin $Bi_{1-x}Sb_x$ films in the range $x = 0 – 0.25$. The thin films with thicknesses $d = (250 \pm 10)$ nm were prepared by thermal evaporation in vacuum of $Bi_{1-x}Sb_x$ polycrystals onto (111) mica substrates and the transport properties (the electrical conductivity, Seebeck coefficient, Hall coefficient, electronic and hole mobility, magnetoresistance) of the films were measured at room temperature. It was established that all anomalies in the concentration dependences of the properties, observed earlier in the $Bi_{1-x}Sb_x$ bulk crystals and attributed to electronic phase transitions, were reproduced in thin films. The data obtained represent another evidence of the existence of the concentration peculiarities in the transport properties of $Bi_{1-x}Sb_x$ solid solutions, indicate a good correspondence between the compositions of $Bi_{1-x}Sb_x$ initial polycrystals and those of the thin films, and should be taken into account when interpreting the results of studies and predicting properties of $Bi_{1-x}Sb_x$ crystals and thin films. Bibl. 21. Fig. 4.

Key words: $Bi_{1-x}Sb_x$, solid solution, thin film, concentration, phase transition, thermoelectric properties, galvanomagnetic properties

Introduction

$Bi_{1-x}Sb_x$ solid solutions have attracted much attention as promising n-type low-temperature thermoelectric (TE) materials for refrigeration devices at temperatures below ~ 200 K [1-3]. Besides, these materials are among the physical objects whose unique properties continue to be revealed more and more every year, surprising us with the manifestation of new physical effects. Recently, interest in studying $Bi_{1-x}Sb_x$ crystals and thin films has sharply increased after it was established that they exhibit properties of 3D-topological insulators [4,5] in which a strong spin-orbit interaction leads to the appearance of topologically protected metallic surface states with a Dirac dispersion law. However, by now, the simultaneous coexistence of the topological and good TE properties, which is also observed for other promising TE materials (e.g. V_2VI_3 compounds), has not found an unambiguous explanation, but in recent years several works have appeared, related to possible effects of topological surface states on controlling TE properties of $Bi_{1-x}Sb_x$ crystals and thin films [6, 7].

Due to the structural and electrochemical similarities of Bi and Sb semimetals, these elements form a continuous series of $Bi_{1-x}Sb_x$ solid solutions [8], which makes it possible to study in detail the effect of the composition on the crystal structure, band structure and physical properties. It is known that although $Bi_{1-x}Sb_x$ solid solutions have a rhombohedral crystal structure in the entire concentration range, the band structure changes in a non-monotonic way [9-12] (Fig. 1). In the valence band of pure Bi, there are subbands of "light" (L_a) and "heavy" (T) holes and, as a result of the overlap of the hole T and electron L_s bands, Bi exhibits semimetallic properties. With an increase in the *Sb* concentration, the distance between the conduction band L_s and the subband L_a decreases and at $x = 0.023$ - 0.04 (different authors indicate different

values of this concentration) a gapless state is observed, the L_s and L_a bands invert. With a further increase in x, the gap between them increases again. Simultaneously with an increase in x, the overlap of T and Ls bands decreases, disappearing at $x = 0.06 \div 0.07$, and a semimetal – indirect semiconductor transition occurs. Then, at $x = 0.08 \div 0.09$, the ceilings of T and Ls of the valence bands converge, and in the concentration range $x = 0.09 - 0.15$ the semiconductor becomes direct-gap. The maximum value of the energy gap in the semiconductor region ($E_g \sim 0.025$ eV) is reached near $x = 0.15 \div 0.17$. With a subsequent increase in x, at $x \sim 0.15$, the semiconductor becomes indirect-gap again and at $x > 0.22$, $Bi_{1-x}Sb_x$ solid solutions acquire semimetal properties. Thus, the Bi1-xSbx system is characterized by a number of electronic phase transitions, the presence of which should be reflected at the concentration dependences of properties.

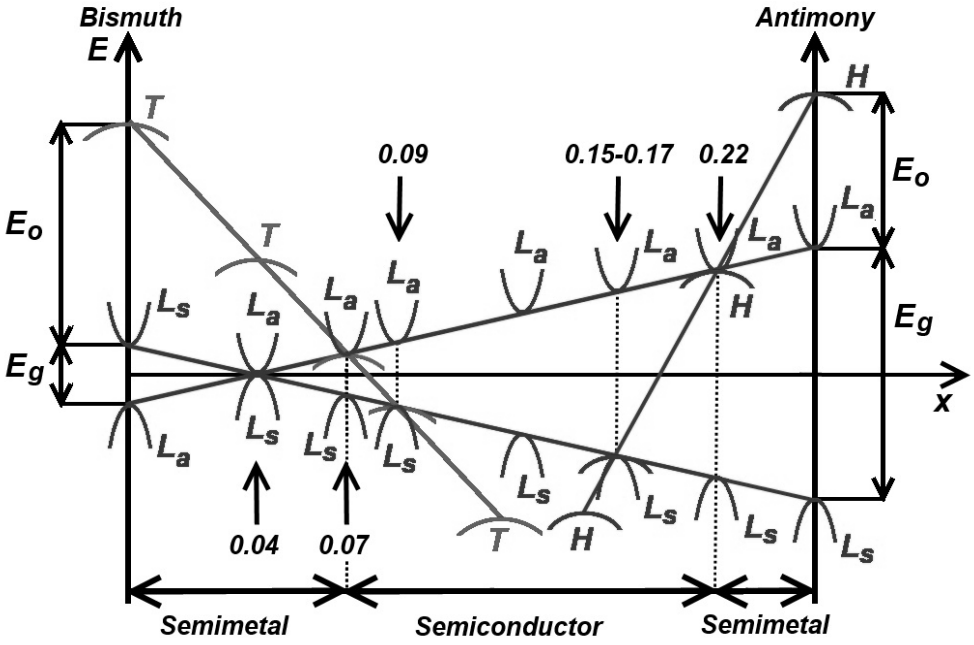

Fig. 1. Electronic band structure of the $Bi_{1-x}Sb_x$ solid solutions

Although the majority of studies on the fundamental properties of $Bi_{1-x}Sb_x$ solid solutions were carried out using single crystals, at present, an increasing number of works are devoted to the study of polycrystals [13-16]. This is due to both the great simplicity and cost-effectiveness of manufacturing polycrystalline materials and the convenience of manufacturing TE devices of various types from them. It was found that the nature of the concentration and temperature dependences of the TE properties of polycrystals and $Bi_{1-x}Sb_x$ single crystals is basically the same, although the grain size has a significant effect on the properties of polycrystals.

Earlier, we revealed a nonmonotonic behavior of the concentration dependences of TE properties in polycrystalline $Bi_{1-x}Sb_x$ solid solutions in the vicinity of $x = 0.01$, 0.03, 0.07, 0.08, 0.15, 0.22 [17 – 25] and attributed the concentration anomalies of properties in the vicinity of $x = 0.01$ to percolation effects in the impurity subsystem of crystal, and other anomalies to corresponding electronic phase transitions (to a gapless state, semimetal - semiconductor, indirect – direct-band-gap semiconductor).

Currently, in connection with the development of nanotechnology, low-dimensional structures (thin films, quantum wires, quantum dots) are widely used in various fields of science and technology, including

thermoelectricity. The possibility of enhancing the dimensionless TE figure of merit ($ZT = (S^2 \div T)/\lambda$, where S is the Seebeck coefficient, λ is electrical conductivity, λ is total thermal conductivity, and T is absolute temperature) in low-dimensional structures [26] have stimulated studies of $Bi_{1-x}Sb_x$ thin-film structures. In particular, it was of interest to find out whether the revealed concentration anomalies would be observed in the thin films obtained from the bulk crystals. When studying thin $Bi_{1-x}Sb_x$ films in the range x = 0 – 0.09, we have showed [27] that concentration anomalies of properties are also reproduced in the thin films. It was interesting to expand the range of compositions under study, taking into account that the highest Z values are observed in the concentration range x = 0.12-0.15 [1 – 3]. In addition, it was of interest to find out whether technological factors or measurement conditions influence the fact of the presence of anomalies or the nature of their manifestation.

The objects of the present study were the $Bi_{1-x}Sb_x$ thin films with thicknesses $d = (250 \pm 10)$ nm prepared by thermal evaporation in vacuum onto mica substrates at T_s = 380 K of $Bi_{1-x}Sb_x$ polycrystals in the composition range x = 0 – 0.25.

As a result of the conducted studies, it was found that in the dependences of TE and galvanomagnetic properties on composition of thin $Bi_{1-x}Sb_x$ films in the range x = 0 - 0.25, concentration anomalies were found as well as in $Bi_{1-x}Sb_x$ polycrystals, and that changes in the polycrystal preparation technology and in the magnetic field value in which the galvanomagnetic properties are measured, do not change the general character of the dependences of the TE and galvanomagnetic properties on the composition.

Experimental details

The $Bi_{1-x}Sb_x$ thin films with the thicknesses $d = (250 \pm 10)$ nm were obtained by the thermal evaporation of $Bi_{1-x}Sb_x$ polycrystals (x = 0 – 0.25) in a vacuum (~ 10^{-6} Pa) from a single source and their deposition onto (111) mica substrates at a temperature T_S = 380 K with a rate of 0.1 – 0.3 nm/s. Fabrication technique of the polycrystalline Bi1-xSbx samples of various compositions (x = 0 - 0.25) for the thin films obtaining is described in [27]. The only difference was that in the present work we used samples that were annealed for 720 hours after synthesis, and the samples used to obtain films in the work [27] were annealed for 1200 hours.

The film thicknesses and the condensation rate were controlled using a calibrated quartz resonator. The crystal structures and phase composition of the initial materials and thin films were characterized by the X-ray diffraction method. In the X-ray diffraction patterns for thin films similarly to the initial bulk crystals, only $Bi_{1-x}Sb_x$ lines were seen. The obtained $Bi_{1-x}Sb_x$ films had a mosaic structure with a trigonal axis perpendicular to the film surface. Using X-ray photoelectronic spectroscopy and microprobe analysis, it was shown that the film composition corresponded to the initial material composition with an accuracy (Δx) not worse than $\Delta x = \pm 0.002$.

The measurements of the transport properties were carried out at room temperature on as-prepared films. The electrical conductivity σ, the Hall coefficient R_H and magnetoresistance $\Delta\rho/\rho$ were measured by a conventional d_c method on bulk parallelepiped-shaped samples and double Hall-cross shaped thin films. Ohmic contacts were prepared by soldering indium to the bulk or film surfaces. The used value of the magnetic field (B = 0.05 T) corresponded to a weak magnetic field in contrast to work [27], where a magnetic field equal to B = 0.9 T was used, which corresponded to the region of a strong magnetic field. It is known that in the weak magnetic field, RH value does not depend on B and $\Delta\rho/\rho$ increases of quadratic function. The error in the R_H, σ and $\Delta\rho/\rho$ measurements did not exceed ±5 %. The Seebeck coefficient S was measured relative to Cu with an accuracy of ±3 %. The component of the TE power perpendicular to the trigonal axis was measured. The calculation of the Hall mobilities of electrons μ_n and holes μ_p was

carried out taking into account two types of charge carriers and assuming that $n = p$ (which is observed with a high degree of accuracy in $Bi_{1-x}Sb_x$ solid solutions) according to the equations:

$$\sigma = en\left(\mu_n + \mu_p\right); \quad R_H = \frac{1}{en}\frac{\mu_n - \mu_p}{\mu_n + \mu_p}; \quad \frac{\Delta\rho}{\rho B^2} = \mu_n \mu_p \tag{1}$$

Since the mobility of electrons μ_n exceeds the mobility of holes μ_p, the sign of R_H for Bi and $Bi_{1-x}Sb_x$ solid solutions is determined by the mobility of electrons. This explains the resulting negative sign of R_H and S in bulk crystals. From the results of measuring σ, R_H, $\Delta\rho/\rho$, and S values and taking into account the value of B, the values of $n = p$, μ_n, μ_p and TE power factor $P(x) = S_2\,\sigma$ were calculated.

Results

In Figs 2-4, the concentration dependences $R_H(x)$, $S(x)$, $\Delta\rho/\rho(x)$, $\mu_n(x)$, $\mu_p(x)$, and $P(x)$ are presented for the $Bi_{1-x}Sb_x$ bulk crystals and thin films. It can be seen that all dependences exhibit a distinctly non-monotonic oscillatory behavior.

According to the measurement of S, all obtained thin films, like the initial polycrystals, had an electronic type of conductivity. From the Fig. 2 (a) it can be seen that $S(x)$ dependences for bulk polycrystals and thin films are very similar. The addition of Sb atoms to bismuth to $x \sim 0.10$ leads to a significant increase in S, due to the reduction of the overlap of T and L_s bands and the formation of a semiconductor region (Fig. 1).

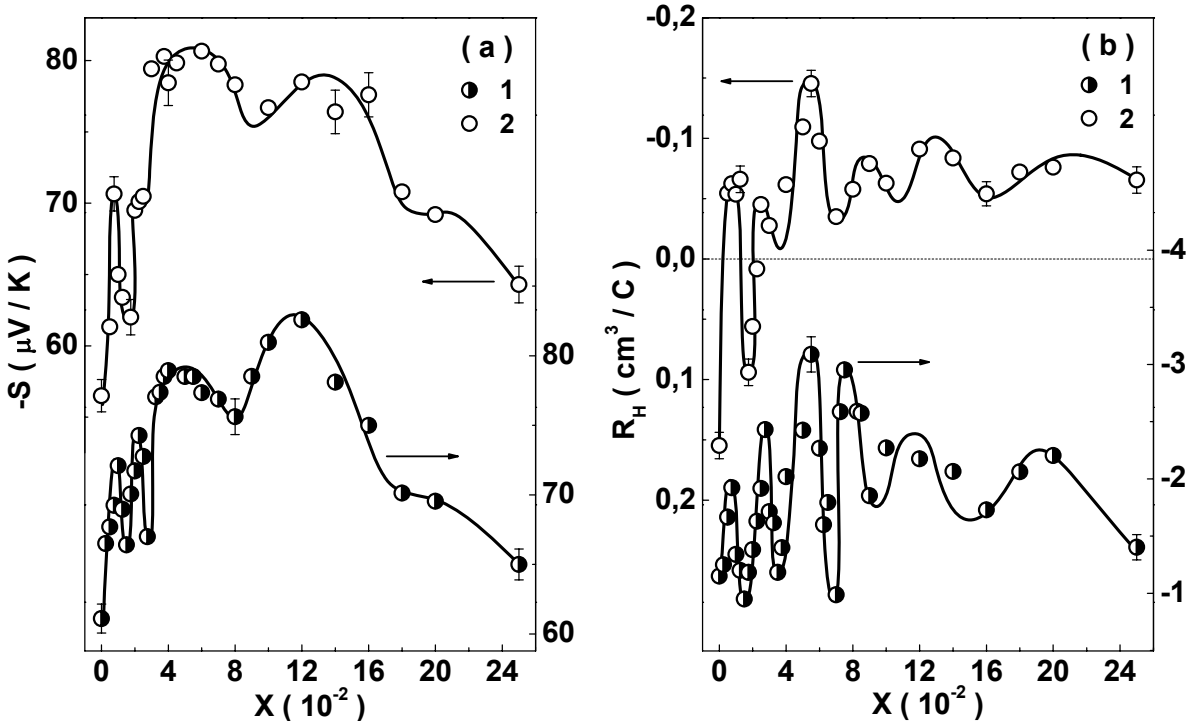

Fig. 2. Room-temperature dependences of the Seebeck coefficient S (a) and the Hall coefficient R_H (b) on the composition x of the $Bi_{1-x}Sb_x$ polycrystals (1) and thin films (2). Solid lines are guides to the eye.

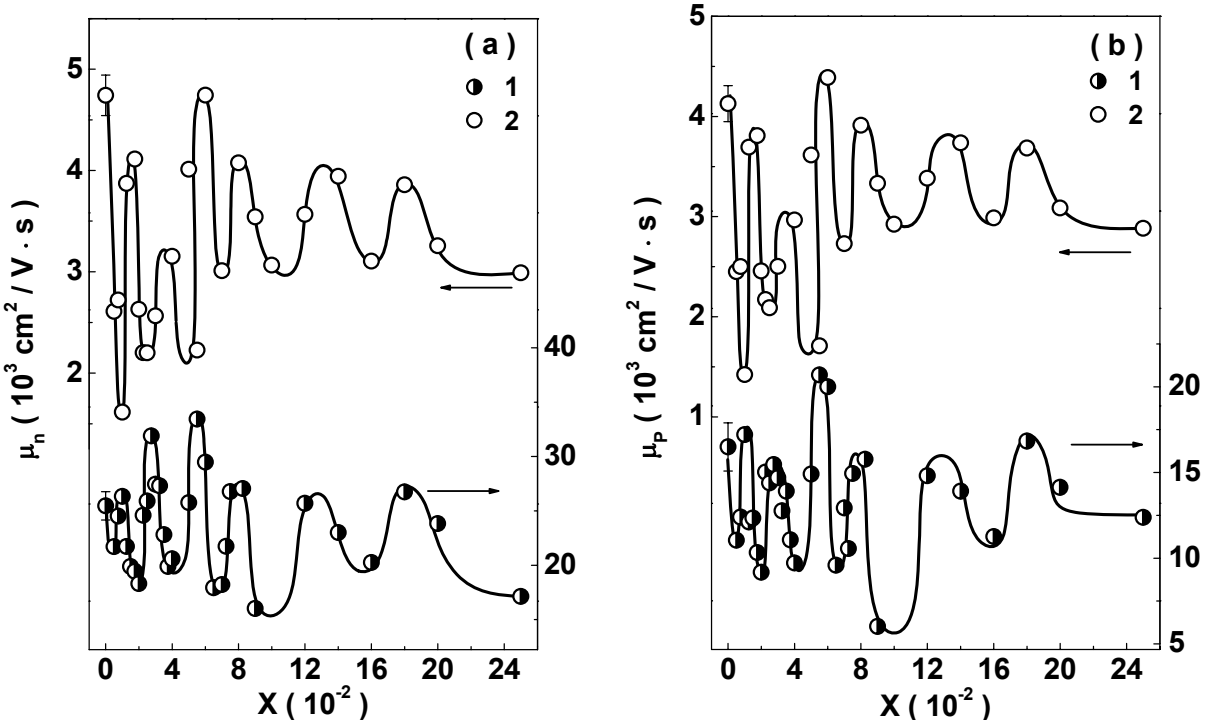

Fig. 3. Room-temperature dependences of the electron μ_n (a) and hole μ_p (b) mobilities on composition x of the $Bi_{1-x}Sb_x$ polycrystals (1) and thin films (2). Solid lines are guides to the eye.

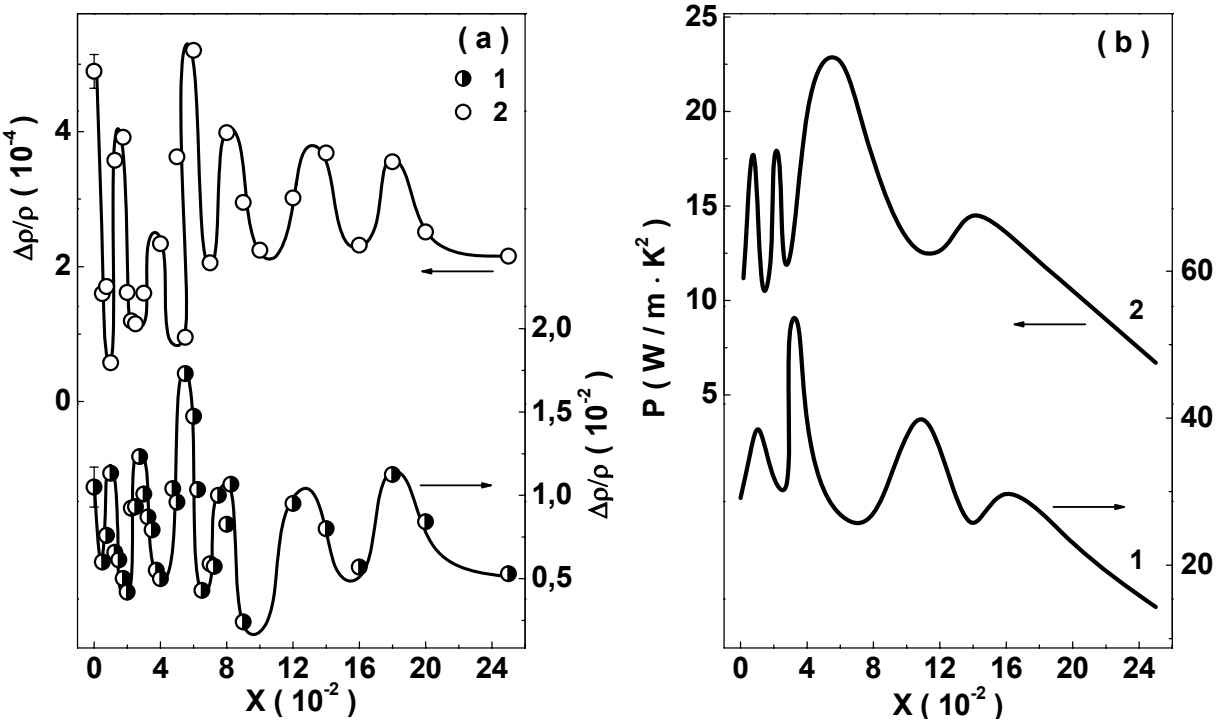

Fig. 4. Room-temperature dependences of magnetoresistance Δρ/ρ and thermoelectric power factor $P = S^2 \sigma$ on composition x of the $Bi_{1-x}Sb_x$ polycrystals (1) and thin films (2). Solid lines are guides to the eye.

After that, *S* decreases. However, we are talking only about the general trend of S change in the range $x = 0 - 0.25$. Meanwhile, the $S(x)$ dependence for both bulk crystals and thin films exhibit several

peaks or inflections near the compositions x = 0.01, 0.02, 0.05, 0.12, and 0.18 which we attributed [17 – 25] to a percolation and electronic phase transitions.

In accordance with the R_H measurements, all the initial polycrystals also had an electronic type of conductivity. In the R_H (x) dependence for polycrystals (Fig. 2,b), in addition to the indicated anomalies in $S(x)$ dependence (Fig. 2,a), we were able at $x \sim 0.08$ to reveal the peak associated with an indirect-gap - a direct-gap semiconductor transition, when the T-band top coincides with the L_s-band top [24, 25]. In $S(x)$ dependence, in contrast to dependence R_H (x), there is one diffuse anomalous section in the range $x = 0.05 – 0.08$ (Fig. 2*a*).

The dependence R_H (x) for thin films (Fig. 2,b) turned out to be more complex: R_H (x) curve had a number of features connected with the change of conductivity type. Bi had p-type conductivity ($R_H > 0$) but introduction of the first portions of Sb (to $x \sim 0.007$) led to inversion sign of conductivity ($p \rightarrow n$). Then, at $x \sim 0.01$, the conductivity type changed again ($n \rightarrow p$) and followed by a new change in the sign of the conductivity at $x \sim 0.02$ ($p \rightarrow n$). After that, with a further increase in x, the R_H sign for all films was negative ($R_H < 0$), as for bulk crystals. The reason for the difference between the R_H and S signs may be as follows. According to [28], in Bi monocrystals, R_H has a positive sign only along the direction of the trigonal axis, and in the perpendicular directions, the sign changes to a negative one. Unlike R_H, the coefficient S in any crystallographic directions remains negative. $Bi_{1-x}Sb_x$ films were grown along the direction of the trigonal axis [001], which was perpendicular to the plane of the substrate. That is why a positive R_H sign and a negative S sign were observed for Bi films what we showed in our work [29]. The introduction of Sb leads to an elastic distortions of crystal lattice, and with increasing x, orientation along the trigonal axis [001] becomes less and less perfect, and at a certain concentration of Sb, orientation practically disappears. A convincing fact confirming this assumption is the negative R_H sign observed by the authors of [30] in polycrystalline Bi films in which there is no anisotropy of properties.

Let us point out the following circumstance. As noted above, it was previously assumed [17 – 25] that in the range x=0.005-0.01, there is a percolation transition from an impurity discontinuum to an impurity continuum, which is with a high degree of probability is accompanied by ordering processes [31]. These processes can stimulate the formation of a more perfect oriented structure and determine inversion of conductivity type ($n \rightarrow p$). A subsequent increase in Sb concentration makes again the structure less perfect and leads to the inversion of the conductivity sign ($p \rightarrow n$). Approach to transition to a gapless state leads to a decrease in RH but it no longer causes an inversion of the conduction type ($n \rightarrow p$) since a significant number of impurity atoms makes the oriented structure even more imperfect. Thus, the alternating change in the R_H sign reflects in some way the change in the degree of structure perfection (degree of orientation), which, in turn, is associated with the presence of phase transitions. In a sense, a conductivity type can be used to estimate the degree of anisotropy in the film structure. This, of course, only applies to the case if the type of conductivity depends on the direction in the crystal.

Let us note that in the work [27] in which the $Bi_{1-x}Sb_x$ films were studied only in the concentration range $x = 0 – 0.1$, no change in the sign of R_H was observed at the percolation transition near $x = 0.01$. Perhaps this was due to the fact that the R_H measurements were carried out in a strong magnetic field (B = 0.9 T), and not in a weak magnetic field (B = 0.05 T), as in the present work.

A change in the R_H sign in films depending on x complicates the comparison of the $R_H(x)$ dependences for bulk and film samples. However, it can be seen (Fig. 2*b*) that despite the alternating change of R_H sign in the range $x = 0 – 0.02$, the character of the $R_H(x)$ dependence remains the same as for bulk crystals, having extrema corresponding to the phase transitions of the above types, if we take the R_H value of Bi as the reference point. In other words, a change in R_H sign does not prevent observation of the concentration anomalies.

The calculation of the μ_n and μp values using equation (1) showed that the dependences $\mu_n(x)$ and μ_p (x) have also a pronounced nonmonotonic character (Fig. 3). There are several clear maxima at $x \sim 0.01$, ~ 0.03, ~ 0.06, ~ 0.08, ~ 0.14 and ~ 0.18. These concentrations correspond to the characteristic compositions (Fig. 1) at which there are qualitative changes in the $Bi_{1-x}Sb_x$ band energy structure. It should be noted that, in these dependences, as well as in the R_H (x) dependence, two maxima can be distinguished, corresponding to the semimetal – indirect-gap semiconductor transition and indirect-gap semiconductor - direct-gap semiconductor ($x \sim 0.06$ and $x \sim 0.08$, respectively). The dependence $\Delta\rho/\rho$ (x) (Fig. 4*a*) actually repeats the character of the dependences $\mu_n(x)$ and μ_p (x).

It was shown theoretically [32] that the $Bi_{1-x}Sb_x$ band structure depends not only on the composition and thickness of the film, but also on the orientation of the film on the substrate. Therefore, it can be expected that at low Sb concentrations, when the degree of anisotropy in the film is sufficiently high, the extrema on the concentration dependences of the properties of the films can be shifted relative to these positions in the crystal. Some shift of the maxima on the dependences $\Delta\rho/\rho$ (x), $\mu_n(x)$ and μ_p (x) for bulk crystals and films in the range of compositions $x = 0$ - 0.1 is related, apparently, to this circumstance.

In Fig. 4,b, the concentration dependences of TE power factor $P = S_2\ \sigma$ for bulk crystals and thin films are presented. The lower values of P in thin films compared to bulk crystals can be explained by lower values of electrical conductivity in thin films, since the values of the Seebeck coefficient, are practically the same in crystals and films (Fig. 2*a*). Fig. 4 shows that the $P(x)$ dependence, as well as the dependences on the composition for all other kinetic coefficients of crystals and films, has a distinctly nonmonotonic character. The compositions at which the maximum values of P are observed, are different for crystals and thin films (at $x \sim 0.03$ and $x \sim 0.06$, respectively). however, these data correspond to 300 K, while the highest values of TE figure of merit correspond to temperatures below 200 K [1 – 3]. Therefore, our immediate task is to obtain the temperature dependences of the kinetic coefficients of thin $Bi_{1-x}Sb_x$ films.

Thus, we can conclude that the concentration anomalies of TE and galvanomagnetic properties observed for $Bi_{1-x}Sb_x$ polycrystals and attributed [17 – 25] to critical phenomena accompanying phase transitions, are reproduced in the thin films obtained from these crystals. A change in the technology for preparing initial bulk crystals (the reduction in the annealing time of bulk from 1200 to 720 hours) does not change the behavior of the concentration dependences of kinetic coefficient of bulk crystals and thin films qualitatively. The nature of the magnetic field (strong or weak) in which the galvanomagnetic properties are measured does not change the general character of the dependences of the properties on the composition and the presence of anomalies, but only affects the value of RH and $\Delta\rho/\rho$.

However, it should be noted that this is observed in sufficiently "thick" films ($d = 250 \pm 10$ nm), when quantum size effects (e.g, the oscillating nature of the d - dependences of properties) are practically not manifested. The transition to very thin films and manifestation of these effects can significantly change the physical picture. However, in a number of cases, thin-film TE energy converters are used with layer thicknesses when size quantum effects do not manifest themselves.

Conclusions

1. It was established that the concentration anomalies of TE and galvanomagnetic properties associated with the manifestation of critical phenomena accompanying percolation and electronic phase transitions observed in $Bi_{1-x}Sb_x$ polycrystals in the composition range $x = 0 – 0.25$, are largely reproducible in thin $Bi_{1-x}Sb_x$ films with thicknesses $d = (250 \pm 10)$ nm obtained from these crystals by thermal evaporation in vacuum on mica substrates.
2. A change in the magnetic field value used in the measurement of R_H and magnetoresistance, a change in

the technology of polycrystals of which the films were made (a decrease in the annealing time from 1200 to 720 hours) do not affect the fact of the presence of concentration anomalies of properties both in polycrystals and in thin films.

3. The alternation of the RH sign in the range $x = 0 – 0.02$ with changing the composition under a constancy of sign of the Seebeck coefficient in $Bi_{1-x}Sb_x$ thin films was found. The sign of the R_H in a film depends on the degree of film anisotropy, which, in turn, depends on the presence of a phase transition. A change in the R_H sign with a changing the composition is not an obstacle to the detection of anomalies in the concentration dependences of properties.
4. The results obtained is one more confirmation of the fact of the presence of percolation and electronic phase transitions in the $Bi_{1-x}Sb_x$ solid solutions which manifest themselves in critical phenomena observed not only in crystals, but also in films.
5. Good agreement of the critical compositions in the concentration dependences of the properties of the $Bi_{1-x}Sb_x$ crystals and thin films, indicates good reproducibility of the compositions of polycrystals in thin films obtained from these polycrystals.
6. The existence of the concentration anomalies of TE and galvanomagnetic properties in $Bi_{1-x}Sb_x$ bulk and thin film states should be taken into account when interpreting the results of studies, predicting TE properties, and using the $Bi_{1-x}Sb_x$ polycrystals and thin films in TE devices.

Acknowledgements This work was supported by the Ministry of Education and Science of Ukraine (Project # M 0625)

References

1. Anatychuk L.I. (1979). Termoelementy i termoelektricheskie ustroistva: spravochnik [Thermoelements and thermoelectric devices: reference book] Kyiv, Naukova dumka [in Russian].
2. Lenoir B., Scherrer H. and Caillat T. (2001). An overview of recent developments for BiSb alloys, Chapter 4, In: Tritt T.M. (ed.) Semiconductors and Semimetals: Recent Trends in Thermoelectric Materials Research I, Vol. 69. San Diego, Academic Press.
3. Uher C. (ed.) (2016). Materials aspect of thermoelectricity. CRC Press, Boca Raton: Taylor & Francis Group.
4. Fu L., Kane C.L. and Mele E.J. (2007). Topological insulators in three dimensions. Phys. Rev. Lett., 98(10), 106803.
5. Hsieh D., Qian D., Wray L., Xia Y., Hor Y.S., Cava R.J. and Hasan M.Z. (2008). A topological Dirac insulator in a quantum spin Hall phase. Nature, 452, 970-974.
6. Takahashi R. and Murakami S. (2012). Thermoelectric transport in topological insulators Semicond. Sci. Technol., 27(12), 124005-8.
7. Müchler L., Casper F., Yan B., Chadov S., and Felser C. (2013). Topological insulators and thermoelectric materials. Phys. Stat. Solidi RRL, 7(1-2), 91-100.
8. Ugay Ya.A., Goncharov Ye.G., Semenova G.V. and Lazarev V.B. (1989). Phase equilibria between phosphorus, arsenic and bismuth. Moscow, Nauka (in Russian).
9. Brandt N.B., Chudinov S.M., and Karavaev V.G. (1976). Investigation of the zero-gap state induced by a magnetic field in bismuth-antimony alloys. Sov. Phys. JETP, 43(6), 1198-1209; Zh. Eksp. Teor. Fiz. 70, 2296-2317 (in Russian)
10. Yasaki T. and Abe Y. (1968). Galvanomagnetic investigations of the $Bi_{1-x}Sb_x$ ($0 < x < 0.15$) system at 77 K. J. Phys. Soc. Jpn., 24(2), 290-295.

11. Mironova G.A., Sudakova M.B., Ponomarev Ya.G. (1980). Dispersion law of carriers in the $Bi_{1-x}Sb_x$ alloys. Sov. Phys. Solid State, 22(12), 2124; Fizika tverd. tela, 22(12), 1980, pp. 3628-3634 (in Russian).
12. Mironova G.A., Sudakova M.B., Ponomarev Ya.G. (1980). Investigation of the band structure of semiconducting $Bi_{1-x}Sb_x$ alloys. Sov. Phys. JETP, 51(5), 918-929.
13. Kitagawa H., Noguchi H., Kiyabu T., Itoh M. and Noda Y. (2004). Thermoelectric properties of Bi-Sb semiconducting alloys prepared by quenching and annealing. J. Phys. Chem. Solids, 65(7), 1223-1227.
14. Malik K., Das D., Mondal D., Chattopadhyay D., Deb A.K., Bandyopadhyay S. and Banerjee A. (20112). Sb concentration dependent structural and resistive properties of polycrystalline Bi-Sb alloys. J. Appl. Phys., 112(12), 083706.
15. Dutta S., Shubha V. and Ramesh T.G. and D'Sa F. (2009). Thermal and electronic properties of $Bi_{1-x}Sb_x$ alloys. J. Alloy Compd., 467(1), 305–309.
16. Lenoir B., Dauscher A., Cassart M., Ravich Y.I. and Scherrer H. (1998). Effect of antimony content on the thermoelectric figure of merit of $Bi_{1-x}Sb_x$ alloys. J. Phys. Chem. Solids., 59(1), 129-134.
17. Rogacheva E.I. and Drozdova A.A. (2006). Thermoelectric properties of polycrystalline bismuth-antimony solid solutions. J. Thermoelectricity, 2, 22-28.
18. Rogacheva E.I., Yakovleva A.A. (Drozdova A.A.), Pinegin V.I. and Dresselhaus M.S. (2008). Concentration anomalies of properties in Bi-Sb semimetallic solid solutions. J. Phys. Chem. Solids, 69(2-3), 580-584.
19. Rogacheva E.I., Drozdova A.A., Nashchekina O.N., Dresselhaus M.S. and Dresselhaus G.(2009). Transition into a gapless state and concentration anomalies in the properties of $Bi_{1-x}Sb_x$ solid solutions. Appl. Phys. Lett., 94(20), 202111.
20. Rogacheva E.I., Drozdova A.A. and Nashchekina O.N., Percolation effects in semimetallic Bi-Sb solid solutions, Phys. Stat. sol. (a), 207(2), 2010, pp. 344–347.
21. Rogacheva E.I., Doroshenko A.N., Nashchekina O.N. and Yu.V. Men′shov. (2013). Thermal conductivity in $Bi_{1-x}Sb_x$ solid solutions. J. Electron. Mater., 42(7), 2098-2102.
22. Rogacheva E.I., Doroshenko A.N., Pinegin V.I. and Dresselhaus M.S. (2013). Electronic phase transitions and structural instability in $Bi_{1-x}Sb_x$ solid solutions. J. Thermoelectricity, 6, 13-20.
23. Rogacheva E.I., Doroshenko A.N., Nashchekina O.N. and Dresselhaus M.S. (2016). Specific heat critical behavior in $Bi_{1-x}Sb_x$ solid solutions. Appl. Phys. Lett., 109(13), 131906.
24. Doroshenko A.N., Rogacheva E.I., Drozdova A.A., Martynova K.V., Men'shov Yu.V. (2016). Thermoelectric properties of polycrystalline $Bi_{1-x}Sb_x$ solid solutions in the concentration range x = 0 – 0.25. J. Thermoelectricity, 4, 23-36.
25. Rogacheva E.I., Doroshenko A.N., Drozdova A.A., Nashchekina O.N., Men'shov Yu.V.(2020). Galvanomagnetic properties of polycrystalline $Bi_{1-x}Sb_x$ solid solutions in the concentration range x = 0 - 0.25. Functional Materials, 27(3) 488-496. https://doi.org/10.15407/fm27.03.488
26. Dresselhaus M.S., Lin Y.-M., Cronin S.B., Rabin O, Black M.R., Dresselhaus G. (2001). Quantum wells and quantum wires for potential thermoelectric applications, In Tritt T.M. (ed.) Semiconductors and Semimetals: Recent Trends in Thermoelectric Materials Research III, Vol. 71. Academic Press, San Diego, CA.
27. Rogacheva E.I., Nashchekina O.N., Orlova D.S., Doroshenko A.N., Dresselhaus M.S. (2017). Influence of composition on the thermoelectric properties of $Bi_{1-x}Sb_x$ thin films. J. Electron. Mater. 46(7), 3821-3825.
29. Jain A.L. (1959). Temperature dependence of the electrical properties of bismuth-antimony alloys. Phys. Rev. B 114(6), 1518 -1528.

30. Rogacheva E.I., Grigorov S.N., Nashchekina O.N., Lyubchenko S.G., Dresselhaus M.S. (2003). Quantum size effects in n-type Bi thin films. Appl. Phys. Lett. 82, 2628-2630.
31. Petrosyan V.I., Molin V.N. Dagman E.I., Tavger B.A., Skripkina P.A., Alexandrov L.N.(1971). Quantum size transition semimetal-semiconductor in super-thin Bi films. Phys. Metallov i Metallovedenie, 31, 725-730 (in Russian)
32. Rogacheva E.I. (2003). Self-organization processes in impurity subsystem of solid solution. J. Phys. Chem. Solids, 64(9-10), 1579-1583.
33. Tang Sh., Dresselhaus M.S. (2012). Phase diagrams of $Bi_{1-x}Sb_x$ thin films with different growth orientations. Phys.Rev.B, 86(7), 075436(1-6). DOI: 10.1103/PhysRevB.86.075436

Submitted 07.04.2020

Рогачова О.І., *докт. фіз.-мат. наук, професор*
Дорошенко Г.М.,
СіпатовО.Ю. *докт. фіз.-мат. наук, професор*

Національний технічний університет "Харківський політехнічний інститут",
вул. Кирпичова, 2, м. Харків 61002, Україна,
e-mail: rogachova.olena@gmail.com

ЕЛЕКТРОННІ ФАЗОВІ ПЕРЕХОДИ У ТОНКИХ ПЛІВКАХ $Bi_{1-X}Sb_X$

Метою даної роботи було вивчення концентраційних залежностей ТЕ та гальваномагнітних властивостей тонких плівок $Bi_{1-x}Sb_x$ в інтервалі x = 0 – 0.25. Тонкі плівки $Bi_{1-x}Sb_x$ товщиною d = (250 ± 10) нм були виготовлені термічним випаровуванням у вакуумі кристалів $Bi_{1-x}Sb_x$ на (111) слюдяні підкладки, а транспортні властивості (електропровідність, коефіцієнт Зеєбека, коефіцієнт Холла, рухливість електронів і дірок, магнетоопір) плівок вимірювались за кімнатної температури. Було встановлено, що всі аномалії на концентраційних залежностях властивостей, що спостерігалися раніше в масивних кристалах $Bi_{1-x}Sb_x$ і пов'язувалися із електронними фазовими переходами, відтворювались у тонких плівках. Отримані дані, з одного боку,– це ще один доказ існування концентраційних особливостей у транспортних властивостях твердих розчинів $Bi_{1-x}Sb_x$, а, з другого боку, ці дані вказують на добру відповідність складів вихідних кристалів складам тонких плівок. Одержані результати слід враховувати при інтерпретації результатів досліджень та прогнозуванні властивостей кристалів і тонких плівок $Bi_{1-x}Sb_x$. Бібл. 21, рис. 4.

Ключові слова: $Bi_{1-x}Sb_x$, твердий розчин, тонка плівка; концентрація, фазовий перехід, термоелектричні властивості, гальваномагнітні властивості.

Рогачова Е.И., *докт. фіз.-мат. наук, професор*
Дорошенко Г.М.,
Сипатов А.Ю. *докт. фіз.-мат. наук, професор*

Национальный технический университет
"Харьковский политехнический институт"
ул. Кирпичева, 2, г.. Харьков 61002, Украина,
e-mail: rogachova.olena@gmail.com

ЭЛЕКТРОННЫЕ ФАЗОВЫХ ПЕРЕХОДОВ В ТОНКИХ ПЛЕНКАХ $Bi_{1-x}Sb_x$

Целью данной работы было изучение концентрационных зависимостей ТО и гальваномагнитных свойств тонких пленок $Bi_{1-x}Sb_x$ в интервале x = 0 - 0.25. Тонкие пленки Bi1-xSbx толщиной d = (250 ± 10) нм были изготовлены термическим испарением в вакууме кристаллов $Bi_{1-x}Sb_x$ на (111) слюдяные подложки, а транспортные свойства (электропроводность, коэффициент Зеебека, коэффициент Холла, подвижность электронов и дырок, магнитное)пленок измерялись при комнатной температуре. Было установлено, что все аномалии на концентрационных зависимостях свойств, которые наблюдались ранее в массивных кристаллах $Bi_{1-x}Sb_x$ и связаны с электронными фазовыми переходами, воспроизводились в тонких пленках. Полученные данные, с одной стороны, - это еще одно доказательство существования концентрационных особенностей в транспортных свойствах твердых растворов $Bi_{1-x}Sb_x$, а с другой стороны, эти данные указывают на хорошую соответствие складов выходных кристаллов составам тонких пленок. Полученные результаты следует учитывать при интерпретации результатов исследований и прогнозировании свойств кристаллов и тонких пленок $Bi_{1-x}Sb_x$. Библ. 21, рис. 4.

Ключевые слова: *Bi_1-xSbx,* твердый раствор тонкая пленка; концентрация; фазовый переход; термоэлектрические свойства; гальваномагнитные свойства

References

1. Anatychuk L.I. (1979). Termoelementy i termoelektricheskie ustroistva: spravochnik [Thermoelements and thermoelectric devices: reference book] Kyiv, Naukova dumka [in Russian].
2. Lenoir B., Scherrer H. and Caillat T. (2001). An overview of recent developments for BiSb alloys, Chapter 4, In: Tritt T.M. (ed.) Semiconductors and Semimetals: Recent Trends in Thermoelectric Materials Research I, Vol. 69. San Diego, Academic Press.
3. Uher C. (ed.) (2016). Materials aspect of thermoelectricity. CRC Press, Boca Raton: Taylor & Francis Group.
4. Fu L., Kane C.L. and Mele E.J. (2007). Topological insulators in three dimensions. Phys. Rev. Lett., 98(10), 106803.
5. Hsieh D., Qian D., Wray L., Xia Y., Hor Y.S., Cava R.J. and Hasan M.Z. (2008). A topological Dirac insulator in a quantum spin Hall phase. Nature, 452, 970-974.
6. Takahashi R. and Murakami S. (2012). Thermoelectric transport in topological insulators Semicond. Sci. Technol., 27(12), 124005-8.
7. Müchler L., Casper F., Yan B., Chadov S., and Felser C. (2013). Topological insulators and thermoelectric materials. Phys. Stat. Solidi RRL, 7(1-2), 91-100.

8. Ugay Ya.A., Goncharov Ye.G., Semenova G.V. and Lazarev V.B. (1989). Phase equilibria between phosphorus, arsenic and bismuth. Moscow, Nauka (in Russian).
9. Brandt N.B., Chudinov S.M., and Karavaev V.G. (1976). Investigation of the zero-gap state induced by a magnetic field in bismuth-antimony alloys. Sov. Phys. JETP, 43(6), 1198-1209; Zh. Eksp. Teor. Fiz. 70, 2296-2317 (in Russian)
10. Yasaki T. and Abe Y. (1968). Galvanomagnetic investigations of the $Bi_{1-x}Sb_x$ ($0 < x < 0.15$) system at 77 K. J. Phys. Soc. Jpn., 24(2), 290-295.
11. Mironova G.A., Sudakova M.B., Ponomarev Ya.G. (1980). Dispersion law of carriers in the $Bi_{1-x}Sb_x$ alloys. Sov. Phys. Solid State, 22(12), 2124; Fizika tverd. tela, 22(12), 1980, pp. 3628-3634 (in Russian).
12. Mironova G.A., Sudakova M.B., Ponomarev Ya.G. (1980). Investigation of the band structure of semiconducting $Bi_{1-x}Sb_x$ alloys. Sov. Phys. JETP, 51(5), 918-929.
13. Kitagawa H., Noguchi H., Kiyabu T., Itoh M. and Noda Y. (2004). Thermoelectric properties of Bi-Sb semiconducting alloys prepared by quenching and annealing. J. Phys. Chem. Solids, 65(7), 1223-1227.
14. Malik K., Das D., Mondal D., Chattopadhyay D., Deb A.K., Bandyopadhyay S. and Banerjee A. (20112). Sb concentration dependent structural and resistive properties of polycrystalline Bi-Sb alloys. J. Appl. Phys., 112(12), 083706.
15. Dutta S., Shubha V. and Ramesh T.G. and D'Sa F. (2009). Thermal and electronic properties of $Bi_{1-x}Sb_x$ alloys. J. Alloy Compd., 467(1), 305–309.
16. Lenoir B., Dauscher A., Cassart M., Ravich Y.I. and Scherrer H. (1998). Effect of antimony content on the thermoelectric figure of merit of $Bi_{1-x}Sb_x$ alloys. J. Phys. Chem. Solids., 59(1), 129-134.
17. Rogacheva E.I. and Drozdova A.A. (2006). Thermoelectric properties of polycrystalline bismuth-antimony solid solutions. J. Thermoelectricity, 2, 22-28.
18. Rogacheva E.I., Yakovleva A.A. (Drozdova A.A.), Pinegin V.I. and Dresselhaus M.S. (2008). Concentration anomalies of properties in Bi-Sb semimetallic solid solutions. J. Phys. Chem. Solids, 69(2-3), 580-584.
19. Rogacheva E.I., Drozdova A.A., Nashchekina O.N., Dresselhaus M.S. and Dresselhaus G.(2009). Transition into a gapless state and concentration anomalies in the properties of $Bi_{1-x}Sb_x$ solid solutions. Appl. Phys. Lett., 94(20), 202111.
20. Rogacheva E.I., Drozdova A.A. and Nashchekina O.N., Percolation effects in semimetallic Bi-Sb solid solutions, Phys. Stat. sol. (a), 207(2), 2010, pp. 344–347.
21. Rogacheva E.I., Doroshenko A.N., Nashchekina O.N. and Yu.V. Men′shov. (2013). Thermal conductivity in $Bi_{1-x}Sb_x$ solid solutions. J. Electron. Mater., 42(7), 2098-2102.
22. Rogacheva E.I., Doroshenko A.N., Pinegin V.I. and Dresselhaus M.S. (2013). Electronic phase transitions and structural instability in $Bi_{1-x}Sb_x$ solid solutions. J. Thermoelectricity, 6, 13-20.
23. Rogacheva E.I., Doroshenko A.N., Nashchekina O.N. and Dresselhaus M.S. (2016). Specific heat critical behavior in $Bi_{1-x}Sb_x$ solid solutions. Appl. Phys. Lett., 109(13), 131906.
24. Doroshenko A.N., Rogacheva E.I., Drozdova A.A., Martynova K.V., Men'shov Yu.V. (2016). Thermoelectric properties of polycrystalline $Bi_{1-x}Sb_x$ solid solutions in the concentration range $x = 0 – 0.25$. J. Thermoelectricity, 4, 23-36.
25. Rogacheva E.I., Doroshenko A.N., Drozdova A.A., Nashchekina O.N., Men'shov Yu.V.(2020). Galvanomagnetic properties of polycrystalline $Bi_{1-x}Sb_x$ solid solutions in the concentration range $x = 0 - 0.25$. Functional Materials, 27(3) 488-496. https://doi.org/10.15407/fm27.03.488
26. Dresselhaus M.S., Lin Y.-M., Cronin S.B., Rabin O, Black M.R., Dresselhaus G. (2001). Quantum wells and quantum wires for potential thermoelectric applications, In Tritt T.M. (ed.) Semiconductors and

Semimetals: Recent Trends in Thermoelectric Materials Research III, Vol. 71. Academic Press, San Diego, CA.

27. Rogacheva E.I., Nashchekina O.N., Orlova D.S., Doroshenko A.N., Dresselhaus M.S. (2017). Influence of composition on the thermoelectric properties of $Bi_{1-x}Sb_x$ thin films. J. Electron. Mater. 46(7), p. 3821-3825.
29. Jain A.L. (1959). Temperature dependence of the electrical properties of bismuth-antimony alloys. Phys. Rev. B 114(6), 1518 -1528.
30. Rogacheva E.I., Grigorov S.N., Nashchekina O.N., Lyubchenko S.G., Dresselhaus M.S. (2003). Quantum size effects in n-type Bi thin films. Appl. Phys. Lett. 82, 2628-2630.
31. Petrosyan V.I., Molin V.N. Dagman E.I., Tavger B.A., Skripkina P.A., Alexandrov L.N.(1971). Quantum size transition semimetal-semiconductor in super-thin Bi films. Phys. Metallov i Metallovedenie, 31, 725-730 (in Russian)
32. Rogacheva E.I. (2003). Self-organization processes in impurity subsystem of solid solution. J. Phys. Chem. Solids, 64(9-10), 1579-1583.
33. Tang Sh., Dresselhaus M.S. (2012). Phase diagrams of $Bi_{1-x}Sb_x$ thin films with different growth orientations. Phys.Rev.B, 86(7), 075436(1-6). DOI: 10.1103/PhysRevB.86.075436

Submitted 07.04.2020

N.A. Godovanets[1],
I.A. Konstantynovych *cand. phys.– math. sciences, dochent*[1,2],
A.V. Konstantynovych *doc. phys.– math. sciences, dochent*[2],
S.D. Shugani[1]

[1]Chernivtsi National University, 2 Kotsiubynskyi Str.,
Chernivtsi, Ukraine, 58012, *e-mail: anatych@gmail.com*
[2]Institute of Thermoelectricity of the NAS and MES of Ukraine,
1, Nauky str., Chernivtsi, 58029, Ukraine; *e-mail: dj_kneo@ukr.net aconst@ukr.net*
i.konstantynovych@chnu.edu.ua

GYROTROPIC THERMOELEMENT IN UNIFORM AND NON-UNIFORM MAGNETIC FIELDS

Using computer simulation, the temperature distributions in the working medium of gyrotropic thermoelements in uniform and non-uniform magnetic fields have been determined. Temperature dependences of the efficiency of gyrotropic thermoelements in uniform and non-uniform magnetic fields are determined. It has been established that the efficiency of generator gyrotropic thermoelements is higher in a non-uniform magnetic field than that in a uniform field. Bibl. 19, Fig. 3.
Key words: Nernst-Ettingshausen coefficient, gyrotropic thermoelement, non-uniform magnetic field, thermoelectric material, thermomagnetic figure of merit, efficiency.

Introduction

Nowadays, one of the promising areas of thermoelectric progress is the development of new types of thermoelements, including gyrotropic, and a more detailed study of those already known. In recent years, a number of works on gyrotropic thermoelements in constant magnetic fields have been published [1 – 18], and some parameters of these thermoelements in non-uniform magnetic fields have also been considered [7]. The gyrotropic thermoelements whose efficiency increases due to the excitation of eddy thermoelectric currents in a gyrotropic thermoelectric medium, make it possible to obtain elevated thermoelectric voltages and differ from the known multifunctionality; they are promising for use in special thermal generators , as well as in measuring equipment. However, these opportunities are used but little, so their development will increase the element base of thermoelectricity, improve the competitiveness of both thermoelectric converters and gyrotropic thermoelements, and allow developing more advanced thermoelectric products based on them, and improving their quality and reliability.

Therefore, the topicality of the work lies in the need for further study of gyrotropic thermoelements in uniform and non-uniform magnetic fields, to increase their efficiency and reliability and to create thermoelectric energy converters with improved characteristics.

The objective of this work is to evaluate the efficiency of gyrotropic thermoelements in uniform and non-uniform magnetic fields in the mode of electric energy generation.

Mathematical Model

To study the parameters of gyrotropic thermoelements, it is necessary to solve the following

equation of thermal conductivity with the corresponding boundary conditions:

$$\kappa\Delta T + \rho_0 j^2 + 2\alpha_a \left(j_y \frac{\partial T}{\partial x} - j_x \frac{\partial T}{\partial y} \right) = 0, \tag{1}$$

where T is the temperature; κ is the thermal conductivity of gyrotropic medium; ρ_0 is the electrical resistivity; x, y are the coordinates; j, j_x, j_y are the modulus and projections of the electric current density vector; $\alpha_\perp = Q_\perp B$ is the asymmetric part of the thermoEMF tensor; $Q_\perp$ is transverse Nernst-Ettingshausen coefficient; B is magnetic field induction.

$$\alpha = \begin{pmatrix} \alpha_0 & \alpha_a & 0 \\ -\alpha_a & \alpha_0 & 0 \\ 0 & 0 & \alpha_\perp \end{pmatrix}, \tag{2}$$

Where $\alpha_0, \alpha_\perp$ are the diagonal components of the thermoEMF tensor.

To obtain eddy currents, it is advisable to consider spiral thermocouples. Considering the axial symmetry, (1) we have

$$\Delta T + \frac{j_\varphi^{\ 2}}{\kappa\sigma} + \frac{1}{\kappa} j_\varphi 2\alpha_a(r) \frac{\partial T}{\partial r} = 0, \tag{3}$$

where σ is the electrical conductivity, φ is the angle, r is the radius, j_φ is the - angular component of current density, which is determined by the expression

$$j_\varphi = \sigma Q_\perp(r) B(r) \frac{dT}{dr}. \tag{4}$$

Whereas thermoEMF is set by the expression

$$E = 2\pi r Q_\perp(r) B(r) \frac{dT}{dr}. \tag{5}$$

The thermomagnetic figure of merit of the gyrotropic material

$$Z_Q(r) = \frac{Q_\perp^2(r) B^2(r)}{\kappa\rho}. \tag{6}$$

Non-uniformity can be obtained by changing the magnetic field B in a homogeneous gyrotropic medium, or by creating an anisotropy of the Nernst-Ettingshausen coefficient $Q^\perp$ in the ring at a constant magnetic field B. Let us consider the case when the magnetic field B in the ring changes along the radius of the ring, at a constant Nernst-Ettingshausen coefficient $Q^\perp$.

To solve (3) taking into account (4) and (5) and considering the boundary conditions, we obtain the expression for the efficiency of a spiral gyrotropic thermoelement in a non-uniform magnetic field

$$\eta = \frac{1}{6}\frac{\left(1 \pm \sqrt{1 + 6Z_Q(T_1 - T_2)}\right)^2}{6Z_Q(T_1 - T_2) - \left(1 \pm \sqrt{1 + 6Z_Q(T_1 - T_2)}\right)^2 - 2Z_Q T_1\left(1 \pm \sqrt{1 + 6Z_Q(T_1 - T_2)}\right)} \quad (7)$$

were

$$Z_Q = \frac{Q_\perp^2 B^2(r)}{\kappa\rho}. \quad (8)$$

Using (6), (7) one can calculate the efficiency of the gyrotropic spiral thermoelement in a non-uniform magnetic field.

Computer simulation results

Comsol Multiphysics software package was used to build a computer model of a spiral-shaped gyrotropic thermocouple [19]. The calculation of temperature distributions in the gyrotropic thermocouple was carried out by the finite element method. Using computer simulations, the temperature distributions for the *InSb* material in the temperature range 300 - 700 K and the magnetic field with induction B = 1 T were determined.

Fig.1 shows the temperature dependences of the figure of merit for thermoelectric materials *InSb, InAs* and *Bi2Te3*. It is seen that the best material for the manufacture of generator gyrotropic thermocouples is *InSb*, which is consistent with the experimental results presented in [1].

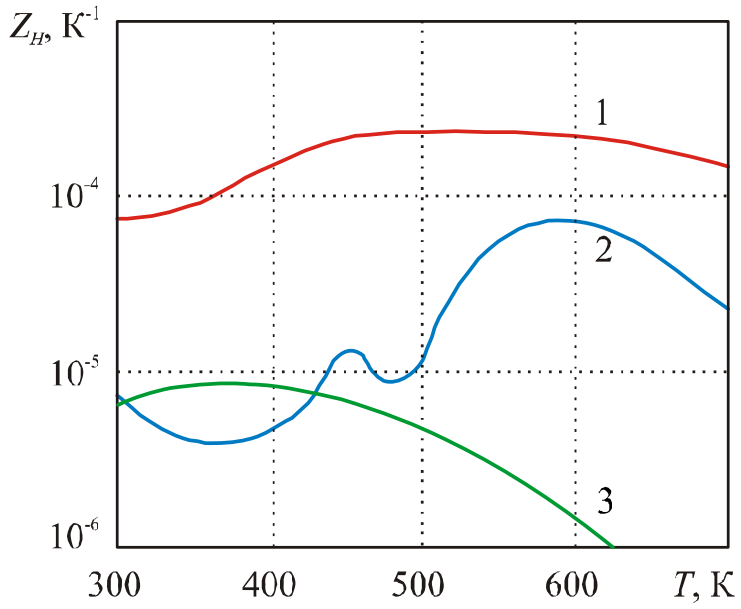

Fig. 1. Temperature dependences of the figure of merit of thermoelectric materials for gyrotropic thermoelements (1 – InSb, 2 – InAs, 3 – Bi_2Te_3).

Fig. 2 shows 3D mesh models of the finite element method *(a)* and temperature distribution *(b)* in a spiral gyrotropic thermoelement.

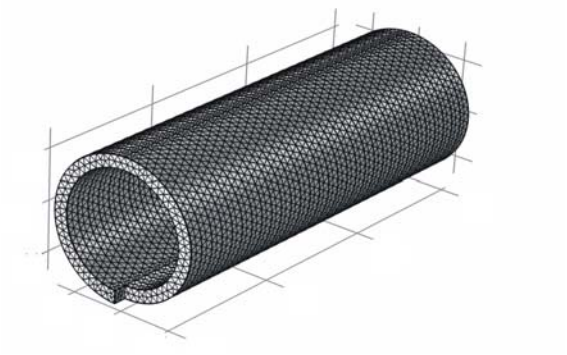

a)

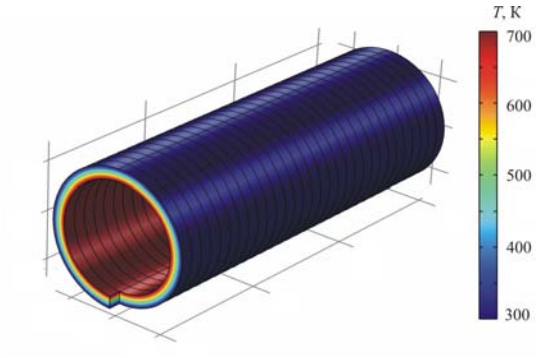

b)

Fig. 2. 3D mesh models of the finite element method (a) and temperature distribution (b) in a gyrotropic spiral thermoelement.

According to the calculations, the dependences of efficiency on the hot side temperature temperature of thermoelement T_2 at the constant cold side T_1 = 300 K for *InSb* are constructed (Fig. 3).

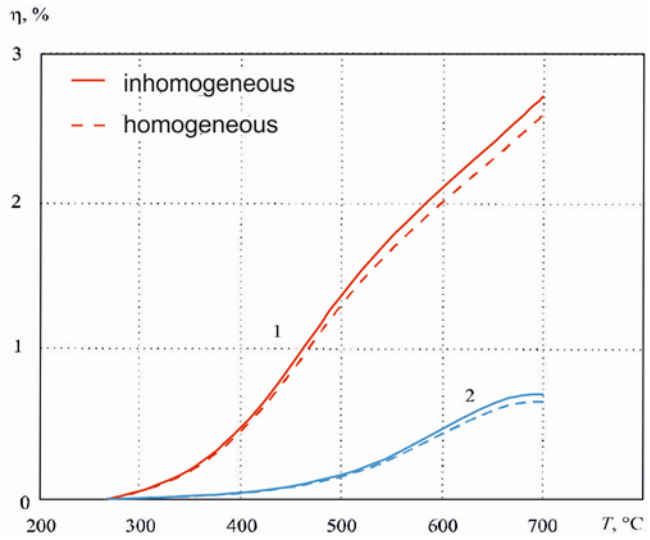

Fig. 3. Temperature dependence of the efficiency for cylinder-shaped gyrotropic thermoelement (1 – InSb, 2 – InAs).

The figure shows that the use of non-uniform magnetic fields in spiral thermoelements is more efficient. And spiral thermoelements, whose work is based on the excitation of eddy thermoelectric currents in a homogeneous gyrotropic thermoelectric medium, allow obtaining high thermoelectric voltages and differ from the known ones by multifunctionality, being promising for use both in special thermal generators and in measuring equipment. Studies of gyrotropic thermoelements of rectangular and optimal shapes have also shown efficiency increase in the case of using a non-uniform magnetic field.

Conclusions

1. The parameters of thermoelectric materials (*InSb, InAs* and Bi_2Te_3) for gyrotropic thermoelements are compared. It is established that the best material for the manufacture of generator gyrotropic thermoelements is *InSb,* the average value of the figure of merit of which in the temperature range 400 - 700 K is approximately $4 \cdot 10^{-4}$ K^{-1}.
2. Using computer simulations, the temperature distributions in the working fluid of a spiral-shaped gyrotropic thermoelement for *InSb* and *InAs* thermoelectric material were determined.
3. Temperature dependences of the efficiency are determined. It is established that the maximum efficiency value of spiral-shaped gyrotropic thermoelement for material *InSb* in the range of temperatures 300 - 700 K and magnetic induction of 1 T makes 2.75%.

References

1. Anatychuk L.I. (1979). *Termoelementy i termoelektricheskiie ustroistva [Thermoelements and thermoelectric devices]*. Kyiv: Naukova dumka [in Russian].
2. Samoilovich A.G. (2006). *Termoelektricheskiie i termomagnitnyie metody preobrazovaniia energii [Thermoelectric and thermomagnetic methods of energy conversion]*. Chernivtsi: Ruta [in Russian].
3. Anatychuk. L.I. (2003). *Termoelektrichestvo. T.2. Termoelektricheskiie preobrazovatelu energii [Thermoelectricity. Vol.2. Thermoelectric energy converters]*. Kyiv, Chernivtsi: Naukova Dumka [in Russian].
4. Samoilovich A.G., Korenblit L.L. (1953). The current state of the theory of thermoelectric and thermomagnetic phenomena in semiconductors. *Uspekhi Fizicheskikh Nauk*, 49(2), 243 - 272.
5. Nakamura H., Ikeda K., Yamaguchi S. (1997). Transport coefficients of *InSb* in a strong magnetic field. *Proc. of XVI International Conference on Thermoelectrics*. (Dresden, Germany, 1997, 142 – 146).
6. Anatychuk L.I., Luste O.J., Fedoruk Ya.G., Shinkaruk S.M. (2004). Eddy thermoelectric currents in a gyrotropic medium with radial temperature distribution. *J. Thermoelectricity*, 1, 19 - 24.
7. Luste O.Ya., Fedoruk Ya.G. Gyrotropic thermocouple in an non-uniform magnetic field // Thermoelectricity. - 2006. - №1. - P. 16 - 22.
8. Luste O.J., Fedoruk Ya.G. (2008). Optimization of materials for gyrotropic thermoelements. *J. Thermoelectricity*, 4, 21 - 26.
9. Agayev Z.F., Arasly D.G., Aliyev S.A. (2003). Thermomagnetic converter of IR radiation. *Energy Problems*, 3, 12 - 21.
10. Nemov S.A., Proshin V.I., Tarantasov G.L., Parfenyev R.V., Shamshur D.V., Chernyaev A.V. (2009). Nernst-Ettingshausen transverse effect, resonant scattering and superconductivity in SnTe: In. *Solid State Physics*, 51(1), 461 - 464.

11. Harman T.G., Honig J.M. (1967). *Thermoelectric and thermomagnetic effects and applications*. New York, Mc. Graw - Hill.
12. Nakamura H., Ikeda K. and Yamaguchi S. (1998). Transport coefficients of InSb in a strong magnetic field. Research report. *NIFS series (Nagoya, Japan).*
13. Hiroaki Nakamura, Kazuaki Ikeda, Satarou Yamaguchi. Transport coefficients of InSb in a strong magnetic field. (1997). *Proc. of XVI International conference on Thermoelectrics*. (Dresden, Germany, August 26-29, 1997).
14. Baransky P.I., Gaidar G.P. (2014). Anisotropy of thermoelectric properties of multi-valley semiconductors of cubic symmetry under the influence of external directional effects. *J.Thermoelectricity*, 1, 13.
15. Goldsmid H.J., Volckmann E.H. (1997). Galvanomagnetic and thermoelectric measurements on polycrystalline. *Proc. of 16 International Conference on Thermoelectrics* (Dresden, Germany, August 26 - 29, 1997).
16. Anatychuk L.I., Vikhor L.N. (1997). Low-temperature thermoelectric cooling under optimal legs inhomogeneity in the optimal nonuniform magnetic field. In: *Proc.of the 16 International Conference on Thermoelectrics* (Dresden, August 26-29, 1997).
17. Konstantinovich I.A., Rendigevich O.V. (2016). On the efficiency of gyrotropic thermoelements in generation mode. *J.Thermoelectricity*, 1, 69-74.
18. Zakharchuk T.V, Konstantinovich I.A., Konstantinovich A.V, Forbatyuk A.V. (2019). On the efficiency of spiral gyrotropic thermoelements in cooling mode. *J. Thermoelectricity*, 1, 63-68.
19. *COMSOL Multiphysics User's Guide* (2010).

Submitted 14.04.020

Годованець Н.А.[1],
Константинович І.А. *канд. фіз-мат. наук, доцент*[1,2]**,**
А.В. Константинович *док. фіз.-мат. наук, доцент*[2]**,**
Шугані С.Д.[1]

[1]Чернівецький національний університет ім. Ю. Федьковича,
вул. Коцюбинського 2, Чернівці, 58012, Україна,
[2]Інститут термоелектрики Національної академії наук і Міністерства освіти
і науки України, вул. Науки 1, Чернівці, 58029, Україна
dj_kneo@ukr.net; aconst@ukr.net; i.konstantynovych@chnu.edu.ua

ГІРОТРОПНІ ТЕРМОЕЛЕМЕНТИ В ОДНОРІДНОМУ ТА НЕОДНОРІДНОМУ МАГНІТНИХ ПОЛЯХ

За допомогою комп'ютерного моделювання визначено розподіли температур у робочому тілі гіротропних термоелементів в однорідному та неоднорідному магнітних полях. Визначено температурні залежності ККД гіротропних

термоелементів в однорідному та неоднорідному магнітних полях. Встановлено, що ККД генераторних гіротропних термоелементів більше в неоднорідному магнітному полі ніж в однорідному полі. Бібл. 19, рис. 3.

Ключові слова: коефіцієнт Нернста-Еттінгсгаузена, гіротропний термоелемент, неоднорідне магнітне поле, термоелектричний матеріал, термомагнітна добротність, ККД.

Годованец Н.А. [1],
Константинович И.А.. *канд. физ-мат. наук, доцент*[1,2]**,**
Константинович а.В. *док. физ.-мат. наук, доцент*[2]**,**
Шугани С.Д.[1]

[1]Черновицкий национальный университет им. Ю. Федьковича,
ул. Коцюбинского 2, [2]Черновцы, 58012, Украина,
[2]Институт термоэлектричества НАН и Мон Украины,
ул. Науки 1, Черновцы, 58029, Украина
e-mail: dj_kneo@ukr.net; aconst@ukr.net;
i.konstantynovych@chnu.edu.ua

ГИРОТРОПНОГО ТЕРМОЭЛЕМЕНТ В ОДНОРИДНОМУ ТА НЕОДНОРОДНОМ МАГНИТНОМ ПОЛЯХ

С помощью компьютерного моделирования определены распределения температур в рабочем теле гиротропных термоэлементов в однородном и неоднородном магнитном поле. Определены температурные зависимости КПД гиротропных термоэлементов в однородном и неоднородном магнитном поле. Установлено, что КПД генераторных гиротропных термоэлементов больше в неоднородном магнитном поле чем в однородном поле. Библ. 19, рис. 3.

Ключевые слова: коэффициент Нернста-Эттингсгаузена, гиротропный термоэлемент, неоднородное магнитное поле, термоэлектрический материал, термомагнитная добротность, КПД..

References

1. Anatychuk L.I. (1979). *Termoelementy i termoelektricheskiie ustroistva [Thermoelements and thermoelectric devices]*. Kyiv: Naukova dumka [in Russian].
2. Samoilovich A.G. (2006). *Termoelektricheskiie i termomagnitnyie metody preobrazovaniia energii [Thermoelectric and thermomagnetic methods of energy conversion]*. Chernivtsi: Ruta [in Russian].
3. Anatychuk. L.I. (2003). *Termoelektrichestvo. T.2. Termoelektricheskiie preobrazovatelu energii [Thermoelectricity. Vol.2. Thermoelectric energy converters]*. Kyiv, Chernivtsi: Naukova Dumka [in Russian].

4. Samoilovich A.G., Korenblit L.L. (1953). The current state of the theory of thermoelectric and thermomagnetic phenomena in semiconductors. *Uspekhi Fizicheskikh Nauk*, 49(2), 243 - 272.
5. Nakamura H., Ikeda K., Yamaguchi S. (1997). Transport coefficients of *InSb* in a strong magnetic field. *Proc. of XVI International Conference on Thermoelectrics*. (Dresden, Germany, 1997, 142 – 146).
6. Anatychuk L.I., Luste O.J., Fedoruk Ya.G., Shinkaruk S.M. (2004). Eddy thermoelectric currents in a gyrotropic medium with radial temperature distribution. *J. Thermoelectricity*, 1, 19 - 24.
7. Luste O.Ya., Fedoruk Ya.G. Gyrotropic thermocouple in an non-uniform magnetic field // Thermoelectricity. - 2006. - №1. - P. 16 - 22.
8. Luste O.J., Fedoruk Ya.G. (2008). Optimization of materials for gyrotropic thermoelements. *J. Thermoelectricity*, 4, 21 - 26.
9. Agayev Z.F., Arasly D.G., Aliyev S.A. (2003). Thermomagnetic converter of IR radiation. *Energy Problems*, 3, 12 - 21.
10. Nemov S.A., Proshin V.I., Tarantasov G.L., Parfenyev R.V., Shamshur D.V., Chernyaev A.V. (2009). Nernst-Ettingshausen transverse effect, resonant scattering and superconductivity in SnTe: In. *Solid State Physics*, 51(1), 461 - 464.
11. Harman T.G., Honig J.M. (1967). *Thermoelectric and thermomagnetic effects and applications*. New York, Mc. Graw - Hill.
12. Nakamura H., Ikeda K. and Yamaguchi S. (1998). Transport coefficients of InSb in a strong magnetic field. Research report. *NIFS series (Nagoya, Japan).*
13. Hiroaki Nakamura, Kazuaki Ikeda, Satarou Yamaguchi. Transport coefficients of InSb in a strong magnetic field. (1997). *Proc. of XVI International conference on Thermoelectrics*. (Dresden, Germany, August 26-29, 1997).
14. Baransky P.I., Gaidar G.P. (2014). Anisotropy of thermoelectric properties of multi-valley semiconductors of cubic symmetry under the influence of external directional effects. *J.Thermoelectricity*, 1, 13.
15. Goldsmid H.J., Volckmann E.H. (1997). Galvanomagnetic and thermoelectric measurements on polycrystalline. *Proc. of 16 International Conference on Thermoelectrics* (Dresden, Germany, August 26 - 29, 1997).
16. Anatychuk L.I., Vikhor L.N. (1997). Low-temperature thermoelectric cooling under optimal legs inhomogeneity in the optimal nonuniform magnetic field. In: *Proc.of the 16 International Conference on Thermoelectrics* (Dresden, August 26-29, 1997).
17. Konstantinovich I.A., Rendigevich O.V. (2016). On the efficiency of gyrotropic thermoelements in generation mode. *J.Thermoelectricity*, 1, 69-74.
18. Zakharchuk T.V, Konstantinovich I.A., Konstantinovich A.V, Forbatyuk A.V. (2019). On the efficiency of spiral gyrotropic thermoelements in cooling mode. *J. Thermoelectricity*, 1, 63-68.
19. *COMSOL Multiphysics User's Guide* (2010).

Submitted 14.04.2020

**Silke Augustin, Thomas Fröhlich,
Gunter Krapf, Jean-Pierre Bergmann,
Michael Grätzel,Jan Ansgar Gerken,
Kiril Schmidt**

Technical University, Ilmenau, Germany,
e-mail: silke.augustin@tu-ilmenau.de

CHALLENGES OF TEMPERATURE MEASUREMENT DURING THE FRICTION STIR WELDING PROCESS

The exact determination of the process zone temperature can be considered as an increasingly important role in the control and monitoring of the friction stir welding process (FSW). At present, temperature measurement is carried out with the aid of a temperature sensor integrated into the tool (usually thermocouples). Since these cannot be attached directly to the joining area, heat dissipation within the tool and to the environment cause measurement deviations as well as a time delay in the temperature measurement. The article describes a process and the challenges that arise in this process, how a direct temperature measurement during the process can be achieved by exploiting the thermoelectric effect between tool and workpiece, without changing the tool by introducing additional temperature sensors. Bibl. 12, Fig. 7.
Keyword: friction stir welding, direct temperature measurement, Seebeck-effect, measurement errors

Вступ

Friction Stir Welding (FSW) was developed and patented by Wayne Thomas at TWI (The Welding Institute) in Great Britain in 1991. It is assigned to the group of solid-state welding processes. In contrast to friction welding, the operating principle in FSW is not based on a relative movement of the workpieces, but by means of a wear-resistant rotating tool. One of the most relevant process variables is the axial force between the tool and the component. This force acts or- thogonally to the welding direction and causes the tool to be completely immersed in and to remain in the joining area. This welding process is characterized by comparatively low joining temperatures below the melting temperature and excellent mechanical weld seam properties in comparison to conventional welding processes, such as arc and laser welding [1]. Friction stir welding is used in aerospace, shipbuilding, medical technology, and automotive engineering. However, the challenges for possible direct temperature measurement, based on the Seebeck effect, are the spindle speeds of the welding tool and the forces acting in the process. Thus, high demands on the design of the measuring device and the permanent transmission of the electrical voltage are necessary [2].

The measurement of the joining zone temperature during the process is an increasingly quantifiable indicator, as it al- lows conclusions to be drawn about the heat input and thus the thermomechanical stress on the microstructure [2 – 4]. Temperatures are currently measured by thermography or thermocouples, which are integrated into the welding tool [5]. However, the latter method is very costly and inaccurate, as the thermocouple does not contact the friction point be- tween

the shoulder of the tool and the workpiece. In addition, various publications have described that the thermocou- ples were either destroyed or changed in their position during the welding process so that an exact temperature meas- urement was not possible [3]. Measurement deviations and time delays can occur due to heat conduction in the tool or the heat transfer to the environment. An alternative to inserting thermocouples in the tool is the Tool-Workpiece- Thermocouple method (TWT method), in which the occurring electrical thermoelectric voltage between tool and work- piece can be measured and then converted into a temperature value. However, this method places high demands on the used measuring circuits and the experimental determination of the various influencing parameters, as these have a deci- sive influence on the uncertainty of the measured temperature. In the following, the application of this method is de- scribed using the example of a robotized friction stir welding system and the results achieved are presented and dis-cussed.

Fundamentals of temperature measurement with thermocouples

If there is a temperature difference $T = T_1 - T_2$ at the ends of a metallic conductor ($T_1 > T_2$), the electrons at the warm end are of higher thermal energy than the electrons at the cold end. As a result, the electron diffusion, which is the rea- son for the occurrence of a potential difference E along the conductor.

$$E = \oint \frac{dU}{dT} \cdot \frac{dT}{dx} \cdot dx \tag{1}$$

The quotient dU/dT, describing the occurring differential thermoelectric voltage U along the conductor as a function of the temperature difference, is material-dependent and referred to as the Seebeck coefficient S(T) of the material.

The absolute thermoelectric emf of the conductor cannot be measured directly, but only in relation to the absolute thermoelectric emf of a conductor made of another material. This can be explained by the connecting wires of the volt- meter (mostly Cu) that are led from the hot and cold end of the conductor through an unknown temperature field, thus generating further differential, unknown thermoelectric emf. Therefore, two electric conductors with known Seebeck coefficients are connected to form a thermocouple measuring circuit. The underlying physical principle, the Seebeck effect (Fig. 1), indicates that an electric current is generated in a loop of two different conductors A and B when differ- ent temperatures T_1 and T_2 are present at the junctions of the two conductors.

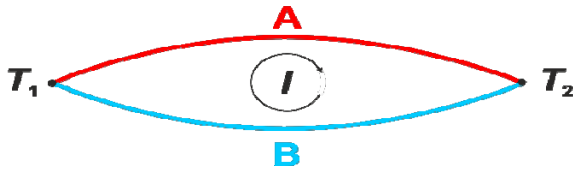

Fig. 1. Schematic representation of the Seebeck effect [6]

For measuring the resulting thermoelectric voltage, the closed circuit is disconnected at one point (Fig. 3) and a voltme- ter is applied. In the most basic case, i.e. at low-temperature differences and for a homogeneous Seebeck coefficient for the entire conductor length, the following applies to the measured thermoelectric emf:

$$U = \left(S_A - S_B\right) \cdot \Delta T \tag{2}$$

The length and the cross-section of the respective conductors are not relevant in this case. It can also be assumed that inhomogeneous conductors, with constant Seebeck coefficients over the entire length of the conductor, the occurring thermoelectric voltage depends only on the temperature difference between the two junctions. Temperature gradients along the homogeneous conductors have no effect on the measured thermoelectric emf since the resulting differential partial voltages along the two conductors cancel each other. [6,7]. On the other hand, however, an additional thermoe-lectric voltage occurs when the Seebeck coefficient changes, e.g. due to mechanical or chemical influences on the con- ductor material, if these inhomogeneities in the conductor material are located in the temperature gradient [8,9,10].

For the basic circuit for temperature measurement with thermocouples, which is most frequently used in technology, the circuit is disconnected at a junction and the voltmeter is connected there via copper wires (Fig. 2).

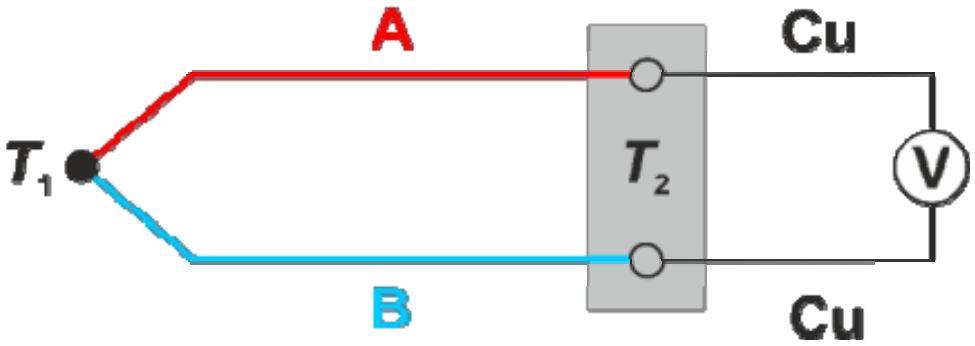

Fig. 2. Basic circuit of temperature measurement with thermocouples

The temperature T_2 must be known and constant over the measuring period. When defining their characteristic curve, internationally standardized thermocouples refer to a temperature T_2, also known as reference junction temperature, of T_V = 0 °C. If this reference junction temperature deviates from 0 °C, a corresponding correction must be made when converting the thermoelectric voltage into temperature.

When it is not possible to lead the thermocouple cables to the cold junction, compensating or thermoelectric cables are used in practice. These cables provide the same thermoelectric material properties as the thermocouple cables used in a limited temperature range (up to approx. 200 °C). Ideally, no additional contributions to the thermoelectric emf should occur when using compensating cables, even if they are in the range of the temperature gradient. In practice, however, additional contributions to the measurement uncertainty occur, which must be taken into consideration in the process of measurement.

The illustrated basic principle of temperature measurement with thermocouples can also be used for direct measurement of the temperature between tools and workpieces in production machines [6].

Tool-Workpiece-Thermocouple (TWT-) Method

In the present paper, the direct measurement of the electrical thermoelectric voltage between workpiece and tool is studied using the example of a robotic system for friction stir welding (Fig. 3).

The average temperature is recorded along the entire contact surface between the tool and the workpiece.

First, it is necessary to investigate which thermoelectric or compensating cables can be connected to the two basic ele- ments of the electric thermoelectric voltage circuit in the welding robot so that a thermoelectric circuit up to the measur- ing device is created. It is to be expected that process-related temperature gradients will occur in the system, which could cause additional thermoelectric voltages with different material combinations. The Production Technology Group [11] has developed a grinding system for the test adaptable to the robotized FSW system (Fig. 4 above). The electrical voltage is to be tapped directly from the rotating tool and led to a thermoelectric cable.

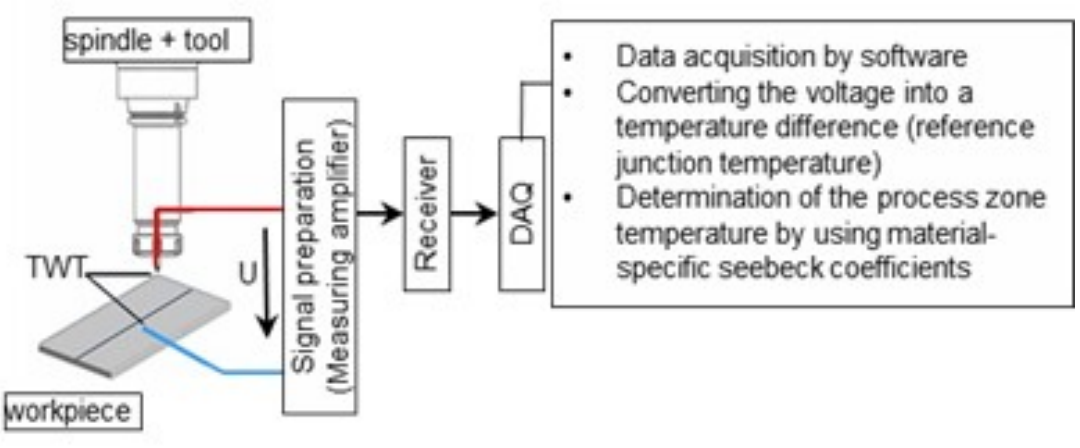

Fig. 3. Basic principle of the Tool-Workpiece- Thermocouple (TWT) Method [11]

The grinding system is electron- ically isolated from the system in order to avoid interferences. The friction stir welding tool used consists of hardened tool steel (1.2344), and the workpieces to be joined are made of the aluminum alloy EN AW 6060 T66 with a sheet thickness of 5 mm, a length of 300 mm and a width of 50 mm. The workpieces were joined by butt joint formation. The individual components, which carry the thermoelectric voltage from the probe to the Cu cable, are made of the same material (1.2344) in order not to interfere with the rules for thermoelectric circuits.

For the following investigations, the friction stir welding tool or workpiece was first extended with thermoelectric ca-bles made of the same materials as the tool and workpiece in order to tap the thermoelectric voltage. Copper cables were connected to these thermoelectric cables, comparable to the basic circuit in Fig. 2, to carry the signal to the meas- uring instrument (Fig. 4).

This design requires the reference point in the thermoelectric circuit to be located at different points in the system. It is not guaranteed that the reference junction temperature of both contact points is identical over the course of time. The heat dissipation through the thermoelectric lines was estimated in advance for heat conduction by analytical calculations and dimensioned in such a way that the same temperature finally prevails at the reference junctions. In the first meas- urements at the system, the temperature of the reference junctions was monitored by means of applied thermocouples to validate the previously calculated minimum lengths. The measurements confirmed the correctness of the assumptions made, the temperature at the reference junctions was the same.

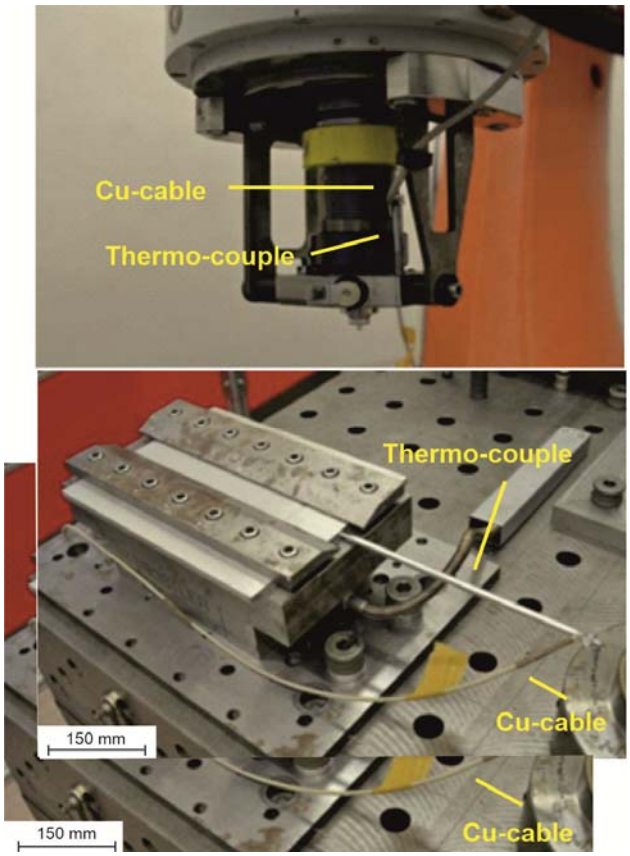

Fig. 4. Fastening of the thermal and copper cable to the tool (top) or workpiece (bottom)

Results

Calibration of the material combination

The used material combination of tool steel (1.2344) and aluminum alloy EN AW 6060 T66 does not belong to the internationally standardized thermocouple material combinations. Therefore, the T-U-characteristic or the Seebeck coefficient of the material pairing was determined at first. The calibration was carried out in a temperature-controlled test rig using a calibrated thermocouple. Figure 6 shows the results for the material combination 1.2344/EN AW 6060 T66.

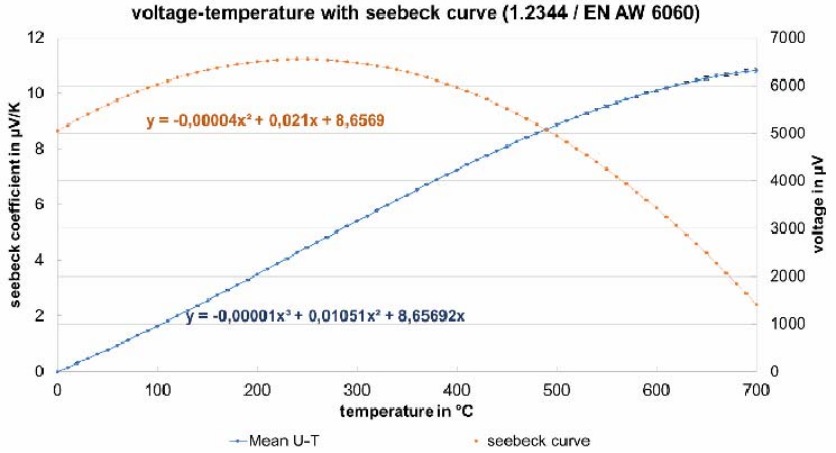

Fig. 5. Result of calibration for 1.2344 and EN AW 6060 [11]

The left ordinate axis shows the determined Seebeck coefficient (orange) and the opposite one the thermo-voltage axis (blue). The Seebeck coefficient was determined with the simplified equation 2. The temperature difference of the sup-porting points was 10 K. The results were firstly used to calculate the temperatures during the welding process in order to prove the basic suitability of the measurement setup. The characteristic curve of the material combination is to be determined more precisely in subsequent tests in the calibration laboratory of the Institute for Process Measurement and Sensor Technology.

Measurements at the robotized FSW welding unit

The temperature measurement experiments are carried out on a serial kinematic 6-axis jointed-arm robot KUKA KR 500 MT 3. The robot is equipped with a modified FSW spindle from MAG, which is fitted with a tool clamping system for hollow shank tapers (HSK 63). The friction stir welding tool and workpiece were integrated into the system as de- scribed in chapter 3. The resulting forces are recorded by a multi-component dynamometer from KISTLER, which is located below the component holder (Fig. 5).

The system was operated with the following welding parameters:

- welding speed: 1000 mm/min
- rotational speed: 5000 min-1
- axial force: 4000 N
- shoulder diameter: 13 mm
- probe diameter: 5 mm
- weld seam length: 250 mm
- plunging depth: 4.5 mm

For validation of the calculated temperatures from the Seebeck coefficients determined during calibration, sheath ther- mocouples type *K* were integrated into the center of the welding zone (stir zone). Therefore, grooves were prepared in the workpiece in which the thermocouples were inserted without damage (Fig. 6). The intention was to prove that the temperature in the welding zone measured with the system set up was almost on the same level as that of the thermo- couples. The thermocouples were positioned 2 mm below the welding surface in the gap between the workpieces has to be joined.

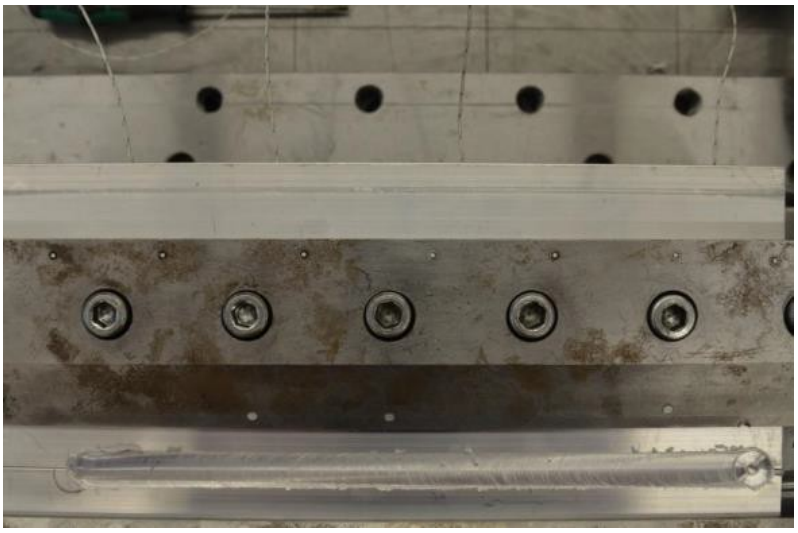

Fig. 6. Positioning of the thermocouples along the weld seam (from left TE1 - TE4)

The measured thermoelectric voltages were filtered with a passive low-pass filter of 1st order of 1 Hz. Figure 8 shows the increase in temperature (red) and force (blue) of the material combination 1.2344 & EN AW 6060 T66 throughout the welding time. It can be clearly noticed that the temperature rises during the plunging phase and reaches a maximum of 450 °C at appr. 12 s. At the same time, a reduction of the axial force to almost 1000 N can be recognized, which is due to a reduction of the yield stress of the aluminum alloy. After the tool has sufficiently plasticized the workpiece material, the contact surface at which the electrical thermoelectric voltage is generated increases. Due to the contact with the still cool tool body and the plasticized workpiece, a temperature decrease of approx. 125 °C can be determined. During the welding phase (starting at t = 15 s), the axial force (4000 N) and the temperature (approx. 500 °C) remain almost constant. The latter criterion corresponds to approx. 75% of the liquidus temperature of EN AW 6060 T66. Im- mediately before the tool retraction, the force and the temperature rise briefly before the welding tool leaves the joining area. This can be explained by a short dwell time before the tool retraction whereby process-related reorientations of the spindle take place. The temperature curves of the thermocouples (TE1 - TE4) also shown in Figure 7, which should be used to validate the results of the direct thermoelectric voltage measurement (referred to as Tweld_ThermV in the dia-gram), always indicate a maximum below the temperature curves. This can be attributed both to a positioning slightly below the surface [7] and to the delay periods of the thermocouples. It was determined after the measurement that ther- mocouple 3 was not positioned exactly, which can be used to justify the deviating temperature curve.

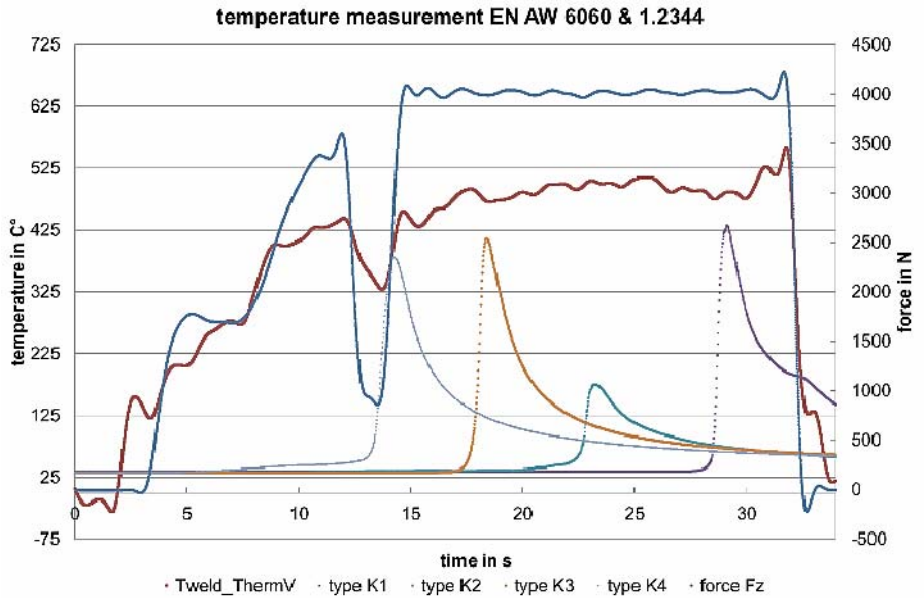

Fig. 7. Results during the welding process [11]

It is also noticeable that interference signals are already recorded before and also after welding, i.e. during the open thermoelectric circuit. This is mainly explained by disturbance variables, e.g. the 50Hz mains frequency (correctable with low-pass filter), the rotational frequency of the rotating spindle or the system-related EMC load. As a result, both the values of the calibration and the results obtained during the welding process must be validated by repeat measure-ments.

Summary and outlook

The measurement results presented in the paper demonstrated that a direct temperature measurement can be accom-plished using the TWT method. The calibration characteristic curve was determined for the material combination used and applied to measure the process zone temperature during the joining process. The achieved measuring values of the calibration should be additionally confirmed by an exact laboratory calibration. During the first measurements on the robotic FSW welding robot, the following influences on the measurement results and their uncertainty were identified:

- uncertainty of the characteristic curve determination,
- EMC load due to system periphery,
- wear of the probe during the welding process,
- not yet identified temperature gradients in the area of material transitions, which cause additional thermoelec-tric voltages.

In the future cooperation between the Production Technology Group and the Institute for Process Measurement and Sensor Technology at the TU Ilmenau, the possibilities of direct temperature measurement based on the Seebeck effect both for friction stir welding and for other welding processes are to be further investigated and verified. The heat trans- fer processes are also to be calculated in advance using numerical simulations [12] and subsequently verified by meas-urement technology.

Conflict of Interest

The authors claim that there are no possible financial or other conflicts over the work

References

1. D. Schmid: Reibrührschweißen von Aluminiumlegierungen mit Stählen für die Automobilindustrie, Dissertation, TU Mün- chen, Herbert Utz Verlag GmbH, 2015.
2. A. Fehrenbacher, C. Smith, N. Duffie, N. Ferrier, F. Pferfferkorn, M. Zinn: Combined Temperature and Force Control for Robotic Friction Stir Welding, ASME, J. Manuf. Sci. Eng 136 (2), 021007 (Jan 15, 2014 року), Paper No: MANU-12-1357; DOI: 10.1115 / 1.4025912.
3. ACF Silva, J. De Backer, G. Bolmsjö: Temperature measurements during friction stir welding, University West, Trollhät- tan, Sweden, Springerlink.com, 2016. DOI 10.1007 / s00170-016-9007-4.
4. E. Cole, A. Fehrenbacher, N. Duffie, M. Zinn, F. Pfefferkorn, N. Ferrier: Weld temperature effects during friction stir weld- ing of dissimilar aluminum alloys 6061-t6 and 7075-t6, Int J Adv Manuf Technol (2014 року) 71: 643-652. DOI 10.1007 / s00170-013-5485-9.
5. A. Fehrenbacher, N. Duffie, N. Ferrier, F. Pfefferkorn, M. Zinn: Effects of tool-workpiece interface temperature on weld quality and quality improvements through temperature control in friction stir welding, The Int. Journ. Adv. Manuf. Techn., Vol. 71, pp. 165-179, 2014/03/01, 2014.
6. F. Bernhard (Hrsg.): Handbuch der Technischen Temperaturmessung, 2. Auflage, Springer-Verlag, 2014.
7. M. Javurek, A. Mittermair: Wo in einem Thermoelement herrscht die gemessene Temperatur? Analyse mittels FE- Simulation, Technisches Messen, Heft 11, 2016, De Gruyter Oldenbourg. DOI 10.1515 / teme-2016-0028.
8. P. Germanow: Messtechnische Untersuchung der Kennlinienstabilität von Thermoelementen, TU Ilmenau, Masterarbeit, 2019.
9. ES Webster: Low-Temperature Drift in MIMS Base-MetalThermocouples, Springer Verlag, Int J Thermophys (2014 року) 35: 574-95. DOI 10.1007 / s10765-014-1581-9.

10. AD Greenen, ES Webster: Thermal Recovery from Cold-Working in Type K Bare-Wire Thermocouples, Springer Ver- lag, Int J Thermophys (2017) 38: 179. DOI 10.1007 / s10765-017-2316-5.
11. M. Baranowski, K. Schmidt, MK Stobrawa: Anwendung des Seebeck-Effekts zur Messung der Prozesszonentemperatur beim Reibrührschweißen, Dokumentation Projektseminar, TU Ilmenau, 2018.
12. MZH Khandkar, JA Khan, AP Reynolds: Prediction of temperature distribution and thermal history during friction stir welding: input torque based model, Sc. and Techn. of Welding & Joining, 8 (3): 165-174, 2003. DOI: 10.1179 / 136217103225010943

Submitted 22.04.2020

Зільке Аугустин, Фрёлих Томас ,
Крапф Гюнтер, Жан-Пьер Бергманн,
Грэтцель Михаэль, Геркен Ян Ансгар ,
Шмидт Кирил

Технічний університет, Ільменау, Німеччина,
e-mail: silke.augustin@tu-ilmenau.de

ПРОБЛЕМИ ВИМІРУ ТЕМПЕРАТУРИ В ПРОЦЕСІ РОТАЦІЙНОГО ЗВАРЮВАННЯ ТЕРТЯМ

Точне визначення температури технологічної зони набуває все більш важливу роль в процесі контролю і моніторингу ротаційного зварювання тертям. В даний час вимірювання температури здійснюється за допомогою вбудованого в інструмент давача температури (зазвичай термопари). Оскільки її не можна прикріпити безпосередньо до області з'єднання, розсіювання тепла всередині інструменту і в навколишнє середовище викликає відхилення в вимірах, а також затримку вимірювання температури в часі. У статті описано процес і пов'язані з ним проблеми. Показано, що пряме вимірювання температури в ході процесу може бути здійснене за рахунок використання термоелектричного ефекту між інструментом і деталлю без заміни інструменту шляхом введення додаткових давачів температури. Бібл. 12, рис. 7.

Ключові слова: ротаційне зварювання тертям, пряме вимірювання температури, ефект Зеєбека, похибки вимірювання

Зильке Аугустин, Фрёлих Томас ,
Крапф Гюнтер, Жан-Пьер Бергманн,
Грэтцель Михаэль, Геркен Ян Ансгар ,
Шмидт Кирил

Технический университет, Ильменау, Германия,
e-mail: silke.augustin@tu-ilmenau.de

ПРОБЛЕМЫ ИЗМЕРЕНИЯ ТЕМПЕРАТУРЫ В ПРОЦЕССЕ РОТАЦИОННОЙ СВАРКИ ТРЕНИЕМ

Точное определение температуры технологической зоны приобретает все более важную роль в процессе контроля и мониторинга ротационной сварки трением. В настоящее время измерение температуры осуществляется с помощью встроенного в инструмент датчика температуры (обычно термопары). Поскольку их нельзя прикрепить непосредственно к области соединения, рассеяние тепла внутри инструмента и в окружающую среду вызывает отклонения в измерениях, а также задержку измерения температуры во времени. В статье описан процесс и связанные с ним проблемы, как прямое измерение температуры в ходе процесса может быть достигнуто за счет использования термоэлектрического эффекта между инструментом и деталью, без замены инструмента путем введения дополнительных датчиков температуры. Библ. 12, рис. 7.

Ключевые слова: ротационная сварка трением, прямое измерение температуры, эффект Зеебека, погрешности измерения

References

1. D. Schmid: Reibrührschweißen von Aluminiumlegierungen mit Stählen für die Automobilindustrie, Dissertation, TU Mün- chen, Herbert Utz Verlag GmbH, 2015.
2. A. Fehrenbacher, C. Smith, N. Duffie, N. Ferrier, F. Pferfferkorn, M. Zinn: Combined Temperature and Force Control for Robotic Friction Stir Welding, ASME, J. Manuf. Sci. Eng 136 (2), 021007 (Jan 15, 2014 року), Paper No: MANU-12-1357; DOI: 10.1115 / 1.4025912.
3. ACF Silva, J. De Backer, G. Bolmsjö: Temperature measurements during friction stir welding, University West, Trollhät- tan, Sweden, Springerlink.com, 2016. DOI 10.1007 / s00170-016-9007-4.
4. E. Cole, A. Fehrenbacher, N. Duffie, M. Zinn, F. Pfefferkorn, N. Ferrier: Weld temperature effects during friction stir weld- ing of dissimilar aluminum alloys 6061-t6 and 7075-t6, Int J Adv Manuf Technol (2014 року) 71: 643-652. DOI 10.1007 / s00170-013-5485-9.
5. A. Fehrenbacher, N. Duffie, N. Ferrier, F. Pfefferkorn, M. Zinn: Effects of tool-workpiece interface temperature on weld quality and quality improvements through temperature control in friction stir welding, The Int. Journ. Adv. Manuf. Techn., Vol. 71, pp. 165-179, 2014/03/01, 2014.
6. F. Bernhard (Hrsg.): Handbuch der Technischen Temperaturmessung, 2. Auflage, Springer-Verlag, 2014.
7. M. Javurek, A. Mittermair: Wo in einem Thermoelement herrscht die gemessene Temperatur? Analyse mittels FE- Simulation, Technisches Messen, Heft 11, 2016, De Gruyter Oldenbourg. DOI 10.1515 / teme-2016-0028.
8. P. Germanow: Messtechnische Untersuchung der Kennlinienstabilität von Thermoelementen, TU Ilmenau, Masterarbeit, 2019.

9. ES Webster: Low-Temperature Drift in MIMS Base-MetalThermocouples, Springer Verlag, Int J Thermophys (2014 року) 35: 574-95. DOI 10.1007 / s10765-014-1581-9.
10. AD Greenen, ES Webster: Thermal Recovery from Cold-Working in Type K Bare-Wire Thermocouples, Springer Ver- lag, Int J Thermophys (2017) 38: 179. DOI 10.1007 / s10765-017-2316-5.
11. M. Baranowski, K. Schmidt, MK Stobrawa: Anwendung des Seebeck-Effekts zur Messung der Prozesszonentemperatur beim Reibrührschweißen, Dokumentation Projektseminar, TU Ilmenau, 2018.
12. MZH Khandkar, JA Khan, AP Reynolds: Prediction of temperature distribution and thermal history during friction stir welding: input torque based model, Sc. and Techn. of Welding & Joining, 8 (3): 165-174, 2003. DOI: 10.1179 / 136217103225010943

Submitted 02.04.2020

Anatychuk L.I. *acad. NAN Ucraine*[1,2],
Kobylianskyi R.R. *cand. phys.– math sciences*[1,2],
Fedoriv R.V.[1,2]

[1]Institute of Thermoelectricity of the NAS and MES of Ukraine,
1, Nauky str., Chernivtsi, 58029, Ukraine, *e-mail:* anatych@gmail.com
[2]Chernivtsi National University, 2 Kotsiubynskyi Str.,
Chernivtsi, Ukraine, 58012,

COMPUTER SIMULATION OF CYCLIC TEMPERATURE EFFECT ON THE HUMAN SKIN

This paper presents the results of computer simulation of cyclic temperature effect on the human skin in a dynamic mode. A three-dimensional computer model of biological tissue was built with regard to thermophysical processes, blood circulation, heat exchange metabolic and phase transition processes. As an example, the case is considered when on the skin surface there is a work tool whose temperature varies in the temperature range [-50 ÷ +50] °C. Temperature distributions in different layers of the human skin in heating and cooling modes have been determined. The results obtained make it possible to predict the depth of biological tissue freezing and heating with a given temperature effect. Bibl. 46,Fig. 10, Tabl. 2.
Keywords: temperature effect, human skin, dynamic mode, computer simulation.

Introduction

It is well known in medical practice that temperature exposure is an important factor in the treatment of many diseases of the human body [1-3]. However, the devices used for this purpose are in most cases bulky, without proper temperature control and thermal reproduction capabilities. To obtain lower temperatures, systems with liquid nitrogen are used [4-8], which significantly limits the possibilities of their use in medical institutions, where the provision of liquid nitrogen is problematic. In addition, the use of liquid nitrogen or the Joule-Thomson effect in the expansion of gases does not allow for the exactly required temperature regimes, and generally reduces the efficiency of using cold in treatment.

This problem can be solved by using thermoelectric cooling (heating) [3, 9-12]. Studies of the thermal effect on biological tissue carried out for many years, the creation of thermoelectric devices on their basis and the use in medical practice confirm their effectiveness. Thermoelectric devices are promising in such areas of medicine as cryotherapy, cryosurgery, ophthalmology, traumatology, neurosurgery, plastic surgery, urology, dermatology, etc. [1-3].

However, the experience of using thermoelectric medical devices has revealed a number of their disadvantages. Among them, the most important is the lack of the ability to control the cooling and heating processes in time. The latter significantly narrows the possibilities of treatment with heat and cold.

Studies show that cooling rates (their dynamics) play a decisive role in treatment [7, 13-25]. Thus, very rapid cooling does not lead to the destruction of biological tissues at all. On the contrary, moderate but cyclic cooling promotes vigorous destruction of tumors. Time cooling and heating functions are also important in the treatment of other diseases.

Thus, the general problem is to develop a fundamental scientific basis for creating a new generation of thermoelectric medical devices, which reproduce the specified functions of cooling and heating in biological tissue. In most cases, it is very difficult to control the cyclic processes of cooling and heating of biological tissue [26, 27]; therefore, it is necessary to learn to predict the depth of freezing and heating of skin layers at a given temperature effect at different points in time.

So, the *purpose of this work* is to determine, using computer simulation, the temperature distributions in different layers of the human skin in a dynamic mode at a given cyclic temperature effect.

Physical model

According to a physical 2D model with axial symmetry (Fig.1), the area of biological tissue of the human body is a structure of three layers of skin (epidermis 1, dermis 2, subcutaneous layer 3) and the internal biological tissue 4 and is characterized by the following thermophysical properties [28-34]: thermal conductivity κ_i, specific heat C_i, density ρ_i, blood perfusion rate ω_{bi}, blood density ρ_b, blood temperature T_b, blood heat capacity C_b and specific heat release Q_{meti} due to metabolic processes and latent heat of phase transition L. Thermophysical properties of skin and biological tissue of the human body in normal [35-39] and frozen states [40, 41] are shown in Tables 1, 2. The respective layers of biological tissue 1-4 are considered as bulk heat sources qi, where:

$$q_i = Q_{met\,i} + \rho_b \cdot C_b \cdot \omega_{bi} \cdot (T_b - T), \quad i = 1..4 . \tag{1}$$

The geometric dimensions of each such layer 1-4 are a_i, b_i. On the surface of the skin is a round work tool 5, the geometric dimensions of which are as follows: thickness $d = 1$ mm and diameter $c = 10$ mm. According to medical recommendations and analysis of known cryoprobes used for cryodestruction, it was determined that the diameter of such probes is from 5 mm to 15 mm [42, 43]. Therefore, in this work, as an example, we took the average value of the probe diameter, which is $c = 10$ mm. The temperatures at the boundaries of the respective layers 1-4 and the work tool 5 are T_1, T_2, T_3, T_4, T_5, T_6. The temperature inside biological tissue is $T_1 = +37$°C. The temperature of the work tool varies in the range $T_7 = [-50 \div +50]$ °C. The ambient temperature is $T_8 = +22$°C. The surface of human skin with a temperature of T_6 is in a state of heat exchange with the environment (heat transfer coefficient α and radiation coefficient ε) at a temperature of T_8. The lateral surface of the skin is adiabatically isolated.

This model does not take into account the thermal contact resistance between the work tool and the human skin, since it is estimated to be insignificant and is $R_c = 2 \cdot 10^{-3}$ m^2·K/W [44].

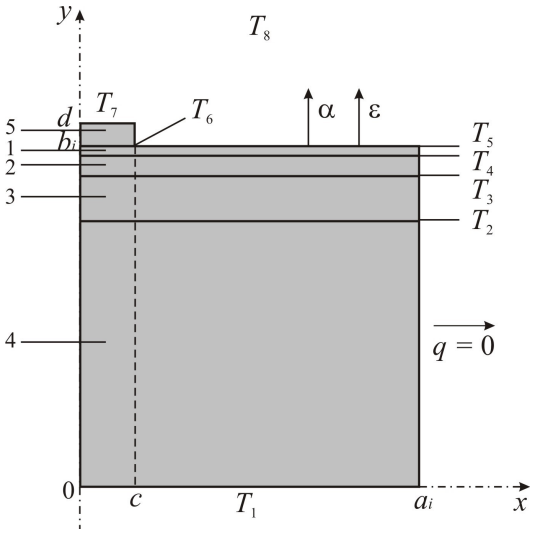

Fig.1. Physical 2D model of the human skin with axial symmetry: 1 – epidermis, 2 – dermis, 3 – subcutaneous layer, 4 – internal biological tissue, 5 – work tool

Table 1

Thermophysical properties of biological tissue of the human body [35-39]

Layers of biological tissue	Epidermis	Dermis	Subcutaneous layer	Internal tissue
Thickness, l (mm)	0.08	2	10	30
Specific heat, C ($J \cdot kg^{-1} \cdot K^{-1}$)	3590	3300	2500	4000
Thermal conductivity, κ ($W \cdot m^{-1} \cdot K^{-1}$)	0.24	0.45	0.19	0.5
Density, ρ ($kg \cdot m^{-3}$)	1200	1200	1000	1000
Metabolism, Q_{met} (W/m^3)	368	368	368	368
Blood perfusion rate, ω_b (ml/s·ml)	0	0.0005	0.0005	0.0005
Blood density, ρ_b ($kg \cdot m^{-3}$)	1060	1060	1060	1060
Blood heat capacity, C_b ($J \cdot kg^{-1} \cdot K^{-1}$)	3770	3770	3770	3770

Table 2

Thermophysical properties of biological tissue of the human body in the normal and frozen states [40, 41]

Thermophysical properties of biological tissue	Value	Measurement units
Heat capacity of normal biological tissue (C_1)	3600	J/m^3 °C
Heat capacity of frozen biological tissue (C_2)	1800	J/m^3 °C
Thermal conductivity of normal biological tissue (κ_1)	0.5	W/m °C
Thermal conductivity of frozen biological tissue (κ_2)	2	W/m °C
Latent heat of phase transition (L)	$250 \cdot 10^3$	J/m^3
Upper temperature of phase transition (T_1)	-1	°C
Lower temperature of phase transition (T_2)	-8	°C

Mathematical model

In general, the equation of heat exchange in biological tissue is given by [45]:

$$C_i \cdot \frac{\partial T}{\partial t} = \nabla \cdot (\kappa_i \cdot \nabla T) + \rho_b \cdot C_b \cdot \omega_{bi} \cdot (T_b - T) + Q_{meti}, \quad i = 1..4, \tag{2}$$

where C_i, κ_i is specific heat and thermal conductivity of respective skin layers, ρ_b is blood density, C_b is specific heat of blood, ω_{bi} is blood perfusion of respective layers, T_b is blood temperature, T is temperature of the biological tissue; Q_{meti} is heat released due to metabolic processes in each layer.

The term on the left side of equation (2) is the rate of change of thermal energy contained in a unit volume of biological tissue. The three terms on the right side of this equation represent, respectively, the rate of change of thermal energy due to thermal conductivity, blood perfusion and metabolic heat.

The equation of heat exchange in the biological tissue (2) is solved with the corresponding boundary conditions. The temperature on the surface of the work tool varies according to the given law in the temperature range T_7 = [-50 ÷ +50] ° C. Inside the biological tissue, the temperature T_1 = + 37 ° C. The lateral surfaces of biological tissue are adiabatically isolated (q = 0), and the upper surface of the skin is in a state of heat exchange (heat exchange coefficient α and radiation coefficient ε) with the environment at a temperature of T8.

$$q_i(x,y,t)\Big|_{\substack{c\le x\le a \\ y=b_i}} = \alpha \cdot (T_8 - T_5) + \varepsilon \cdot \sigma \cdot (T_8^4 - T_5^4), \tag{3}$$

where $q_i(x,y,t)$ is the heat flux density of the i-th layer of the human skin, α is the coefficient of convective heat exchange of the skin surface with the environment, ε is the radiation coefficient, σ is the Boltzmann constant, T_5 is the temperature of the human skin surface, T_8 is the ambient temperature (T_8 = + 22 ° C).

At the initial time moment t = 0 s, it is assumed that the temperature in the entire volume of the skin is T = + 37 °C, i.e. the initial conditions for solving equation (2) are as follows:

$$T_i(x,y,0) = T_b, \qquad i = 1,...,4. \tag{4}$$

As a result of solving the initial-boundary value problem (2) - (4), the distributions of temperature $T_i(x,y,t)$ and heat fluxes $q_i(x,y,t)$ in the corresponding layers of the skin at any time are determined. As an example, in this paper we consider the case in which the temperature of the work tool varies according to a given law in the temperature range T_7 = [-50 ÷ +50] °C. However, it should be noted that the proposed technique allows us to consider cases where the temperature of the work tool $T_f(t)$ changes in any temperature range or according to a predetermined function.

During the freezing process, the cells will undergo a phase change at the freezing point, with the loss of heat of the phase transition (L) and the temperature in these cells will not change. The phase transition in the biological cells occurs in the temperature range (-1 ÷ -8) °C. The properties of the skin and biological tissue in normal and frozen states are given in tables 1, 2 [35-41]. In the temperature range (-1 ÷ -8) °C, when the cells are frozen, the heat of the phase transition is absorbed, which can be

modeled by adding the appropriate value to the heat capacity [40, 41].

When freezing the human skin, vasoconstriction occurs in the capillaries until all blood freezes in the capillaries, and the value ω_{bi} tends to zero. In addition, cells will not be able to generate metabolic heat when frozen and Q_{meti} will be zero at temperatures below zero.

In the frozen state, the properties of the skin and biological tissue will have the following values (5) – (8):

$$C_i = \begin{cases} C_1 & T \geq -1°C \\ \dfrac{L}{-1-(-8)} + \dfrac{C_1 + C_2}{2} & -8°C \leq T \leq -1°C \\ C_2 & T \leq -8°C \end{cases} \tag{5}$$

$$\kappa_i = \begin{cases} \kappa_1 & T \geq -1°C \\ \dfrac{\kappa_1 + \kappa_2}{2} & -8°C \leq T \leq -1°C \\ \kappa_2 & T \leq -8°C \end{cases} \tag{6}$$

$$Q_{met_i} = \begin{cases} 368 & T \geq -1°C \\ 0 & -8°C \leq T \leq -1°C \\ 0 & T \leq -8°C \end{cases} \tag{7}$$

$$\omega_{b_i} = \begin{cases} 0,0005 & T \geq -1°C \\ 0 & -8°C \leq T \leq -1°C \\ 0 & T \leq -8°C \end{cases} \tag{8}$$

Computer model

A three-dimensional computer model of biological tissue was created in a cylindrical coordinate system on the surface of which is a medical work tool. Comsol Multiphysics software package [46] was used to build a computer model, which allows modeling of thermophysical processes in biological tissue, taking into account blood circulation, heat exchange, metabolic processes and phase transition.

The distribution of temperature and heat flux density in biological tissue was calculated by the finite element method, the essence of which is that the object under study is divided into a large number if finite elements and in each of them a function value is sought for that satisfies given second order differential equations with the corresponding boundary conditions. The accuracy of solving the problem posed depends on the level of partitioning and is ensured by a large number of finite elements [46].

As an example, Fig. 3-10 shows the distributions of temperature and isothermal surfaces in the bulk of the human skin, on the surface of which a work tool is located, the temperature of which varies

cyclically according to a predetermined law in the temperature range [-50 ÷ +50] ° C at different points of time.

Results of computer simulation of cyclic temperature effect on the human skin in a dynamic mode

According to the known methods of cryodestruction and coagulation of biological tissue [7, 13, 18-20] the rate of cooling should be at least (40-50) °C/min, and the rate of heating (20-25) °C/min. Therefore, in this paper, as an example, we consider the case when the work tool temperature $T_f(t)$ varies in the range of operating temperatures [-÷+50]°C as follows. First, a cooled work tool is used to carry out cryodestruction of skin at a temperature $T=-50°C$ for t=120 c, then the work tool temperature changes from $-50°C$ to $+50°C$ for the next 240 s, following which skin coagulation is carried out with the heated work tool at $T=+50°C$ for t=120 s. A subsequent temperature reduction to $T=-50°C$ occurs for 120 s, then this temperature effect is repeated cyclically for a better destruction of the human skin. The indicated cyclic temperature effect on the human skin is shown in Fig.2.

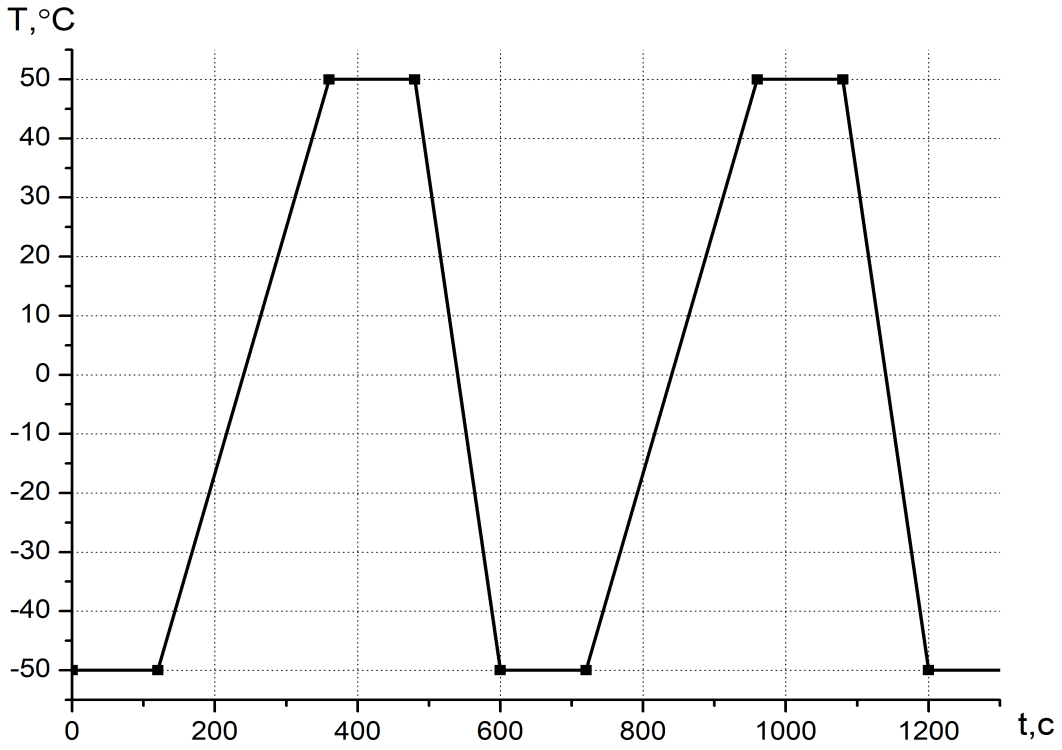

Fig.2. The plot of work tool temperature versus time

Figs. 3-10 show the distributions of temperature and isothermal surfaces in the cross section of biological tissue on the surface of which the work tool is placed, the temperature of which varies according to the above law in the operating temperature range [-50 ÷ +50] ° C at the initial and final moments of cooling-heating cycle.

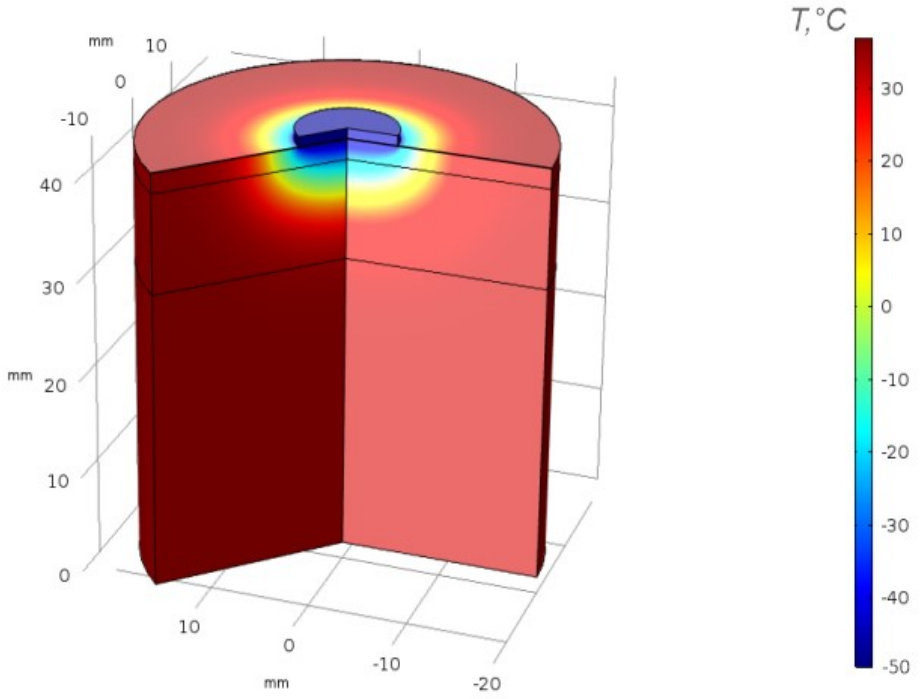

Fig.3. Dostribution of temperature in the bulk of the skin the surface of which accommodates a work tool at a temperature of T=50°C at point of time t=210s

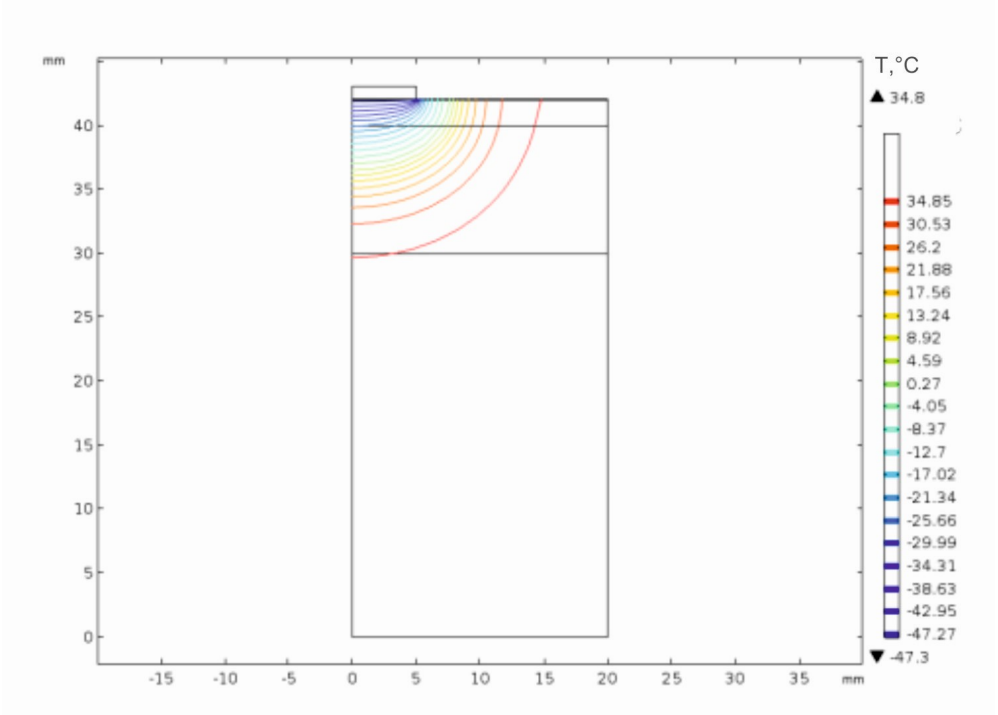

Fig.4. Distribution of isothermal surfaces in the bulk of the skin the surface of which accommodates a work tool at a temperature of T=-50°C at point of time t=120 s

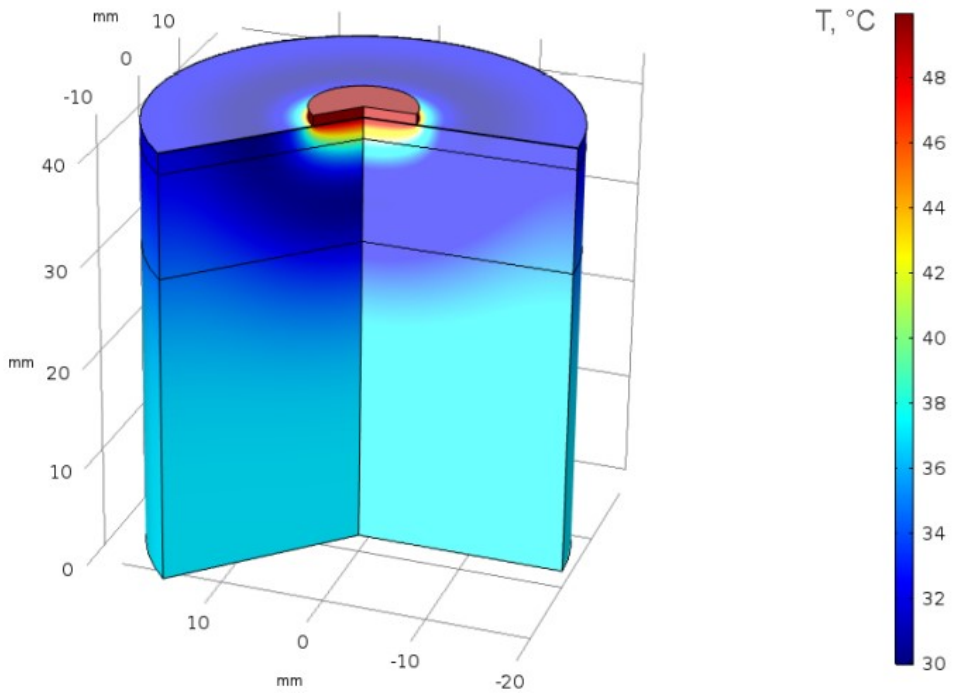

Fig.5. Ditsribution of temperature in the bulk of the skin the surface of which accommodates a work tool at a temperature of T=+50°C at point of time t=480 s

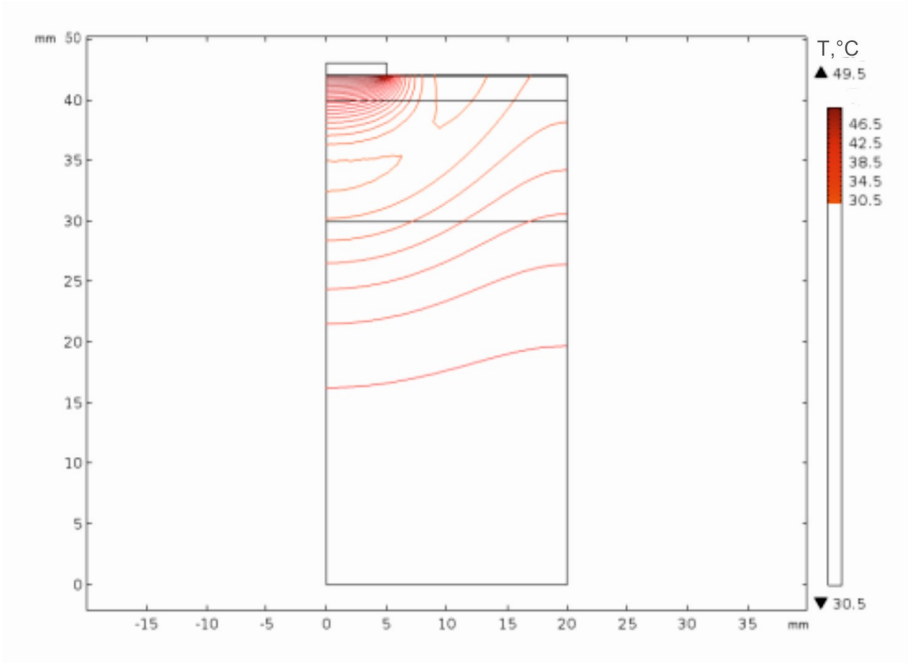

Fig.6. Distribution of isothermal surfaces in the bulk of the skin the surfaces of which accommodates a work tool at a temperature of T=+50°C at point of time t=480 s

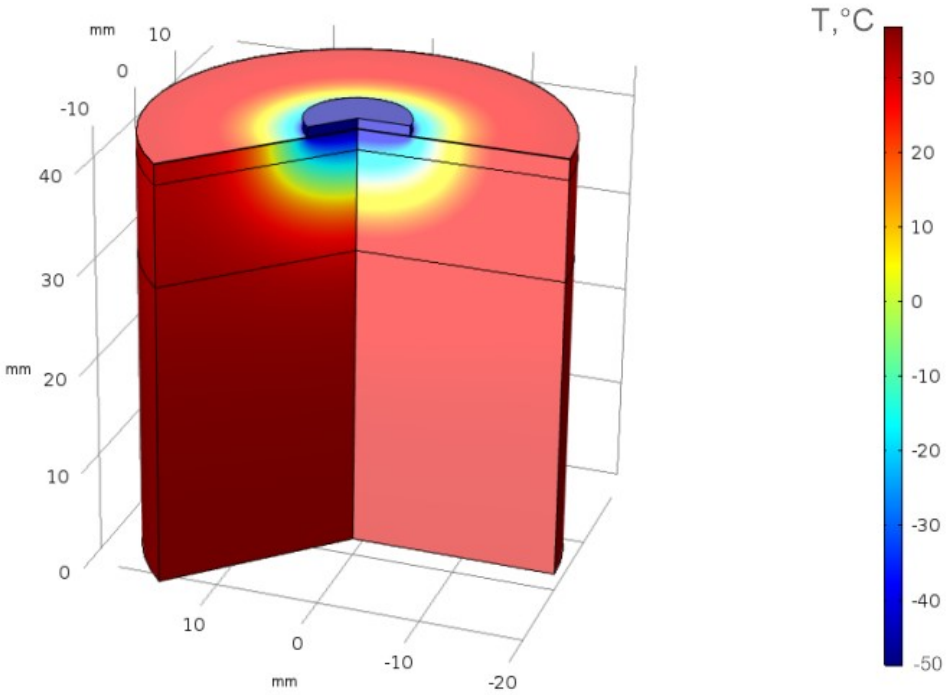

Fig.7. Distribution of temperature in the bulk of the skin the surface of which accomodates a work tool at a temperature of T=-50°C at point of time t=720 s

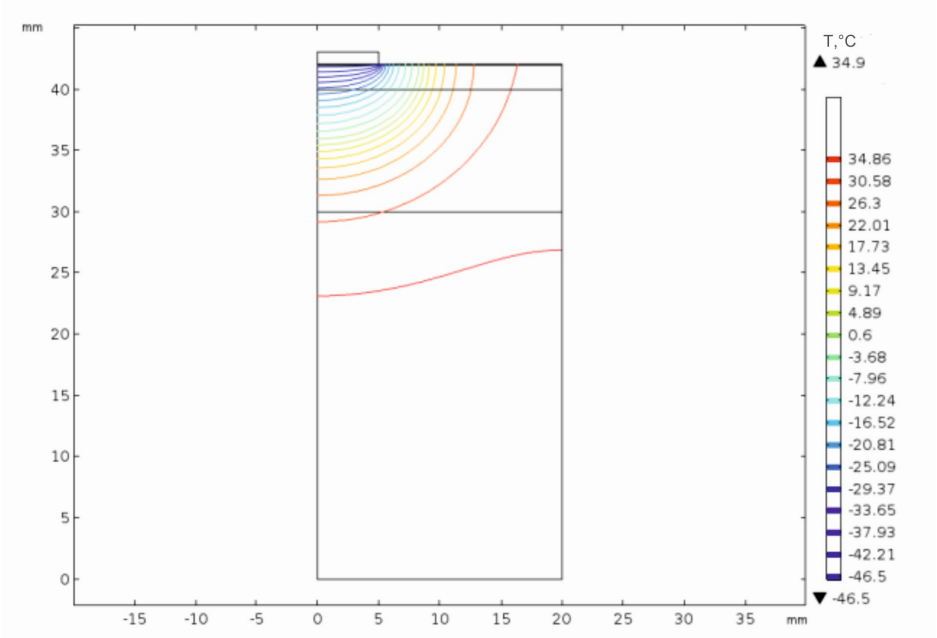

Fig.8. Distribution of isothermal surfaces in the bulk of the skin the surface of which accommodates a work tool at a temperature of T=-50°C at point of time t=720 s

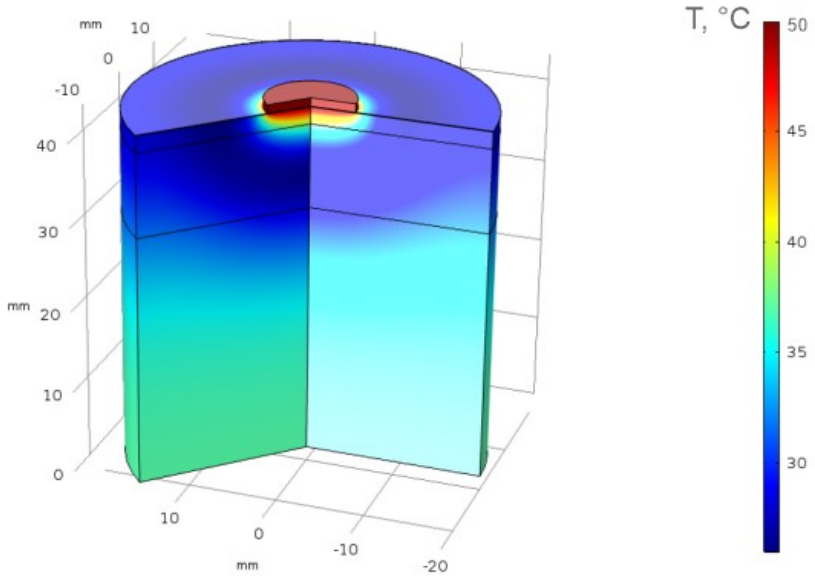

Fig.9. Distribution of temperature in the bulk of the skin the surface of which accommodates a work tool at a temperature of T=+50°C at point of time t=1080 s

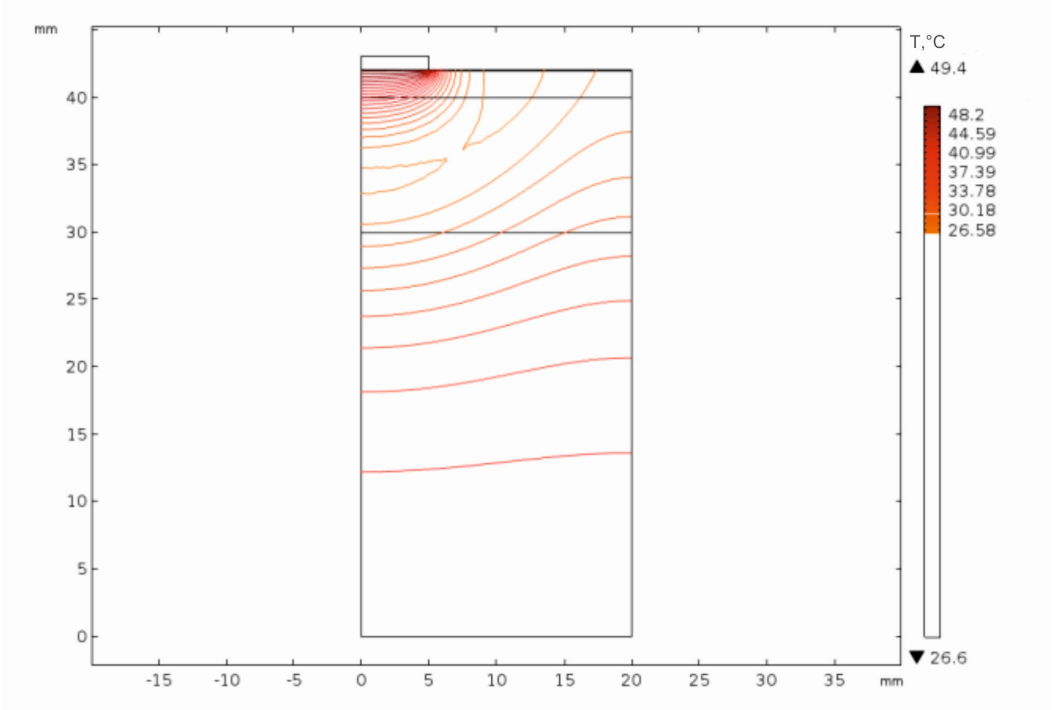

Fig.10. Distribution of isothermal surfaces in the bulk of the skin the surface of which accommodates a work tool at a temperature of T=+50°C at point of time t=1080 s

From Figs. 3-6 it is seen that at *t*=120 s the epidermis is cooled to -48,9°C, the temperature at the epidermis-dermis boundary is -48.3°C, the temperature at the dermis-subcutaneous fat is -25.5°C. And at $t = 480$ s the temperature in the epidermis rises to +49,8°C, at the epidermis-dermis boundary the

temperature is +49.5°C, at the dermis-subcutaneous fat the temperature is +40.3°C. As long as the upper skin layer (epidermis) has the lowest thickness and blood perfusion $\omega_b = 0$, then the temperature inside this layer is close to the work tool temperature. Later, with repeated cyclic temperature exposure (Fig. 7-10), it is observed that at $t = 720$ s after cooling, the temperature inside the skin, for example, at the dermis-subcutaneous fat boundary, reaches -28 ° C, and at $t = 1080$ c after reheating, the temperature at the dermis-subcutaneous fat boundary is + 38 ° C.

It was found that with an increase in the exposure (number of cycles) of temperature effect, a deeper cooling of skin layers and approximately the same heating of the skin are achieved. That is, with a prolonged temperature exposure in the range [-50 ÷ +50] °C one can achieve destruction and coagulation of superficial skin neoplasms.

The results obtained make it possible to predict the depth of freezing and heating of the human skin layers at a given cyclic temperature exposure to achieve the maximum effect during cryodestruction or coagulation. The developed method of computer simulation in a dynamic mode enables one to determine the temperature distribution in different skin layers with a predetermined arbitrary function of changing the work tool temperature with time $T_f(t)$.

Conclusions

1. Computer simulation was used to determine the distributions of temperature in different skin layers in heating and cooling modes with a change of work tool temperature by the predetermined law in the temperature range [-50÷+50]°C. The results obtained give an opportunity to predict the depth of freezing and heating of biological tissue at a given cyclic temperature effect.
2. The method of computer simulation of the distribution of temperature in the human skin is developed, which enables one to predict the results of local temperature effect on the skin and determine at any point of time the distributions of temperature in different skin layers at a predetermined arbitrary temporal function of change in work tool temperature $T_f(t)$.

References

1. Anatychuk L.I. (1979). *Termoelementy i termoelektricheskiie ustroistva: spravochnik [Thermoelements and thermoelectric devices: reference book]*. Kyiv: Naukova dumka [in Rusian].
2. Kolenko E.A. (1967). *Termoelektricheskiie okhlazhdaiushchiiie pribory [Thermoelectric cooling devices]*. 2nd ed. Leningrad: Nauka [in Russian].
3. Anatychuk L.I., Denisenko O.I., Kobylianskyi R.R., Kadeniuk T.Ya., Perepichka M.P.(2017). Suchasni metody krioterapii v dermatologichnii praktytsi [Modern cryotherapy methods in detrmatological practice]. *Klinichna ta Eksperymentalna Patologiia*, XVI, 1(59), 150-156 [in Ukrainian].
4. Denkov V. (1988). On the edge of life. Moscow: Znaniie [Russian transl.]
5. Maruyama S., Nakagawa K., Takeda H. (2008). The flexible cryoprobe using Peltier effect for heat transfer control. *Journal of Biomechanical Science and Engineering*, 138-150.
6. Kochenov V.I. (2000). *Kriokhirurgicheskaia profilakticheskaia onkologiia [Cryosurgical preventive oncology]*. Niznii Novgorod [in Russian].
7. Kochenov V.I. (2003). *Kriologicheskaia profilakticheskaia onkologiia: kratkoie uchebnoie i metodicheskoie posobiie dlia vrachei i studentov [Cryological preventive oncology: a short educational and methodological guide for doctors and students]*. Organization Nizhnii Novgorod Regional Oncological Association of Disabled People (Ed). 2nd revised ed. Nizhnii Novgorod [in

Russian].
8. Kochenov V.I. (1982). Adhesive effect in cryosurgery. *Abstract in the International Abstract Journal*, IV, 8.
9. Moskalyk I.A., Manyk O.M. (2013). On the use of thermoelectric cooling in cryodestruction practice. *J.Thermoelectricity*, 6, 84-92.
10. Anatychuk L.I., Denisenko O.I., Kobylianskyi R.R., Kadenyuk T.Ya. (2015). On the use of thermoelectric cooling in dermatology and cosmetology. *J.Thermoelectricity*, 3, 57-71.
11. Moskalyk I.A. (2015). Pro vykorystannia termoelektrychnykh pryladiv u kriokhirurhii [On the use of thermoelectric devices in cryosurgery]. *Fizyka i khimiia tverdoho tila - Physics and Chemistry of Solid State*, 4, 742-746.
12. Kobylianskyi R.R., Kadenyuk T.Ya. (2016). Pro perspektyvy vykorystannia termoelektryky dlia likuvannia zakhvoriuvan shkiry kholodom [On the prospects of using thermoelectricity for treatment of skin diseases with cold]. *Naukovy visnyk Chernivetskogo universitetu: zbirnyk naukovykh ptrats. Fizyka. Elektronika - Scientific Bulletin of Chernivtsi University: Collection of Scientific Papers. Physics. Electronics,* 5, 1, 67 – 72 [in Ukrainian].
13. Zinkin A.N., Zingilevskaia N.G., Muselian B.B. (1997). *Kriovozdeistvie v otorinolaringologii: metodicheskiie rekomendatsii [Cryotherapy in otorhinolaryngology: guidelines]*. Krasnodar [in Russian].
14. Belous A. M., Bondarenko V.A. (1982). *Strukturnyie izmeneniia biologicheskikh membran pri okhlazhdenii [Structural changes of biological membranes in cooling]*. Kyiv: Naukova dumka [in Russian].
15. Belous A. M., Bondarenko V.A., Babiichuk L.K., et al. (1985). Edinyi mekhanizm povrezhdeniia kletki pri termalnom shoke, zamorazhivanii a postgipertonicheskom lizise [Unified mechanism of cell damage during thermal shock, freezing and posthypertensive lysis]. *Kriobiologiia – Cryobiology*, 2, 25-32 [in Russian].
16. Miller P., Metzner D. (1969). Cryosurgery for tumors of the head and neck. *Trns. Am.Ophthalmol. Otolaringol. Soc*., 73(2), 300-309.
17. D'Hont G. (1974). La cryotherapie en ORL. *Acta. Otorhinolaringol. Belg*., 28(2), 274-278.
18. Mazur P. (1968). Physical-chemical factors underlying cell injury in cryosurgical freezing. In: *Cryosurgery* ed. by R. W. Rand, A. P. Rinfret, H. Leden. Springfield, Illinois, U.S.A.
19. Shafranov V.V., Borkhunova E.N., Kostyliov M.A., et al. (2012). Mekhanizm razrusheniia biologicheskikh tkanei pri lokalnoi kriodestruktsii [Mechanism of desctruction of biological tissues during local cryodesctruction]. *Bulletin of the Russian Academy of Natural Sciences*, 1, 68 – 77 [in Russian].
20. Kandel E.I. (1974). *Kriokhirurgiia [Cryosurgery]*. Moscow: Meditsina [in Russian].
21. Gill W., Fraser I. (1968). A look at cryosurgery. *Scot. Med*, I, 13, 268-273.
22. Derpgolts V.F. (1979). *Mir vody [World of water]*. Leningrad [in Russian].
23. Shafranov V.V., Korotkii N.G. (2000). Vozmozhnosti ispolzovanii metoda CVCh-destruktsii v dermokosmetologii dlia lecheniia keloidnykh rubtsov [Possibilities of using the microwave cryodestruction method in dermocosmetology for the treatment of keloid scars]. *Detskaia khirurgiia - Pediatric Surgery*, 1, 35–37 [in Russian].
24. Van Venrjy G. (1975). Freeze-etching: freezing velocity and crystal size at different size locations in samples. *Cryobiology,* 12(1), 46–61.
25. Bause H. (2004). Kryotherapie lokalisierter klassischer, Neues Verfahren mit Peltier-Elementen (–32°C) Erfahrungsbericht Hamangiome. *Monatsschr Kinderheilkd*. 152:16–22.

26. Ponomarenko G.N. (2002). *Fizioterapiia v kosmetologii [Physiotherapy in cosmetology]*. St.Petersburg: Voienno-Meditsinskaia Akademia [in Russian].
27. Zadorozhnyi B.A. (1985). *Krioterapiia v dermatologii (Biblioteka practicheskogo vracha). [Cryotherapy in dermatology (Library of practicing physician)]*. Kyiv: Zdorovie [in Russian].
28. Anatychuk L.I., Vikhor L.M., Kotsur M.P., Kobylianskyi R.R., Kadenyuk T.Ya. (2016). Optimal control of time dependence of cooling temperature in thermoelectric devices. *J.Thermoelectricity*, 5, 5-11.
29. Anatychuk L.I., Kobylianskyi R.R., Kadenyuk T.Ya. (2017). Computer simulation of local thermal effect on the human skin. *J.Thermoelectricity*, 1, 69-79.
30. Anatychuk L.I., Vikhor L.M., Kobylianskyi R.R., Kadenyuk T.Ya. (2017). Computer simulation and optimization of the dynamic operating modes of thermoelectric device for treatment of skin diseases. *J.Thermoelectricity*, 2, 44-57.
31. Anatychuk L.I., Vikhor L.M., Kobylianskyi R.R., Kadenyuk T.Ya., Zvarich O.V. (2017). Computer simulation and optimization of the dynamic operating modes of thermoelectric reflexotherapy device. *J.Thermoelectricity*, 3, 68-78.
32. Anatychuk L., Vikhor L., Kotsur M., Kobylianskyi R., Kadenyuk T. (2018). Optimal control of time dependence of temperature in thermoelectric devices for medical purposes. *International Journal of Thermophysics* 39:108. https://doi.org/10.1007/s10765-018-2430-z.
33. Anatychuk L.I., Kobylianskyi R.R., Fedoriv R.V. (2019). Method for taking into account the phase transition in biological tissue during computer-aided simulation of cryodestruction process. *J. Thermoelectricity*, 1, 46-58.
34. Anatychuk L.I., Kobylianskyi R.R., Fedoriv R.V. (2019). Computer simulation of human skin cryodestruction process during thermoelectric cooling. *J.Thermoelectricity*, 2, 21-35.
35. Jiang S.C., Ma N., Li H.J., Zhang X.X. (2002). Effects of thermal properties and geometrical dimensions on skin burn injuries. *Burns*, 28, 713-717.
36. Cetingul M.P., Herman C. (2008). Identification of skin lesions from the transient thermal response using infrared imaging technique. *IEEE*, 1219-1222.
37. Ciesielski M., Mochnacki B., Szopa R. (2011). Numerical modeling of biological tissue heating. Admissible thermal dose. *Scientific Research of the Institute of Mathematics and Computer Science*, 1(10), 11-20.
38. Filipoiu Florin, Bogdan Andrei Ioan, Carstea Iulia Maria (2010). Computer-aided analysis of the heat transfer in skin tissue. *Proceedings of the 3-rd WSEAS Int. Conference on Finite Differences - Finite Elements - Finite Volumes - Boundary Elements,* 2010, 53-59.
39. Carstea Daniela, Carstea Ion, Carstea Iulia Maria (2011). Interdisciplinarity in computer-aided analysis of thermal therapies. *WSEAS Transactions on Systems and Control*, 6(4), 115-124.
40. Deng Z.S., Liu J. (2005). Numerical simulation of selective freezing of target biological tissues following injection of solutions with specific thermal properties. *Cryobiology*, 50, 183-192.
41. Lim Han Liang, Gunasekaran Venmathi (2011). *Mathematical modeling of heat distribution during cryosurgery*. https://isn.ucsd.edu/last/courses/beng221/problems/2011/project10.pdf.
42. Shah Vishal N., Orlov Oleg I., Orlov Cinthia, Takebe Manabu, Thomas Matthew, and Plestis Konstadinos (2018). Combined cryo-maze procedure and mitral valve repair through a ministernotomy. *Multimed Man Cardiothorac Surg*. 2018. doi: 10.1510/mmcts.2018.022.
43. Bokeriia L.A., Bokeriia O.L., Kambarov S,Yu., Mota O. R., Zavarina A.Yu., Rubtsov P.P., Mordvinova A.S. (2009). Kriomodifikatsiia operatsii “labirint” v sochetanii s protezirovaniiem mitralnogo klapana, plastikoi trikuspidalnogo klapana i aortokoronarnym shuntirovaniiem

(klinivcheskii sluchai) [Cryomodification of the "labyrinth" operation in combination with mitral valve replacement, tricuspid valve plasty and coronary artery shunting (clinical case)]. *Bulletin of A.N.Bakulev Scientific Centre of Crdiovascular Surgery RAMS*, 5, 65–71.
44. Rykaczewski Konrad (2019). Modeling thermal contact resistance at the finger-object interface. *Temperature*, 6 (1), 85-95.
45. Pennes H.H. (1948)ю Analysis of tissue and arterial blood temperatures in the resting forearm *J. Appl. Physiol.* , 1(2), 93 – 122.
46. *COMSOL Multiphysics User's Guide* (2010).

Submitted 04.05.2020

Анатичук Л.І., *акад. НАН Украини*[1,2]
Кобилянський Р., *канд. физ.-мат. наук*[1,2]
Федорів Р.В.[1,2]

[1]Інститут термоелектрики НАН і МОН України,
вул. Науки, 1, Чернівці, 58029, Україна;
e–mail: anatych@gmail.com
[2]Чернівецький національний університет ім. Юрія Федьковича,
вул. Коцюбинського 2, Чернівці, 58012, Україна

КОМП'ЮТЕРНЕ МОДЕЛЮВАННЯ ЦИКЛІЧНОГО ТЕМПЕРАТУРНОГО ВПЛИВУ НА ШКІРУ ЛЮДИНИ

У роботі наведено результати комп'ютерного моделювання циклічного температурного впливу на шкіру людини у динамічному режимі. Побудовано тривимірну комп'ютерну модель біологічної тканини з врахуванням теплофізичних процесів, кровообігу, теплообміну, процесів метаболізму та фазового переходу. Як приклад, розглянуто випадок, коли на поверхні шкіри знаходиться робочий інструмент, температура якого змінюється циклічно за наперед заданим законом у діапазоні температур [50 ÷ +50] °С. Визначено розподіли температури у різних шарах шкіри людини в режимах охолодження та нагріву. Отримані результати дають можливість прогнозувати глибину промерзання і прогрівання біологічної тканини при заданому температурному впливі. Бібл. 46, рис. 10, табл. 2.

Ключові слова: температурний вплив, шкіра людини, динамічний режим, комп'ютерне моделювання.

Анатычук Л.И., *акад. НАН Украины*[1,2]
Кобылянский Р.Р., *канд. физ.-мат. наук* [1,2]
Федорив Р.В.[1,2]

[1]Институт термоэлектричества НАН и МОН Украины,
ул. Науки, 1, Черновцы, 58029, Украина,
e–mail: anatych@gmail.com;
[2]Черновицкий национальный университет им. Юрия Федьковича,
ул. Коцюбинского, 2, Черновцы, 58012, Украина

КОМПЬЮТЕРНОЕ МОДЕЛИРОВАНИЕ ЦИКЛИЧЕСКИХ ТЕМПЕРАТУРНЫХ ВОЗДЕЙСТВИЙ НА КОЖУ ЧЕЛОВЕКА

В работе приведены результаты компьютерного моделирования циклического температурного воздействия на кожу человека в динамическом режиме. Построено трехмерную компьютерную модель биологической ткани с учетом теплофизических процессов, кровообращения, теплообмена, процессов метаболизма и фазового перехода. В качестве примера, рассмотрен случай, когда на поверхности кожи находится рабочий инструмент, температура которого меняется циклически по заранее заданному закону в диапазоне температур [50 ÷ +50] ° С. Определены распределения температуры в различных слоях кожи человека в режимах охлаждения и нагрева. Полученные результаты дают возможность прогнозировать глубину промерзания и прогревания биологической ткани при заданном температурном воздействии. Библ. 46, рис. 10, табл. 2.

Ключевые слова: температурное воздействие, кожа человека, динамический режим, компьютерное моделирование.

References

1. Anatychuk L.I. (1979). *Termoelementy i termoelektricheskiie ustroistva: spravochnik [Thermoelements and thermoelectric devices: reference book]*. Kyiv: Naukova dumka [in Rusian].
2. Kolenko E.A. (1967). *Termoelektricheskiie okhlazhdaiushchiiie pribory [Thermoelectric cooling devices]*. 2nd ed. Leningrad: Nauka [in Russian].
3. Anatychuk L.I., Denisenko O.I., Kobylianskyi R.R., Kadeniuk T.Ya., Perepichka M.P.(2017). Suchasni metody krioterapii v dermatologichnii praktytsi [Modern cryotherapy methods in detrmatological practice]. *Klinichna ta Eksperymentalna Patologiia*, XVI, 1(59), 150-156 [in Ukrainian].
4. Denkov V. (1988). On the edge of life. Moscow: Znaniie [Russian transl.]
5. Maruyama S., Nakagawa K., Takeda H. (2008). The flexible cryoprobe using Peltier effect for heat transfer control. *Journal of Biomechanical Science and Engineering*, 138-150.
6. Kochenov V.I. (2000). *Kriokhirurgicheskaia profilakticheskaia onkologiia [Cryosurgical preventive oncology]*. Niznii Novgorod [in Russian].
7. Kochenov V.I. (2003). *Kriologicheskaia profilakticheskaia onkologiia: kratkoie uchebnoie i metodicheskoie posobiie dlia vrachei i studentov [Cryological preventive oncology: a short educational and methodological guide for doctors and students]*. Organization Nizhnii Novgorod Regional Oncological Association of Disabled People (Ed). 2nd revised ed. Nizhnii Novgorod [in Russian].
8. Kochenov V.I. (1982). Adhesive effect in cryosurgery. *Abstract in the International Abstract Journal*, IV, 8.
9. Moskalyk I.A., Manyk O.M. (2013). On the use of thermoelectric cooling in cryodestruction

practice. *J.Thermoelectricity*, 6, 84-92.
10. Anatychuk L.I., Denisenko O.I., Kobylianskyi R.R., Kadenyuk T.Ya. (2015). On the use of thermoelectric cooling in dermatology and cosmetology. *J.Thermoelectricity*, 3, 57-71.
11. Moskalyk I.A. (2015). Pro vykorystannia termoelektrychnykh pryladiv u kriokhirurhii [On the use of thermoelectric devices in cryosurgery]. *Fizyka i khimiia tverdoho tila - Physics and Chemistry of Solid State*, 4, 742-746.
12. Kobylianskyi R.R., Kadenyuk T.Ya. (2016). Pro perspektyvy vykorystannia termoelektryky dlia likuvannia zakhvoriuvan shkiry kholodom [On the prospects of using thermoelectricity for treatment of skin diseases with cold]. *Naukovy visnyk Chernivetskogo universitetu: zbirnyk naukovykh ptrats. Fizyka. Elektronika - Scientific Bulletin of Chernivtsi University: Collection of Scientific Papers. Physics. Electronics,* 5, 1, 67 – 72 [in Ukrainian].
13. Zinkin A.N., Zingilevskaia N.G., Muselian B.B. (1997). *Kriovozdeistvie v otorinolaringologii: metodicheskiie rekomendatsii [Cryotherapy in otorhinolaryngology: guidelines]*. Krasnodar [in Russian].
14. Belous A. M., Bondarenko V.A. (1982). *Strukturnyie izmeneniia biologicheskikh membran pri okhlazhdenii [Structural changes of biological membranes in cooling]*. Kyiv: Naukova dumka [in Russian].
15. Belous A. M., Bondarenko V.A., Babiichuk L.K., et al. (1985). Edinyi mekhanizm povrezhdeniia kletki pri termalnom shoke, zamorazhivanii a postgipertonicheskom lizise [Unified mechanism of cell damage during thermal shock, freezing and posthypertensive lysis]. *Kriobiologiia – Cryobiology*, 2, 25-32 [in Russian].
16. Miller P., Metzner D. (1969). Cryosurgery for tumors of the head and neck. *Trns. Am.Ophthalmol. Otolaringol. Soc*., 73(2), 300-309.
17. D'Hont G. (1974). La cryotherapie en ORL. *Acta. Otorhinolaringol. Belg*., 28(2), 274-278.
18. Mazur P. (1968). Physical-chemical factors underlying cell injury in cryosurgical freezing. In: *Cryosurgery* ed. by R. W. Rand, A. P. Rinfret, H. Leden. Springfield, Illinois, U.S.A.
19. Shafranov V.V., Borkhunova E.N., Kostyliov M.A., et al. (2012). Mekhanizm razrusheniia biologicheskikh tkanei pri lokalnoi kriodestruktsii [Mechanism of desctruction of biological tissues during local cryodesctruction]. *Bulletin of the Russian Academy of Natural Sciences*, 1, 68 – 77 [in Russian].
20. Kandel E.I. (1974). *Kriokhirurgiia [Cryosurgery]*. Moscow: Meditsina [in Russian].
21. Gill W., Fraser I. (1968). A look at cryosurgery. *Scot. Med*, I, 13, 268-273.
22. Derpgolts V.F. (1979). *Mir vody [World of water]*. Leningrad [in Russian].
23. Shafranov V.V., Korotkii N.G. (2000). Vozmozhnosti ispolzovanii metoda CVCh-destruktsii v dermokosmetologii dlia lecheniia keloidnykh rubtsov [Possibilities of using the microwave cryodestruction method in dermocosmetology for the treatment of keloid scars]. *Detskaia khirurgiia - Pediatric Surgery*, 1, 35–37 [in Russian].
24. Van Venrjy G. (1975). Freeze-etching: freezing velocity and crystal size at different size locations in samples. *Cryobiology,* 12(1), 46–61.
25. Bause H. (2004). Kryotherapie lokalisierter klassischer, Neues Verfahren mit Peltier-Elementen (–32°C) Erfahrungsbericht Hamangiome. *Monatsschr Kinderheilkd*. 152:16–22.
26. Ponomarenko G.N. (2002). *Fizioterapiia v kosmetologii [Physiotherapy in cosmetology]*. St.Petersburg: Voienno-Meditsinskaia Akademia [in Russian].
27. Zadorozhnyi B.A. (1985). *Krioterapiia v dermatologii (Biblioteka practicheskogo vracha). [Cryotherapy in dermatology (Library of practicing physician)]*. Kyiv: Zdorovie [in Russian].

28. Anatychuk L.I., Vikhor L.M., Kotsur M.P., Kobylianskyi R.R., Kadenyuk T.Ya. (2016). Optimal control of time dependence of cooling temperature in thermoelectric devices. *J.Thermoelectricity*, 5, 5-11.
29. Anatychuk L.I., Kobylianskyi R.R., Kadenyuk T.Ya. (2017). Computer simulation of local thermal effect on the human skin. *J.Thermoelectricity*, 1, 69-79.
30. Anatychuk L.I., Vikhor L.M., Kobylianskyi R.R., Kadenyuk T.Ya. (2017). Computer simulation and optimization of the dynamic operating modes of thermoelectric device for treatment of skin diseases. *J.Thermoelectricity*, 2, 44-57.
31. Anatychuk L.I., Vikhor L.M., Kobylianskyi R.R., Kadenyuk T.Ya., Zvarich O.V. (2017). Computer simulation and optimization of the dynamic operating modes of thermoelectric reflexotherapy device. *J.Thermoelectricity*, 3, 68-78.
32. Anatychuk L., Vikhor L., Kotsur M., Kobylianskyi R., Kadenyuk T. (2018). Optimal control of time dependence of temperature in thermoelectric devices for medical purposes. *International Journal of Thermophysics* 39:108. https://doi.org/10.1007/s10765-018-2430-z.
33. Anatychuk L.I., Kobylianskyi R.R., Fedoriv R.V. (2019). Method for taking into account the phase transition in biological tissue during computer-aided simulation of cryodestruction process. *J. Thermoelectricity*, 1, 46-58.
34. Anatychuk L.I., Kobylianskyi R.R., Fedoriv R.V. (2019). Computer simulation of human skin cryodestruction process during thermoelectric cooling. *J.Thermoelectricity*, 2, 21-35.
35. Jiang S.C., Ma N., Li H.J., Zhang X.X. (2002). Effects of thermal properties and geometrical dimensions on skin burn injuries. *Burns*, 28, 713-717.
36. Cetingul M.P., Herman C. (2008). Identification of skin lesions from the transient thermal response using infrared imaging technique. *IEEE*, 1219-1222.
37. Ciesielski M., Mochnacki B., Szopa R. (2011). Numerical modeling of biological tissue heating. Admissible thermal dose. *Scientific Research of the Institute of Mathematics and Computer Science*, 1(10), 11-20.
38. Filipoiu Florin, Bogdan Andrei Ioan, Carstea Iulia Maria (2010). Computer-aided analysis of the heat transfer in skin tissue. *Proceedings of the 3-rd WSEAS Int. Conference on Finite Differences - Finite Elements - Finite Volumes - Boundary Elements,* 2010, 53-59.
39. Carstea Daniela, Carstea Ion, Carstea Iulia Maria (2011). Interdisciplinarity in computer-aided analysis of thermal therapies. *WSEAS Transactions on Systems and Control*, 6(4), 115-124.
40. Deng Z.S., Liu J. (2005). Numerical simulation of selective freezing of target biological tissues following injection of solutions with specific thermal properties. *Cryobiology*, 50, 183-192.
41. Lim Han Liang, Gunasekaran Venmathi (2011). *Mathematical modeling of heat distribution during cryosurgery*. https://isn.ucsd.edu/last/courses/beng221/problems/2011/project10.pdf.
42. Shah Vishal N., Orlov Oleg I., Orlov Cinthia, Takebe Manabu, Thomas Matthew, and Plestis Konstadinos (2018). Combined cryo-maze procedure and mitral valve repair through a ministernotomy. *Multimed Man Cardiothorac Surg*. 2018. doi: 10.1510/mmcts.2018.022.
43. Bokeriia L.A., Bokeriia O.L., Kambarov S,Yu., Mota O. R., Zavarina A.Yu., Rubtsov P.P., Mordvinova A.S. (2009). Kriomodifikatsiia operatsii “labirint” v sochetanii s protezirovaniiem mitralnogo klapana, plastikoi trikuspidalnogo klapana i aortokoronarnym shuntirovaniiem (klinivcheskii sluchai) [Cryomodification of the "labyrinth" operation in combination with mitral valve replacement, tricuspid valve plasty and coronary artery shunting (clinical case)]. *Bulletin of A.N.Bakulev Scientific Centre of Crdiovascular Surgery RAMS*, 5, 65–71.
44. Rykaczewski Konrad (2019). Modeling thermal contact resistance at the finger-object interface.

Temperature, 6 (1), 85-95.
45. Pennes H.H. (1948)ю Analysis of tissue and arterial blood temperatures in the resting forearm *J. Appl. Physiol.* , 1(2), 93 – 122.
46. *COMSOL Multiphysics User's Guide* (2010).

Submitted 04.05.2020

S.O.Filin

S.O. Filin *doctor of tech. science*

West Pomeranian University of Technology,
Szczecin 17, al.Piastow, Szczecin, 70-310, Poland,
e-mail: sergiy.filin@zut.edu.pl

CALCULATION OF THE COOLING SPEED OF THE THERMOELECTRIC BEVERAGE COOLER WITH "WET" CONTACT

The paper proposes an engineering technique for calculating beverage cooling speed in a thermoelectric cooler with wet and dry contact. By calculation, the previously proven experimentally conclusion was confirmed that filling the gap between the bottle with the drink and the cooler container can significantly increase the speed of the cooler. The results of comparative calculations are presented by the example of an automobile cooler of drinks Car mini-cooler FM 201.001. The ways of improving the design of the cooler in order to increase its speed are proposed. Bibl. 10, Fig. 5, Tab. 3.

Key words: beverage cooler, cooling speed, heat exchange conditions, thermal resistances.

Introduction

This paper is the second part in a series of three works devoted to the development and research of thermoelectric coolers for drinks with wet contact. In the previous paper [1], the market of modern household and automobile thermoelectric beverage coolers was analyzed in terms of their cooling speed. The performance indicators of these devices do not meet the needs of consumers. Based on the results of experimental studies, the efficiency of the use of the so-called "wet" contact to increase the speed of the coolers was shown. Wet contact is the filling of the air gap between the beverage can or bottle and the cooler container with water or other liquid. The theoretical analysis below allows one to determine the main factors influencing the mentioned efficiency. Another goal of this work is to develop a method for calculating the cooling time of a drink in coolers with wet contact and to compare the results of calculations using the example of data from previous experiments.

Calculation model

Initial data and assumptions

1. As in experiment [1], we take water as a cooled drink which is a liquid with the highest heat capacity. This approach eliminates speculations associated with inaccuracy in determining the thermophysical properties of specific drinks.
2. Similarly, as a container for a drink, we take an aluminum can with a capacity of 0.33 liters. Its parameters are standardized and unified in most countries of the world [4].
3. The parameters of the cooler, including the thermoelectric module, are tied to the actual technical characteristics of coolers of the *Car mini-cooler FM 201.001* type used in the experiment (Fig. 1).

Fig. 1. Car beverage cooler Car mini-cooler ФМ 201.001 (left),
separately to the right - its container with a thermoelectric module installed on it.

4. The bottom of the container in the cooler Car mini-cooler FM 201.001 is made as a separate element of non-metallic material, and the bottom of the can is concave. There is a linear direct contact between the can and the bottom along the circumference of the convex part of the bottom. Therefore, when calculating a dry contact cooler, we assume that the bottom surface does not participate in heat exchange between the container and the beverage can.
5. Due to its smallness, we neglect the thermal resistance of the can. However, in the case of a plastic bottle, this component of the total thermal resistance must be considered.
6. We assume that the space between the container and the cooler body is filled with polyurethane foam insulation (Fig. 2).

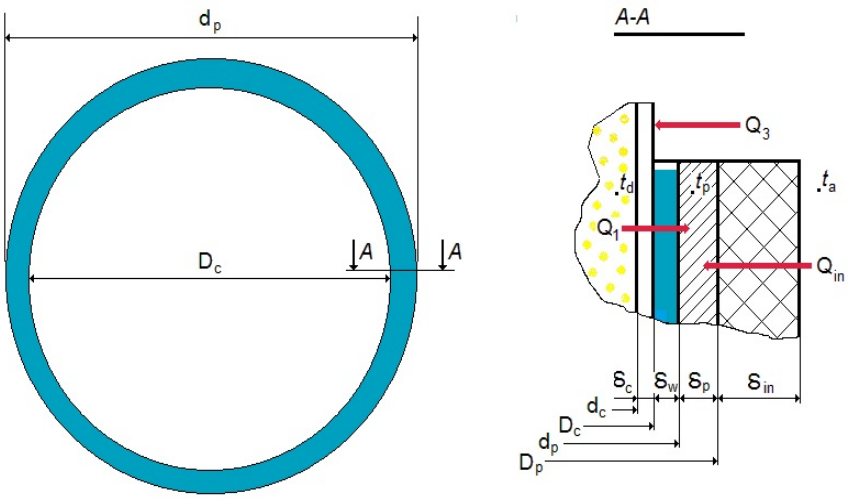

Fig.2. Calculation scheme of beverage cooler.

Table 1

Initial data for the calculation

Parameter	Value	Source	Comment
Cooler capacity			
Material		Manufacturers' data	Aluminum Manganese alloy Al-Mn
Thermal conductivity, λ_p	188 W/m·K	[2]	
Specific mass heat capacity, c_p	985 J/kg K	[2]	
Mass (without bottom part), m_p	113.850 g		Measured
Height, h_p	69 mm		Measured
Inner diameter, d_p	67 mm		Measured
Thickness, δ_p	2 mm		Measured
Water in container			
Thermal conductivity, λ_w	0.55 W/m·K	[3]	At a temperature of 10°C
Specific mass heat capacity, c_w	4200 J/kg·K	[3]	At a temperature of 10°C
Total mass, m_w	15.0 g		Measured
Including mass of water mass in a cylindrical gap, m_{w1}	7.1 g		Calculated
Height, h_w	68 mm		1 mm less than h_p
Layer thickness, δ_w	0.5 mm		$(d_p - D_c)/2$
Beverage can			
Material		[4]	Aluminum alloy АМг2
Thermal conductivity, λ_c	159 W/m·K	[5]	
Specific mass heat capacity, c_c	963 J/kg·K	[5]	
Mass, m_c	13.280 g		Measured
Outer diameter, D_c	66 mm	[4]	
Height, h_c	115.2 mm	[4]	
Thickness, δ_c	0.11...0.30 mm	[4]	0.11 – in the cylindrical part 0.30 – in the lower part
Beverage (water)			
Thermal conductivity, λ_d	0.574 W/m·K	[3]	At a temperature of 15°C[1]
Specific mass heat capacity, c_d	4190 J/kg·K	[3]	At a temperature of 15°C
Mass, m_d	332.0 g		Measured
Insulation			
Material			Foamed polyurethane
Thermal conductivity, λ_{in}	0.029 W/m·K	[6]	
Specific heat capacity, c_{in}	1.47	[6]	
Density, σ_{in}	40 kg/m^3	[6],[7]	
Thickness, δ_{in}	6.5 mm		Measured

[1] Taken as the average temperature of the beverage in the process of cooling.

Calculation of theoretically minimum cooling time

The minimum time τ_{min} for cooling a beverage in a can to a temperature t_f (under ideal conditions of heat exchange at the boundaries of media) can be found from the heat balance of the cold side of the cooler:

$$\left(\bar{Q}_0 - \bar{Q}_2 - \bar{Q}_3 - \bar{Q}_{in}\right)\cdot\tau_{\min} = \bar{Q}_d + \bar{Q}_c + \bar{Q}_w + \bar{Q}_p + \bar{Q}_{in} \quad (1)$$

$$\left(\bar{Q}_0 - \bar{Q}_2 - \bar{Q}_3 - \bar{Q}_{in}\right)\cdot\tau_{\min} =$$

$$= m_d c_d \cdot\left(t_a - t_f\right) + \left(m_w c_w + m_c c_c + m_p c_p\right)\cdot\left(t_a - t_p\right) + \left(m_{in} c_{in}\right)\cdot\frac{t_a - t_p}{2} \quad (2)$$

where: $\bar{Q}_0$ is average cooling capacity of thermoelectric module during cooling; $\bar{Q}_2$ is average heat input from the environment through the bottom of the can, $\bar{Q}_3$ is average power of heat input from the environment to the upper part of the can, not immersed in the container, $\bar{Q}_{in}$ is average power of heat input from the environment through the insulation, Q_d, Q_c, Q_w, Q_p, Q_{in} is the amount of heat removed from the drink, can, water in the gap, container and insulation, respectively, m is mass, c is heat capacity, t_a is air temperature in the room and the initial temperature of all the elements, t_f is finish temperature of the beverage, t_p is average temperature of the cooler at the end of cooling process.

The only unknown value in Eq.(2) is temperature t_p. One can calculate it from the thermal balance of the gap or use the experimental data. Putting into calculation the values $t_a = 25$ °C, $t_f = 10$ °C, $t_p = 8.2$ °C and substituting data from Table 1, we obtain:

Table 2

Intermediate results of calculating thermal balance components

Object	Designation	$m_i c_i$ [J/K]	Q_i, [J]	Percentage
Beverage	$m_d c_d$, Q_d	1382.7	20740.5	87.44%
Can	$m_c c_c$, Q_c	11.95	200.76	0.85%
Water in the gap	$m_w c_w$, Q_w	62.85	1055.88	4.45%
Container	$m_p c_p$, Q_p	102.46	1721.3	7.26%
Insulation	$m_{in} c_{in}$, Q_{in}	0.013	0.1065	0.0005%
Sum	**Σ**	**1560**	**23718.6**	**100%**

It follows from the presented data that, in terms of mass heat capacity, the presence of water in the gap increases the thermal load on the module by less than 5%. The influence of the can (0.85%) is within the experimental error, and therefore, may not be taken into account in engineering calculations, similarly to the effect of insulation, which is absolutely negligible. The role of thermal resistances of the same elements is analyzed below. A similar conclusion in relation to insulation can be made when analyzing the structure of heat inputs. In [9], [10] it was shown that the isolation of the ice form of thermoelectric ice

cube ice makers does not increase the ice maker productivity, because the lion's share of the heat load is the process of the water-ice phase transition. Despite the fact that in our example we are not talking about freezing a beverage, the contribution of heat inputs from the environment is also not vital. Both in the case of ice makers and in coolers, i.e. in the products where the dynamic characteristics are decisive, the thermal resistance of the layers of materials between the cooled object and the source of cold has a greater influence than the mass heat capacity. This thesis is confirmed by the experimental data and further calculations.

Algorithm for calculating the average cooling capacity of the module $\bar{Q}_0$

To be able to use the module manufacturers' data given in Table 3 and in Fig. 3, it is worthwhile to:

1) interpolate the values Q_{omax} and ΔT_{max} between the two temperatures of the hot side of the cooler (the manufacturer provides data for temperatures 27 and 50 °C) for the temperature t_h of the hot heat sink in the steady state, which was measured during the experiment, i.e. for t_h = 32 °C;

2) determine the value of relative current I/I_{max}. In our case it is 2.15/3.4 = 0.63;

3) build dependence Q_{omax} (ΔT_{max}) for this ratio and the above temperature t_h;

4) using the above assumptions, calculate $\Delta T = t_h - t_p$ and graphically determine $\bar{Q}_0$ as shown in Fig. 4.

Another possible option is calculation of $\bar{Q}_0$ by the formula proposed in [8].

Table 3

Technical parameters of module MT-1-1.45-143S

Parameters	**Unit**	**MT 1-1.45-143S**
Current, max	A	3.4
Voltage, max	V	16.6
Coolling Pover, max, (at Th=27°C)	W	33
Temp. Difference, max, (at T_h=27°C in vacuum)	K	70
Resistance (at T_h=27°C amb)	Ohm	4.56 ± 10 %
Width	mm	40+0.5/-0.1
Length	mm	40+0.5/-0.1
Thickness	mm	3.8
Thickness tolerance	mm	±0.3
Parallel Difference	mm	0.05
Wire Length	mm	120+10
Wire Section	mm^2	0.035
Operating temperature, max	°C	90

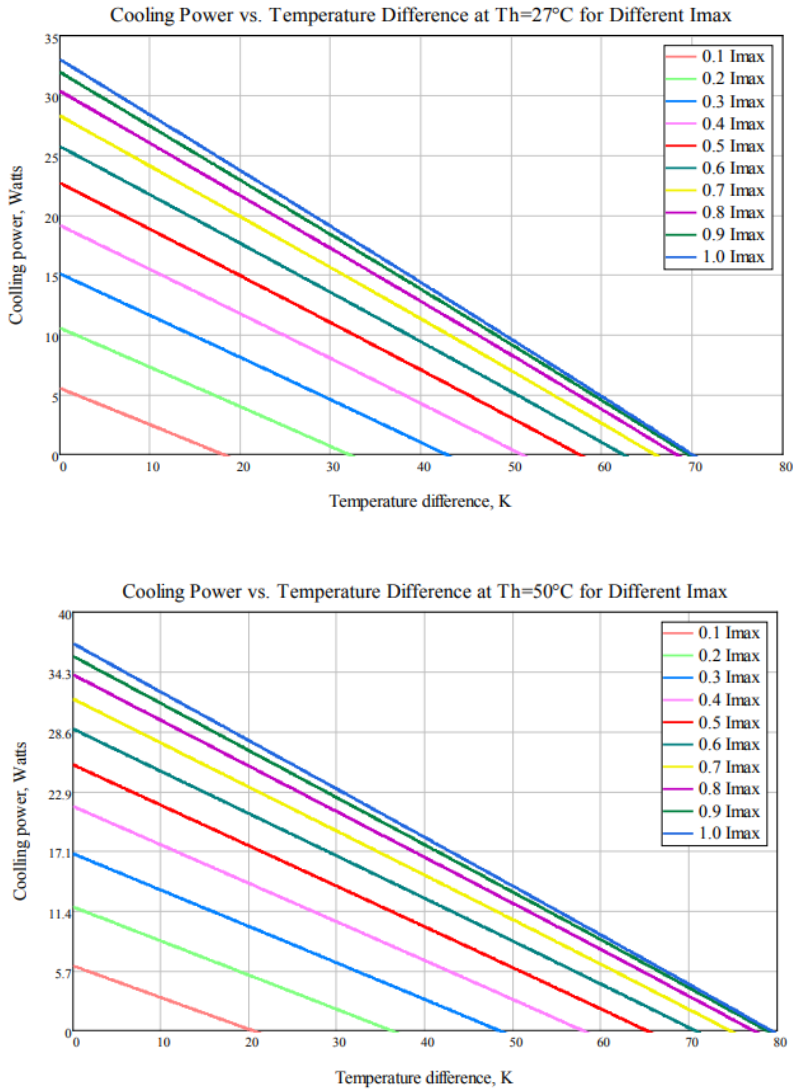

Fig.3. Load characteristics of module MT-1-1.45-143S.

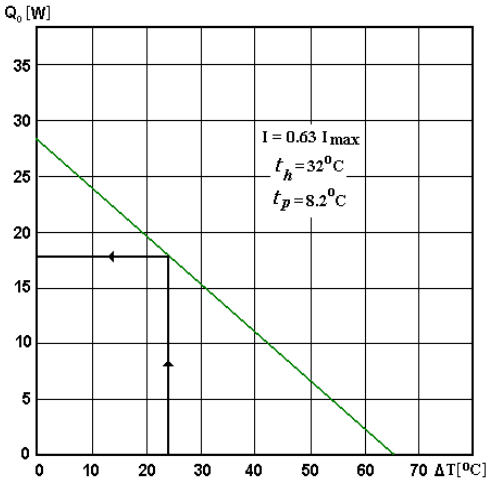

Fig. 4. Graphical method for determining the cooling capacity of the MT-1-1.45-143S module under steady state operation on the manufacturers' database (Fig. 3).

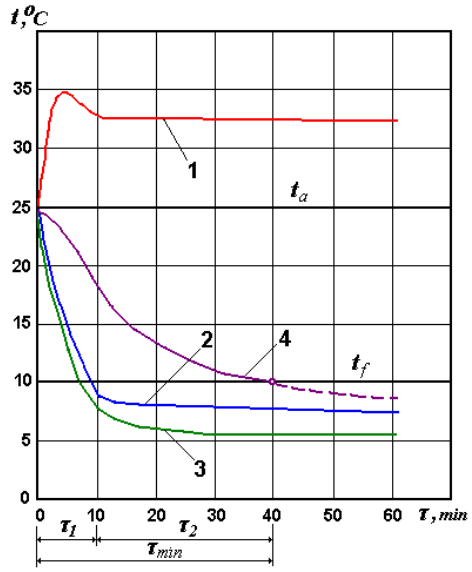

Fig.5. Typical dynamics of temperature change on the cold and hot side of module of thermoelectric cooler at ambient temperature t_a = 25°C:
1 – hot heat sink temperature t_h, 2 – container temperature at wet contact t_{pw},
3 – container temperature at dry contact t_{pd}, 4 – average beverage temperature t_d.

Due to the variability of temperatures on both sides of the thermoelectric module, the value $\bar{Q}_0$ is also not constant. Its relative stabilization occurs approximately 10 minutes after the cooler is turned on (Fig. 5). Therefore, in order to increase the calculation accuracy, one can separately determine the values of Q_{01}, and Q_{02} for two time intervals τ_1 и τ_2 and then use the formula (3)

$$\bar{Q}_0 = \frac{Q_{01} \cdot \tau_1 + Q_{02} \cdot (\tau_{\min} - \tau_1)}{\tau_{\min}} \quad , \tag{3}$$

where τ_1 = 10 minutes.

On substituting (3) into (2) we find τ_{min}.

$$\tau_{\min} = (\frac{\sum Q_i - 10 \cdot 60 \cdot Q_{01}}{Q_{02}}) + 10 \cdot 60 = 1244.9s = 20m48s \quad , \tag{4}$$

where Q_{01} = 20.4 W, Q_{02} = 17.8 W.

The calculation of values $\bar{Q}_2$, $\bar{Q}_3$, $\bar{Q}_{in}$ by the known dependences for heat transfer through a multi-layer wall and for natural convection in air (with regard to the data in Table 4) yielded the following results: $\bar{Q}_2$ = 0.027 W, $\bar{Q}_3$ = 0.063 W, $\bar{Q}_{in}$ = 0.019 W. The sum of these three heat inputs (0.109 W) is as little as 0.6% of the average cooling capacity of module, which makes it possible to ignore them in the engineering calculations.

Actual time of beverage cooling from 25 °C to 10 °C is a factor of 2.5 longer (Table 5), which is due to thermal resistances of layers δ_c , δ_w and δ_p (Fig.2).

Calculation of cooling time with regard to thermal resistances of layers

To take into account the influence of the thermal resistance of the media layers located in the gap between the beverage and the cold source (module), it is necessary to use the thermal balance of the cooled object in a regular thermal mode [3,11]:

$$\sum(m_i c_i)\cdot d(\Delta t_1) = k_\Sigma \cdot F \cdot \Delta t_f \cdot d(\tau) \tag{5}$$

Solving Eq.(5) for τ, we obtain:

$$\tau = \frac{\sum m_i c_i}{k_\Sigma F} \ln \frac{t_a - t_p}{t_f - t_p} \quad , \tag{6}$$

where:

$$k_\Sigma = \frac{1}{\frac{1}{\alpha_d} + \frac{\delta_w}{\lambda_w} + \frac{\delta_p^*}{\lambda_p}} \quad . \tag{7}$$

In relation (6), we separately take into account the heat exchange through the container bottom made of rigid plastic (λ_b = 0.2 W/mK). In relation (7), in the calculation of the container thermal resistance δ_p^*/λ_p, we use the reduced thickness δ^*_p, calculated by formula (8):

$$\delta_p^* = \frac{F_1\delta_1 + (F - F_1)\delta_2}{F} \quad , \tag{8}$$

where: $F_1 = h_p a_m$, $F = \pi d_p h_p$, $\delta_1 = \delta_p + 5\ mm$ (see Fig.1), $\delta_2 = ½(½\pi d_p - a_m/2)$.

Substituting the data from Table 1 and assuming the coefficient of heat transfer from water to the can wall α_d = 140 W/m^{2}K [12,13], we obtain δ^*_p = 36 mm, k_Σ = 122.1 W/m^{2}K.

Conclusions

A laboratory for remote monitoring and control of the heat generation unit operation has been developed. The established laboratory provides an opportunity to study the methods of backup power management due to electricity generated by an array of solar panels located outside the room with the heat generation unit and thermoelectric elements mounted thereupon. **The scientific novelty** of the results obtained lies in the fact that the methods of combining various processes of energy generation from one source and methods of emergency power supply for the control elements of this process have been further developed. **The practical significance** of the results obtained is that the created lab allows holding experiments with different cases of regular stopping of heat generation process in case of unstable or missing power supply for control units. **Prospects for further research** are to develop methods of regular shutdown of the heat generation unit in conditions, when the elements of control and monitoring of the unit are not provided with regular power supply.

The work was supported by the grant of State Fundamental Research Foundation according to contract Ф83-111/2018.

References

1. Deasy, M.J., et al. (2018). Electricity generation from a biomass cookstove with MPPT power

management and passive liquid cooling. *Energy for Sustainable Development*, 43, 162–172, doi:10.1016/j.esd.2018.01.004.
2. Gopi, Nikhil Pattath, and Subhakar Devendran (2015). Autonomy considerations for a standalone photovoltaic system. *Sustainable Energy Technologies and Assessments*, 10, 79–83., doi:10.1016/j.seta.2015.03.005.
3. Eldesoukey, Ayman, and Hamdy Hassan (2019). 3D model of thermoelectric generator (TEG) case study: effect of flow regime on the TEG performance. *Energy Conversion and Management*, 180, 231–239, doi:10.1016/j.enconman.2018.10.104.
4. Yang, Haoqi, et al. (2018). Optimization of thermoelectric generator (TEG) integrated with three-way catalytic converter (TWC) for harvesting engine's exhaust waste heat. *Applied Thermal Engineering*, 144, 628–638, doi:10.1016/j.applthermaleng.2018.07.091.
5. Kütt, Lauri, et al. (2018). Thermoelectric applications for energy harvesting in domestic applications and micro-production units. Part I: Thermoelectric concepts, domestic boilers and biomass stoves. *Renewable and Sustainable Energy Reviews*, 98, 519–544, doi:10.1016/j.rser.2017.03.051.
6. Sornek, Krzysztof, et al. (2019). Comparative analysis of selected thermoelectric generators operating with wood-fired stove. *Energy*, 166, 1303–1313., doi:10.1016/j.energy.2018.10.140.
7. Nuwayhid, Rida Y., et al. (2005). Development and testing of a domestic woodstove thermoelectric generator with natural convection cooling. *Energy Conversion and Management*, 46(9-10), 1631–1643, doi:10.1016/j.enconman.2004.07.006.
8. Zhao, Yulong, et al. (2018). Performance analysis of automobile exhaust thermoelectric generator system with media fluid, *Energy Conversion and Management,* 171, 427–437, doi:10.1016/j.enconman.2018.06.006
9. Champier, Daniel. (2017).Thermoelectric generators: a review of applications. *Energy Conversion and Management,* 140, 167–181, doi:10.1016/j.enconman.2017.02.070.
10. Price-Allison, A., et al. (2019). Emissions performance of high moisture wood fuels burned in a residential stove. *Fuel*, 239, 1038–1045, doi:10.1016/j.fuel.201810.1016/j.fuel.2018.11.090.

Submitted 13.05.2020

Філін С.О. *доктор техн. наук*

Західнопоморський технологічний університет в Щецині
алея Піаст, 17, Щецін, 70-310, Польща,
e-mail: sergiy.filin@zut.edu.pl

РОЗРАХУНОК ШВИДКОДІЇ ТЕРМОЕЛЕКТРИЧНОГО ОХОЛОДЖУВАЧА НАПОЇВ З «МОКРИМИ» КОНТАКТОМ

У статті запропоновано інженерну методику розрахунку швидкості охолодження напою в термоелектричному охолоджувачі з мокрим і сухим контактом. Розрахунковим шляхом був підтверджений раніше доведений експериментально висновок про те, що заповнення щілини між пляшкою з напоєм і ємністю охолоджувача дозволяє істотно підвищити швидкодію охолоджувача. Представлено результати порівняльних розрахунків на прикладі автомобільного

охолоджувача напоїв Car mini-cooler FM 201.001. Запропоновано шляхи удосконалення конструкції охолоджувача з метою підвищення його швидкодії. Бібл. 10, рис. 5, табл. 3.
Ключові слова: охолоджувач напоїв, швидкість охолодження, умови теплообміну, теплові опори.

Филин С.О. *доктор техн. наук*

Западнопоморский технологический университет в Щецине
аллея Пиастов, 17, Щецин, 70-310, Польша,
e-mail: sergiy.filin@zut.edu.pl

РАСЧЁТ БЫСТРОДЕЙСТВИЯ ТЕРМОЭЛЕКТРИЧЕСКОГО ОХЛАДИТЕЛЯ НАПИТКОВ С «МОКРЫМ» КОНТАКТОМ

В статье предложнена инженерная методика рассчёта скорости охлаждения напитка в термоэлектрическом охладителе с «мокрым» и «сухим» контактами. Расчётным путём был подтверждён ранее доказанный экспериментально вывод о том, что заполнение щели между бутылкой с напитком и ёмкостью охладителя позволяет существенно повысить быстродействие охладителя. Представлены результаты сравнительных расчётов на примере автомобильного охладителя напитков Car mini-cooler ФМ 201.001. Предложены пути усовершенствования конструкции охладителя с целью повышения его быстродействия. Библ. 10, рис. 5, табл. 3.
Ключевые слова: охладитель напитков, скорость охлаждения, условия теплообмена, тепловые сопротивления.

References

1. Deasy, M.J., et al. (2018). Electricity generation from a biomass cookstove with MPPT power management and passive liquid cooling. *Energy for Sustainable Development*, 43, 162–172, doi:10.1016/j.esd.2018.01.004.
2. Gopi, Nikhil Pattath, and Subhakar Devendran (2015). Autonomy considerations for a standalone photovoltaic system. *Sustainable Energy Technologies and Assessments*, 10, 79–83., doi:10.1016/j.seta.2015.03.005.
3. Eldesoukey, Ayman, and Hamdy Hassan (2019). 3D model of thermoelectric generator (TEG) case study: effect of flow regime on the TEG performance. *Energy Conversion and Management*, 180, 231–239, doi:10.1016/j.enconman.2018.10.104.
4. Yang, Haoqi, et al. (2018). Optimization of thermoelectric generator (TEG) integrated with three-way catalytic converter (TWC) for harvesting engine's exhaust waste heat. *Applied Thermal Engineering*, 144, 628–638, doi:10.1016/j.applthermaleng.2018.07.091.
5. Kütt, Lauri, et al. (2018). Thermoelectric applications for energy harvesting in domestic applications and micro-production units. Part I: Thermoelectric concepts, domestic boilers and biomass stoves. *Renewable and Sustainable Energy Reviews*, 98, 519–544, doi:10.1016/j.rser.2017.03.051.
6. Sornek, Krzysztof, et al. (2019). Comparative analysis of selected thermoelectric generators operating with wood-fired stove. *Energy*, 166, 1303–1313., doi:10.1016/j.energy.2018.10.140.

7. Nuwayhid, Rida Y., et al. (2005). Development and testing of a domestic woodstove thermoelectric generator with natural convection cooling. *Energy Conversion and Management*, 46(9-10), 1631–1643, doi:10.1016/j.enconman.2004.07.006.
8. Zhao, Yulong, et al. (2018). Performance analysis of automobile exhaust thermoelectric generator system with media fluid, *Energy Conversion and Management,* 171, 427–437, doi: 10.1016/j.enconman.2018.06.006
9. Champier, Daniel. (2017).Thermoelectric generators: a review of applications. *Energy Conversion and Management,* 140, 167–181, doi:10.1016/j.enconman.2017.02.070.
10. Price-Allison, A., et al. (2019). Emissions performance of high moisture wood fuels burned in a residential stove. *Fuel*, 239, 1038–1045, doi:10.1016/j.fuel.201810.1016/j.fuel.2018.11.090.

Submitted 13.05.2020

V.M.Grabov, *doct. phys.– math. sciences, professor*,
E.V. Demidov, *cand. phys.– math. sciences,*
V.A.Komarov, *cand. phys.– math. sciences, docent*, **A.V. Suslov,**
V.A.Gerega, D.D.Yefimov

The Herzen State Pedagogical University,
48 Moyka Embankment, St-Petersburg, 191186, Russia

THERMOELECTRIC PROPERTIES OF THIN FILMS OF BISMUTH AND BISMUTH-ANTIMONY SOLID SOLUTION

The temperature dependences of the resistivity and thermoEMF were investigated by the method that excludes the occurrence of external strain in the film-substrate system, and the thermoelectric power factor was calculated in the temperature range of 77 to 300K for bismuth-antimony solid solution films on substrates with different thermal expansion coefficients. It has been found that to get the maximum thermoEMF, the ratio of the crystallite size and film thickness is critically important, which is due to the different confinement of electrons and holes mobility by the surface and crystallite boundaries. The maximum thermoEMF and power factor correspond to thick block films of $Bi_{0.88}Sb_{0.12}$ on mica.The research was supported by the Ministry of Education of the Russian Federation as part of a state assignment (project No. FSZN-2020-0026). Bibl. 19, Fig. 7, Tabl. 1.

Key words: bismuth, bismuth-antimony, thermoEMF, size effect, power factor

Introduction

The bismuth-antimony solid solution is known as the most effective low-temperature (temperatures below 200 K) thermoelectric material. At the same time, works of recent years show the possibility of using quantum and classical size effects in electronic phenomena, as well as internal strains to increase the thermoelectric figure of merit of materials [1 – 5].

The thermoelectric figure of merit (Z) in low-dimensional structures and nanostructures in comparison with homogeneous bulk materials can increase both due to an increase in the power factor (P), due to the peculiarities of the densities of states in the vicinity of the bottom of the lower dimensional quantization subband [5, 6] and due to a decrease in thermal conductivity due to the scattering of phonons at the interfaces [7]. Another mechanism for changing the thermoelectric power can be a change in the ratio of the contribution of electrons and holes to the thermoEMF due to different restriction of their mobilities by the surface and crystallite boundaries in a thin film [8, 9].

Straintronics offers another possibility in the task of increasing the thermoelectric figure of merit [10]. Straintronics (from the English “strain” - tension) is a new scientific direction of condensed matter physics, using physical effects in solids caused by strains arising in micro- and nanolayers and heterostructures under the action of external control fields, leading to changes in the band structure, electric, magnetic, optical and other properties of materials [11]. The possibilities of straintronics become obvious if we pay attention to the fact that some theoretical calculations and some experimental results show that the use of high pressures can significantly increase the ZT of some

materials [12]. However, this approach is not widely used due to the technological complexity of creating high pressures in finished devices. It is deformation that can be an analogue of high pressures, which, in the case of thin-film materials, can be easily created in several ways, in particular, by using substrates with different lattice parameters and coefficients of thermal expansion, deposition of films on bent substrates or their controlled bending directly during operation, and much more. In low-dimensional structures located on substrates, it is possible to create record elastic strains, for example, vitrified bismuth wires of submicron size withstand relative elongations of 2-3% [13]. This is equivalent to the value of elastic strains in bulk crystals corresponding to mechanical stress up to 1 GPa, which approximately corresponds to the values used in the study of bulk crystals of this type. At present, active research in the field of straintronics is just beginning.

Within the framework of this work, the possibilities of increasing the thermoelectric figure of merit of thin films of bismuth and bismuth-antimony solid solution are experimentally investigated using the above approaches.

Experimental procedure

Bismuth films with a thickness of 10 nm to 1 μm and bismuth-antimony films with an antimony concentration from 3 to 15 at. % Sb were investigated. Plates of monocrystalline mica (muscovite) and a polyamide film were used as substrates. The coefficient of linear thermal expansion (CLTE) of these materials is 8×10^{-6} K^{-1} and $45*10^{-6}$ K^{-1}, respectively. The CLTE of bismuth in the trigonal plane is 10.5×10^{-6} K^{-1}. Thus, mica substrates cause in-plane tensile strain, while polyimide substrates cause in-plane compression strain of the film at temperatures below the film formation temperature.

Various methods were used to obtain films with different structural perfection. The main method for the preparation of thin-film samples was thermal deposition in high vacuum (10^{-5} Torr). In this case, for the films of the bismuth-antimony solid solution, the method of discrete evaporation was used, which makes it possible to obtain a homogeneous distribution of the solid solution components throughout the volume. Using this method, under optimal production conditions [14], it is possible to obtain films with crystallite size more than an order of magnitude larger than the film thickness (for bismuth) and several times larger than the film thickness (for bismuth – antimony solid solution). To obtain films with a single crystal structure, the method of zone recrystallization of a film under a protective coating was used [8]. In order to obtain films with block sizes of the order of the film thickness, we used a technique based on growing a film in a high vacuum on preformed nanoclusters [15]. The structure of the films was monitored by atomic force microscopy and X-ray structural analysis. All films were oriented in the (111) plane parallel to the substrate plane.

On the obtained films, the temperature dependences of the thermoEMF and resistivity were investigated in the temperature range of 77 to 300 K at a stepwise temperature change with temperature stabilization at the measurement point. To measure the thermoEMF, we used a technique that excludes distortion by the installation components of natural strain in the film – substrate system, presented in [16].

Experimental results and their discussion

As indicated in the introduction, in bismuth films, the crystallite boundaries and the surface restrict the mobility of electrons and holes in different ways, which leads to significant changes in the value of the Hall coefficient depending on the ratio between the thickness and crystallite size. The

mobility of electrons is to a greater extent restricted by the surface at low temperatures and the mobility of holes – by crystallite boundaries. In order to study the influence of the above phenomenon on the thermoEMF, which, like the Hall effect, is a difference effect, bismuth films on mica with significant differences in crystallite size have been investigated. We studied films with crystallite size of the order of the film thickness (No. 1,4 in Figs. 1 and 2), obtained using bismuth nanoclusters in accordance with the method developed in [15], films with crystallite size more than an order of magnitude larger than their thickness (No. 2,5 in Figs. 1 and 2), obtained by thermal evaporation in high vacuum under optimal conditions [14] with subsequent annealing, and single-crystal films obtained by zone recrystallization (No. 3,6 in Figs. 1 and 2) [8].

Figs. 1 and 2 show the temperature dependences of the thermoEMF and resistivity of bismuth films with a thickness of 300 nm (No. 1, 2, 3) and 1000 nm (No. 4, 5, 6). It can be seen from the presented dependences that for films of the same thickness, with a decrease in the crystallite size, the absolute value of the thermoEMF increases at low temperatures, which, as in the case of the Hall effect, is due to the greater restriction of the hole mobility by the crystallite boundaries in comparison with the electron mobility. For film No. 4, the absolute value of the thermoEMF at 77 K exceeds the analogous value for bulk bismuth (α_{11} = -45 μV / K). In this case, the effect of crystallites on the mobility of charge carriers for films obtained using bismuth nanoclusters can vary significantly from sample to sample, which can be seen from a comparison of the resistivity of these films at low temperatures: for a film 1000 nm thick, the resistivity at 77 K is almost 2 times higher in comparison with a film with a thickness of 300 nm, obtained in a similar way (Fig. 2).

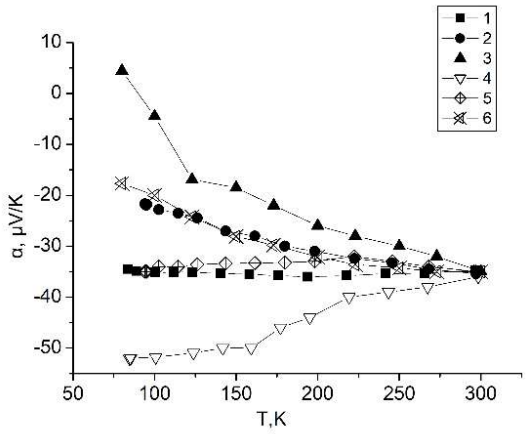

Fig.1 . Temperature dependence of thermoEMF for bismuth films on mica substrate

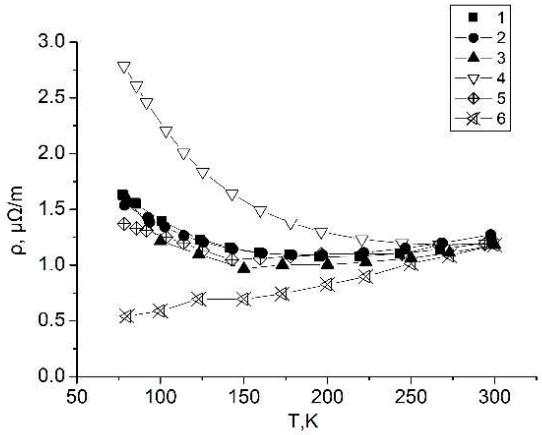

Fig. 2 Temperature dependence of resistivity for bismuth films on mica substrate

In [1, 2], it was theoretically shown for the first time that the quantization of the energy of charge carriers in thin films and wires can lead to an increase in the thermoEMF and a significant increase in *ZT*. A significant thermoEMF increase in thin films due to the quantum size effect should occur at thicknesses h commensurate with the de Broglie wavelength of charge carriers $= 2\pi h/\sqrt{2E_F m^*}$. In bismuth single crystals, charge carriers have a sufficiently large λ value, which in the direction of the C_3 axis is 67 nm for electrons and 11 nm for holes at a temperature of 77 K. In this work, an attempt is made to experimentally discover the influence of the quantum size effect on the thermoelectric properties of thin films of bismuth on mica.

Figure 3 shows the temperature dependences of the thermoEMF of bismuth films with a thickness of 10 nm to 1 μm, obtained by thermal spraying under optimal conditions [14] with annealing. It can be seen from the presented dependences that at low temperatures for films with a thickness of 1 μm to 27 nm, the absolute value of the negative thermoEMF decreases with decreasing film thickness, and for the thin film itself, the thermoEMF at low temperatures goes into the positive region. In this case, due to the peculiarities of the formation of thin-film structures, with a decrease in film thickness, an increase in the ratio between crystallite size and the thickness of the film (*D/h*) occurs. As indicated above, in this case, with a decrease in the film thickness, the electron mobility is more significantly restricted with respect to the hole mobility, which leads to a decrease in the contribution of electrons to the thermoEMF and a decrease in its absolute value for thinner films. However, for films with a thickness of less than 27 nm at low temperatures, an increase in the absolute value of the thermoEMF begins (inset in Fig. 3), while the dependence on the thickness *D/h* remains the same as for films with a greater thickness; therefore, the change in the character of the thickness dependence of the thermoEMF for films thickness less than 27 nm cannot be due to various restrictions of the mobility of electrons and holes by the surface and boundaries of crystallites. Probably, an increase in the absolute value of the thermoEMF with a decrease in the thickness of the bismuth films is associated with a change in the electronic energy spectrum due to the quantum size effect.

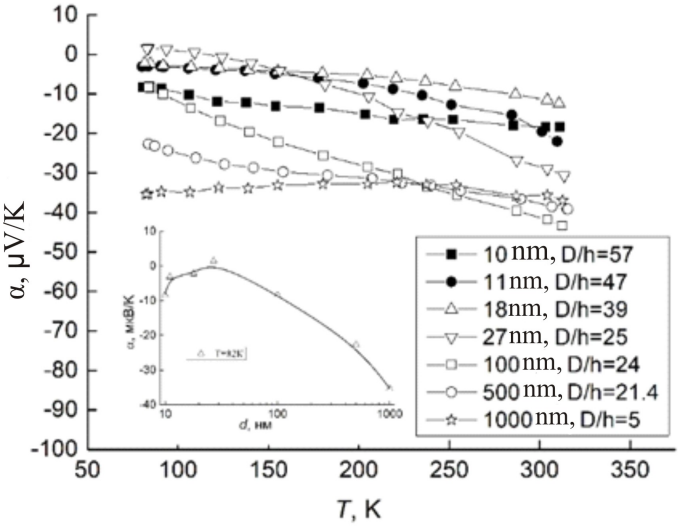

Fig. 3. Temperature dependences of thermoEMF of bismuth films of thickness from 10 nm to 1 μm. D/h is the ratio of crystallite size to film thickness

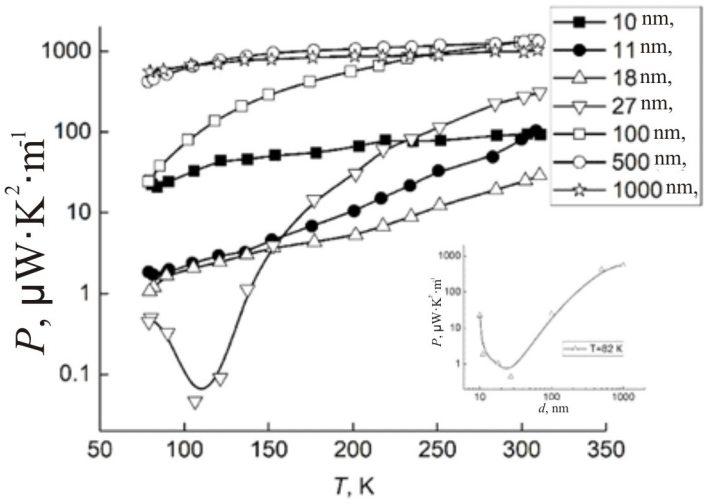

Fig. 4. Temperature dependences of thermoelectric power factor of bismuth films of thickness from 10 nm to 1 μm. D/h is the ratio of crystallite size to film thickness

For bismuth-antimony films this effect was not found, apparently, due to the lower efficiency of annealing in the task of increasing the crystallite size (Table 1) for thin films of bismuth-antimony solid solution and, as a result, smaller values of the coherence length of charge carriers as compared to films of pure bismuth, the large values of which are critical for observing coherent phenomena [17].

Using the measured temperature dependences of resistivity and thermoEMF for the studied films, the thermoelectric power factor P was calculated (Fig. 4). The highest value of thermoelectric power for all temperatures is observed for films with a thickness of 500-1000 nm. However, its thickness dependence is non-monotonic at low temperatures. For films less than 27 nm thick, the power factor begins to grow with a decrease in the film thickness, which, like an increase in the absolute value of the thermoEMF, is caused by a change in the band structure of the films due to the manifestation of quantum coherence of charge carriers.

In order to experimentally study the possibility of using internal mechanical stresses to improve the thermoelectric properties of thin films of the bismuth-antimony system, in this work, the thermoelectric properties of thin films of a bismuth-antimony solid solution on substrates with different thermal expansion coefficients: polyimide and mica (muscovite) are investigated. Under the influence of the difference in thermal expansion of the film and substrate materials, bismuth films on polyimide are in a state of in-plane compression, and bismuth films on mica, in a state of in-plane tension at a temperature below the film formation temperature. When analyzing the results, we used the values of the average crystallite size of the films of the bismuth-antimony system obtained by the methods developed in [18, 19] and presented in Table.

An increase in the concentration of antimony in the film is accompanied by an increase in the absolute value of the thermoEMF at low temperatures, which reflects a change in the thermoEMF in single crystals with a change in their composition (Fig. 5 and Fig. 6). A decrease in the film thickness in films of a bismuth-antimony solid solution leads to a decrease in the thermoEMF in absolute value in the low-temperature region, while a decrease in the crystallite size leads to an increase in its absolute value, in complete analogy with pure bismuth films.

The effect of film strain, due to the difference in the thermal expansion of the film and substrate materials, leads to a different type of the temperature dependences of the thermoEMF in bismuth-antimony films on mica and polyimide substrates.

Table

Crystallite size of bismuth and bismuth-antimony solid solution films, μm.

Substrate material	Thickness, μm / Compo-sition, at.% Sb	1	0.5	0.5
Mica	0	5.4	10.7	3.6
	3	6.8	5.6	4.3
	5	8.2	1.8	3.2
	8	2.2	3.5	–
	12	3.8	3.2	2
	15	2.7	–	1.6
Polyimide	0	2.0	1.4	1.3
	3	1.0	0.8	0.6
	5	–	–	0.9
	8	1.2	0.7	–
	12	1.1	0.7	–
	15	1.0	–	–

The use of films on substrates with a high thermal expansion leads to a decrease in the absolute value of the thermoEMF, especially in the low-temperature region. The maximum values of the thermoEMF and power factor correspond to $Bi_{0.88}Sb_{0.12}$ films on mica and polyimide (Fig. 6, 7).

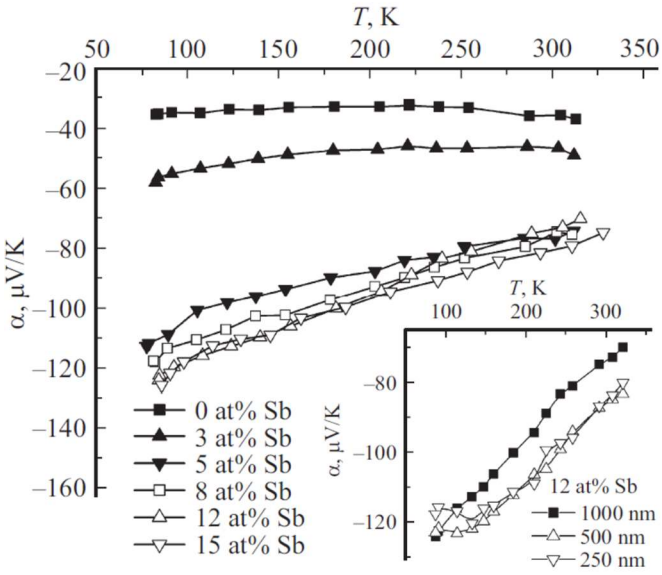

Fig. 5 ThermoEMF of films 1000 nm thick of different composition on mica. On the inset — thermoEMF of $Bi_{0.88}Sb_{0.12}$ films of different thicknesses.

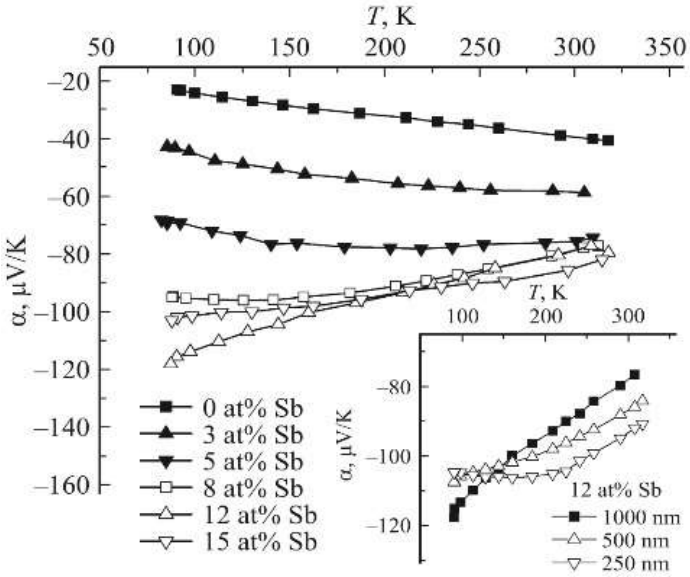

Fig. 6. ThermoEMF of films 1000 nm thick of different composition on polyimide. On the inset — thermoEMF of $Bi_{0.88}Sb_{0.12}$ films of different thicknesses.

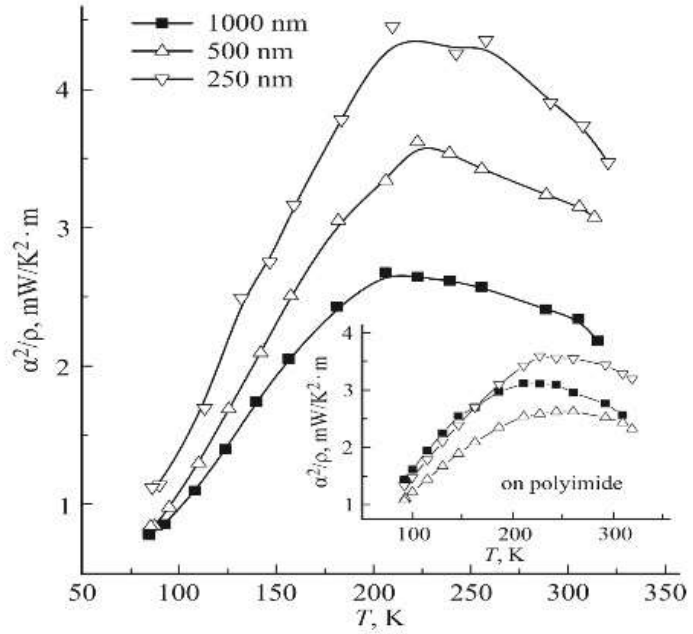

Fig. 7. Power factor of $Bi_{0.88}Sb_{0.12}$ films of different thicknesses on mica.
On the inset — power factor of $Bi_{0.88}Sb_{0.12}$ films of different thicknesses on polyimide.

Conclusions

It has been established that the use of films on substrates with a high thermal expansion leads to a decrease in the thermoEMF, especially in the low-temperature region. The maximum thermoEMF and power factor correspond to thick block films of $Bi_{0.88}Sb_{0.12}$ on mica. In these films, the maximum power factor of 4 * mW / K^{2}m was obtained at temperatures of 200-250 K. The study of ultrathin monocrystalline bismuth-antimony films with an achievable minimum defectiveness and a high surface perfection, which provides a long coherence length of charge carriers with a predominance of specular reflection from the film surfaces, seems to be promising for achieving high values of thermoelectric power. However, the technology for creating such films has not been developed yet.

References

1. Hicks L.D., Dresselhaus M.S. (1993). Effect of quantum-well structures on the thermoelectric figure of merit. *Phys. Rev. B*, 47, 12727.
2. Dresselhaus M.S., Dresselhaus G., Sun X., Zhang Z., Cronin S. B., Koga T. (1999). Low-dimensional thermoelectric materials. *Phys. Solid State,* 41, 679.
3. Nikolaeva A.A., Konopko L.A., Gitsu D.V., Huber T.E., Para G.I., Tsurkan A. (2008). Influence of magnetic field, elastic tension and dimensions on the thermoelectric properties of bismuth

4. Dmitriev A.V., Zviagin I.P. (2010). Sovremennyie tendentsii razvitiia fiziki termoelektricheskikh materialov [Modern development trends of thermoelectric materials]. *Uspekhi Fizicheskikh Nauk-Advances in Physical Sciences*, 180(8), 821–838 [in Russian].
5. Ovsyannikov S.V., Shchennikov V.V., Vorontsov G.V., Manakov A.Y., Likhacheva A.Y., Kulbachinskii V.A. (2008). Giant improvement of thermoelectric power factor of Bi_2Te_3 under

pressure. *J.Applied Physics*, 104, 053713.

6. Demidov E.V., Grabov V.M., Komarov V.A., Suslov A.V., Suslov M.V. (2017). The method of measuring the thermoelectric power in the thin films of the semimetals and narrow-gap semiconductors formed on the thin substrates. *Journal of Physics: Conference Series*, 857, 012006.
7. Grabov V.M., Demidov E.V., Ivanova E.K., Komarov V.A., Kablukova N.S., Krushelnitskiy A.N., Staritsyn M.V. (2017). Influence of annealing at a higher than solidus temperature on the structure

8. Grabov V.M., Komarov V.A., Demidov E.V., Khristich E.E. (2011). The occurrence of the classic size effect in single crystal bismuth films. *Moldavian Journal of the Physical Sciences*, 10(1), 87-95.
9. Grabov V.M., Demidov E.V., Komarov V.A. (2011). Ogranicheniie podvizhnosti nositelei zariada v plionkakh vismuta, obuslovlennoie ikh blochnoi strukturoi [Restriction of charge carrier mobility in bismuth films due to their block structure]. *Poverkhnost', sinkhrotronnyie i neitronnyie issledovaniia – J.Surf.Invest.:X-Ray, Synchrotron Neutron Techn*., 2, 81-85 [in Russian].
10. Kusagaya K., Hagino H., Tanaka S. Miyazaki, K., Takashiri M. (2015).Structural and thermoelectric properties of nanocrystalline bismuth telluride thin films under compressive and tensile strain. *J. Electronic Materials*, 44(6), 1632.
11. Bukharaieva A.A., Zvezdin A.K., Piatakov A.P., Fetisov Yu.K. (2018). Streintronika – novoie napravleniie mikro- i nanoelektroniki i nauki o materialakh [Straintronics – a new direction of micro- and nanoelectronics and materials science]. *Uspekhi Fizicheskikh Nauk- Advances in Physical Sciences*, 188, 1288-1330 [in Russian].
12. Ovsyannikov S.V., Shchennikov V.V., Vorontsov G.V., Manakov A.Y., Likhacheva A.Y., Kulbachinskii V.A. (2008). Giant improvement of thermoelectric power factor of Bi2Te3 under pressure. *J.Applied Physics*, 104, 053713.
13. Nikolaeva A., Huber T., Konopko L., Tsurkan A. Features of Lifshits electron topological transitions induced by anisotropic deformation in thin wires of doped bismuth. // J. Low Temp. Phys. - № 159. - 2010. - P. 258.
14. Grabov V.M., Demidov E.V., Komarov V.A. (2010). Optimizatsiia rezhimov termicheskogo osazhdeniia v vakuume plionok vismuta pri kontrole ikh defektnosti metodom atomno-silovoi mikroskopii [Optimization of thermal deposition in vacuum of bismuth films while monitoring their defectiveness by atomic force microscopy]. *Fizika Tverdogo Tela- Solid State Physics*, 52(6), 1219 – 1222 [in Russian].
15. Grabov V.M., Demidov E.V., Komarov V.A., Kiseleva N.I. (2011). Thermoelectric properties of bismuth films having nanoblock structure. *J.Thermoelectricity*, 4, 73-79.
16. Demidov E.V., Grabov V.M., Komarov V.A., Suslov A.V., Suslov M.V. (2017). The method of measuring the thermoelectric power in the thin films of the semimetals and narrow-gap semiconductors formed on the thin substrates. *Journal of Physics: Conference Series*, 857, 012006.
17. Demidov E.V., Grabov V.M., Komarov V.A., Krushelnitskiy A.N., Suslov A.V., Suslov M.V. (2019). Osobennosti proiavleniia kvantovo-razmernogo effekta v yavleniiakh perenosa v tonkikh plionkah vismuta na podlozhkakh iz sliudy [Peculiarities of quantum size effect manifestation in transport phenomena in bismuth thin films on mica substrates]. *Fizika i Teknika Poluprovodnikov – Semiconductors*, 53(6), 736-740 [in Russian].

18. Grabov V.M., Demidov E.V., Komarov V.A., Klimantov M.M. (2009). Atomno-silovaia mikroskopiia dekorirovannykh oksidirovaniiem defektov plionok vismuta [Atomic-force microscopy of bismuth films decorated with oxidation of defects]. *Fizika Tverdogo Tela - Physics of the Solid State*, 51(4), 800-802 [in Russian].
19. Grabov V.M., Demidov E.V., Komarov V.A. (2008). Atomno-silovaia mikroskopiia plionok vismuta [Atomic-force microscopy of bismuth films]. *Fizika Tverdogo Tela – Physics of the Solid State*, 50(7), 1312-1316 [in Russian].

18.05.2020

В.М. Грабов, *докт. фіз-мат. наук, професор,*
Є.В. Демидов, *канд. фіз-мат. наук,*
В.А. Комаров, *канд. фіз-мат. наук, доцент,* **А.В. Суслов,**
В.А. Герега, Д.Д. Єфімов

Російський державний педагогічний університет ім. А. І. Герцена,
наб. р. Мойки, Санкт-Петербург, 191186, Росія

ТЕРМОЕЛЕКТРИЧНІ ВЛАСТИВОСТІ ТОНКИХ ПЛІВОК ВІСМУТУ І ТВЕРДОГО РОЗЧИНУ ВІСМУТ-СУРМА

Методом, що виключає виникнення зовнішніх деформаційних впливів на систему плівка-підкладка, були досліджені температурні залежності питомого опору і термоЕРС, розрахований фактор термоелектричної потужності в інтервалі температур 77-300К для плівок твердого розчину вісмут-сурма на підкладках з різним коефіцієнтом температурного розширення. Встановлено, що для отримання максимальної термоЕРС критично важливим є співвідношення розміру кристалітів і товщини плівки, що обумовлено різним обмеженням рухливостей електронів і дірок поверхнею і межами кристалітів. Максимальне значення термоЕРС і фактора потужності відповідає товстим блоковим плівкам $Bi_{0.88}Sb_{0.12}$ на слюді. Робота виконана в рамках державного завдання за фінансової підтримки Міносвіти Росії (проект № FSZN-2020-0026). Бібл. 19, Рис. 7, Табл. 1.
Ключові слова: вісмут, вісмут-сурма, термо, розмірний ефект, фактор потужності

В.М. Грабов, *докт. физ-мат. наук, професор,*
Е.В. Демидов, *канд. физ-мат. наук*
В.А. Комаров, *канд. фіз-мат. наук, доцент*, **А.В. Суслов,**
В.А. Герега, Д.Д. Ефимов

Российский государственный педагогический университет им. А. И. Герцена,
наб. р. Мойки, Санкт-Петербург, 191186, Россия

ТЕРМОЭЛЕКТРИЧЕСКИЕ СВОЙСТВА ТОНКИХ ПЛЕНОК ВИСМУТА И ТВЕРДОГО РАСТВОРА ВИСМУТ-СУРЬМА

Методом, исключающим возникновение внешних деформационных воздействий на систему пленка−подложка, были исследованы температурные зависимости удельного сопротивления и термоэдс, рассчитан фактор термоэлектрической мощности в интервале температур 77-300К для пленок твердого раствора висмут-сурьма на подложках с различным коэффициентом температурного расширения. Установлено, что для получения максимальной термоэдс критически важным является соотношения размера кристаллитов и толщины пленки, что обусловлено различным ограничением подвижностей электронов и дырок поверхностью и границами кристаллитов. Максимальное значение термоэдс и фактора мощности соответствует толстым блочным пленкам $Bi_{0.88}Sb_{0.12}$ на слюде.
Работа выполнена в рамках государственного задания при финансовой поддержке Минпросвещения России (проект № FSZN-2020-0026). Библ. 19, Рис. 7, Табл. 1.
Ключевые слова: висмут, висмут-сурьма, термоэдс, размерный эффект, фактор мощности

References

1. Hicks L.D., Dresselhaus M.S. (1993). Effect of quantum-well structures on the thermoelectric figure of merit. *Phys. Rev. B*, 47, 12727.
2. Dresselhaus M.S., Dresselhaus G., Sun X., Zhang Z., Cronin S. B., Koga T. (1999). Low-dimensional thermoelectric materials. *Phys. Solid State,* 41, 679.
3. Nikolaeva A.A., Konopko L.A., Gitsu D.V., Huber T.E., Para G.I., Tsurkan A. (2008). Influence of magnetic field, elastic tension and dimensions on the thermoelectric properties of bismuth
4. Dmitriev A.V., Zviagin I.P. (2010). Sovremennyie tendentsii razvitiia fiziki termoelektricheskikh materialov [Modern development trends of thermoelectric materials]. *Uspekhi Fizicheskikh Nauk-Advances in Physical Sciences*, 180(8), 821–838 [in Russian].
5. Ovsyannikov S.V., Shchennikov V.V., Vorontsov G.V., Manakov A.Y., Likhacheva A.Y., Kulbachinskii V.A. (2008). Giant improvement of thermoelectric power factor of Bi_2Te_3 under pressure. *J.Applied Physics*, 104, 053713.
6. Demidov E.V., Grabov V.M., Komarov V.A., Suslov A.V., Suslov M.V. (2017). The method of measuring the thermoelectric power in the thin films of the semimetals and narrow-gap semiconductors formed on the thin substrates. *Journal of Physics: Conference Series*, 857, 012006.
7. Grabov V.M., Demidov E.V., Ivanova E.K., Komarov V.A., Kablukova N.S., Krushelnitskiy A.N., Staritsyn M.V. (2017). Influence of annealing at a higher than solidus temperature on the structure
8. Grabov V.M., Komarov V.A., Demidov E.V., Khristich E.E. (2011). The occurrence of the classic size effect in single crystal bismuth films. *Moldavian Journal of the Physical Sciences*, 10(1), 87-95.
9. Grabov V.M., Demidov E.V., Komarov V.A. (2011). Ogranicheniie podvizhnosti nositelei zariada v plionkakh vismuta, obuslovlennoie ikh blochnoi strukturoi [Restriction of charge carrier mobility in bismuth films due to their block structure]. *Poverkhnost', sinkhrotronnyie i neitronnyie issledovaniia – J.Surf.Invest.:X-Ray, Synchrotron Neutron Techn*., 2, 81-85 [in Russian].

10. Kusagaya K., Hagino H., Tanaka S. Miyazaki, K., Takashiri M. (2015).Structural and thermoelectric properties of nanocrystalline bismuth telluride thin films under compressive and tensile strain. *J. Electronic Materials*, 44(6), 1632.
11. Bukharaieva A.A., Zvezdin A.K., Piatakov A.P., Fetisov Yu.K. (2018). Streintronika – novoie napravleniie mikro- i nanoelektroniki i nauki o materialakh [Straintronics – a new direction of micro- and nanoelectronics and materials science]. *Uspekhi Fizicheskikh Nauk- Advances in Physical Sciences*, 188, 1288-1330 [in Russian].
12. Ovsyannikov S.V., Shchennikov V.V., Vorontsov G.V., Manakov A.Y., Likhacheva A.Y., Kulbachinskii V.A. (2008). Giant improvement of thermoelectric power factor of Bi2Te3 under pressure. *J.Applied Physics*, 104, 053713.
13. Nikolaeva A., Huber T., Konopko L., Tsurkan A. Features of Lifshits electron topological transitions induced by anisotropic deformation in thin wires of doped bismuth. // J. Low Temp. Phys. - № 159. - 2010. - P. 258.
14. Grabov V.M., Demidov E.V., Komarov V.A. (2010). Optimizatsiia rezhimov termicheskogo osazhdeniia v vakuume plionok vismuta pri kontrole ikh defektnosti metodom atomno-silovoi mikroskopii [Optimization of thermal deposition in vacuum of bismuth films while monitoring their defectiveness by atomic force microscopy]. *Fizika Tverdogo Tela- Solid State Physics*, 52(6), 1219 – 1222 [in Russian].
15. Grabov V.M., Demidov E.V., Komarov V.A., Kiseleva N.I. (2011). Thermoelectric properties of bismuth films having nanoblock structure. *J.Thermoelectricity*, 4, 73-79.
16. Demidov E.V., Grabov V.M., Komarov V.A., Suslov A.V., Suslov M.V. (2017). The method of measuring the thermoelectric power in the thin films of the semimetals and narrow-gap semiconductors formed on the thin substrates. *Journal of Physics: Conference Series*, 857, 012006.
17. Demidov E.V., Grabov V.M., Komarov V.A., Krushelnitskiy A.N., Suslov A.V., Suslov M.V. (2019). Osobennosti proiavleniia kvantovo-razmernogo effekta v yavleniiakh perenosa v tonkikh plionkah vismuta na podlozhkakh iz sliudy [Peculiarities of quantum size effect manifestation in transport phenomena in bismuth thin films on mica substrates]. *Fizika i Teknika Poluprovodnikov – Semiconductors*, 53(6), 736-740 [in Russian].
18. Grabov V.M., Demidov E.V., Komarov V.A., Klimantov M.M. (2009). Atomno-silovaia mikroskopiia dekorirovannykh oksidirovaniiem defektov plionok vismuta [Atomic-force microscopy of bismuth films decorated with oxidation of defects]. *Fizika Tverdogo Tela - Physics of the Solid State*, 51(4), 800-802 [in Russian].
19. Grabov V.M., Demidov E.V., Komarov V.A. (2008). Atomno-silovaia mikroskopiia plionok vismuta [Atomic-force microscopy of bismuth films]. *Fizika Tverdogo Tela – Physics of the Solid State*, 50(7), 1312-1316 [in Russian].

18.05.2020

ARTICLE SUBMISSION GUIDELINES

For publication in a specialized journal, scientific works are accepted that have never been printed before. The article should be written on an actual topic, contain the results of an in-depth scientific study, the novelty and justification of scientific conclusions for the purpose of the article (the task in view).

The materials published in the journal are subject to internal and external review which is carried out by members of the editorial board and international editorial board of the journal or experts of the relevant field. Reviewing is done on the basis of confidentiality. In the event of a negative review or substantial remarks, the article may be rejected or returned to the author(s) for revision. In the case when the author(s) disagrees with the opinion of the reviewer, an additional independent review may be done by the editorial board. After the author makes changes in accordance with the comments of the reviewer, the article is signed to print.

The editorial board has the right to refuse to publish manuscripts containing previously published data, as well as materials that do not fit the profile of the journal or materials of research pursued in violation of ethical norms (for instance, conflicts between authors or between authors and organization, plagiarism, etc.). The editorial board of the journal reserves the right to edit and reduce the manuscripts without violating the author's content. Rejected manuscripts are not returned to the authors.

Submission of manuscript to the journal

The manuscript is submitted to the editorial office of the journal in paper form in duplicate and in electronic form on an electronic medium (disc, memory stick). The electronic version of the article shall fully correspond to the paper version. The manuscript must be signed by all co-authors or a responsible representative.

In some cases it is allowed to send an article by e-mail instead of an electronic medium (disc, memory stick).

English-speaking authors submit their manuscripts in English. Russian-speaking and Ukrainian-speaking authors submit their manuscripts in English and in Russian or Ukrainian, respectively. Page format is A4. The number of pages shall not exceed 15 (together with References and extended abstracts). By agreement with the editorial board, the number of pages can be increased.

To the manuscript is added:

1. Official recommendation letter, signed by the head of the institution where the work was carried out.

2. License agreement on the transfer of copyright (the form of the agreement can be obtained from the editorial office of the journal or downloaded from the journal website – Dohovir.pdf). The license agreement comes into force after the acceptance of the article for publication. Signing of the license agreement by the author(s) means that they are acquainted and agree with the terms of the agreement.

3. Information about each of the authors – full name, position, place of work, academic title, academic degree, contact information (phone number, e-mail address), ORCID code (if available). Information about the authors is submitted as follows:

authors from Ukraine - in three languages, namely Ukrainian, Russian and English;

authors from the CIS countries - in two languages, namely Russian and English;

authors from foreign countries – in English.

4. Medium with the text of the article, figures, tables, information about the authors in electronic form.

5. Colored photo of the author(s). Black-and-white photos are not accepted by the editorial staff. With the number of authors more than two, their photos are not shown.

Requirements for article design

The article should be structured according to the following sections:

- *Introduction*. Contains the problem statement, relevance of the chosen topic, analysis of recent research and publications, purpose and objectives.
- *Presentation of the main research material* and the results obtained.
- *Conclusions* summing up the work and the prospects for further research in this direction.
- *References*.

The first page of the article contains information:

1) in the upper left corner – UDC identifier (for authors from Ukraine and the CIS countries);

2) surname(s) and initials, academic degree and scientific title of the author(s);

3) the name of the institution where the author(s) work, the postal address, telephone number, e-mail address of the author(s);

4) article title;

5) abstract to the article – not more than 1 800 characters. The abstract should reflect the consistent logic of describing the results and describe the main objectives of the study, summarize the most significant results;

6) key words – not more than 8 words.

The text of the article is printed in Times New Roman, font size 11 pt, line spacing 1.2 on A4 size paper, justified alignment. There should be no hyphenation in the article.

Page setup: "mirror margins" – top margin – 2.5 cm, bottom margin – 2.0 cm, inside – 2.0 cm, outside – 3.0 cm, from the edge to page header and page footer – 1.27 cm.

Graphic materials, pictures shall be submitted in color or, as an exception, black and white, in .opj or .cdr formats, .jpg or .tif formats being also permissible. According to author's choice, the tables and partially the text can be also in color.

Figures are printed on separate pages. The text in the figures must be in the font size 10 pt. On the charts, the units of measure are separated by commas. Figures are numbered in the order of their arrangement in the text, parts of the figures are numbered with letters – a, b, .. On the back of the figure, the title of the article, the author (authors) and the figure number are written in pencil. Scanned images and graphs are not allowed to be inserted.

Tables are provided on separate pages and must be executed using the MSWord table editor. Using pseudo-graph characters to design tables is inadmissible.

Formulae shall be typed in Equation or MatType formula editors. Articles with formulae written by hand are not accepted for printing. It is necessary to give definitions of quantities that are first used in the text, and then use the appropriate term.

Captions to figures and tables are printed in the manuscript after the references.

Reference list shall appear at the end of the article. References are numbered consecutively in the order in which they are quoted in the text of the article. References to unpublished and unfinished works are inadmissible.

Attention! In connection with the inclusion of the journal in the international bibliographic abstract database, the reference list should consist of two blocks: CITED LITERATURE and REFERENCES (this requirement also applies to English articles):

CITED LITERATURE – sources in the original language, executed in accordance with the

Ukrainian standard of bibliographic description DSTU 8302:2015. With the aid of VAK.in.ua (http://vak.in.ua) you can automatically, quickly and easily execute your "Cited literature" list in conformity with the requirements of State Certification Commission of Ukraine and prepare references to scientific sources in Ukraine in understandable and unified manner. This portal facilitates the processing of scientific sources when writing your publications, dissertations and other scientific papers.

REFERENCES – the same cited literature list transliterated in Roman alphabet (recommendations according to international bibliographic standard APA-2010, guidelines for drawing up a transliterated reference list "References" are on the site http//www.dse.org.ua, section for authors).

To speed up the publication of the article, please adhere to the following rules:

- in the upper left corner of the first page of the article – the UDC identifier;
- family name and initials of the author(s);
- academic degree, scientific title;

begin a new line, Times New Roman font, size 12 pt, line spacing 1.2, center alignment;

- name of organization, address (street, city, zip code, country), e-mail of the author(s);

begin a new line 1 cm below the name and initials of the author(s), Times New Roman font, size 11 pt, line spacing 1.2, center alignment;

- the title of the article is arranged 1 cm below the name of organization, in capital letters, semi-bold, font Times New Roman, size 12 pt, line spacing 1.2, center alignment. The title of the article shall be concrete and possibly concise;
- the abstract is arranged 1 cm below the title of the article, font Times New Roman, size 10 pt, in italics, line spacing 1.2, justified alignment in Ukrainian or Russian (for Ukrainian-speaking and Russian-speaking authors, respectively);
- key words are arranged below the abstract, font Times New Roman, size 10 pt, line spacing 1.2, justified alignment. The language of the key words corresponds to that of the abstract. Heading "Key words" - font Times New Roman, size 10 pt, semi-bold;
- the main text of the article is arranged 1 cm below the abstract, indent 1 cm, font Times New Roman, size 11 pt, line space spacing 1.2, justified alignment;
- formulae are typed in formula editor, fonts Symbol, Times New Roman. Font size is "normal" – 12 pt, "large index" – 7 pt, "small index" – 5 pt, "large symbol" – 18 pt, "small symbol" – 12 pt. The formula is arranged in the text, center aligned and shall not occupy more than 5/6 of the line width, formulae are numbered in parentheses on the right;
- dimensions of all quantities used in the article are represented in the International System of Units (SI) with the explication of the symbols employed;
- figures are arranged in the text. The figures and pictures shall be clear and contrast; the plot axes – parallel to sheet edges, thus eliminating possible displacement of angles in scaling; figures are submitted in color, black-and-white figures are not accepted by the editorial staff of the journal;
- tables are arranged in the text. The width of the table shall be 1 cm less than the line width. Above the table its ordinary number is indicated, right alignment. Continuous table numbering throughout the text. The title of the table is arranged below its number, center alignment;

• references should appear at the end of the article. References within the text should be enclosed in square brackets behind the text. References should be numbered in order of first appearance in the text. Examples of various reference types are given below.

Examples of LITERATURE CITED

Journal articles

Anatychuk L.I., Mykhailovsky V.Ya., Maksymuk M.V., Andrusiak I.S. Experimental research on thermoelectric automobile starting pre-heater operated with diesel fuel. *J.Thermoelectricity*. 2016. №4. P.84–94.

Books

Anatychuk L.I. *Thermoelements and thermoelectric devices. Handbook.* Kyiv, Naukova dumka, 1979. 768 p.

Patents

Patent of Ukraine № 85293. Anatychuk L.I., Luste O.J., Nitsovych O.V. Thermoelement.

Conference proceedings

Lysko V.V. *State of the art and expected progress in metrology of thermoelectric materials.* Proceedings of the XVII International Forum on Thermoelectricity (May 14-18, 2017, Belfast). Chernivtsi, 2017. 64 p.

Authors' abstracts

Kobylianskyi R.R. *Thermoelectric devices for treatment of skin diseases*: extended abstract of candidate's thesis. Chernivtsi, 2011. 20 p.

Examples of REFERENCES

Journal articles

Gorskiy P.V. (2015). Ob usloviakh vysokoi dobrotnosti i metodikakh poiska perspektivnykh sverhreshetochnykh termoelektricheskikh materialov [On the conditions of high figure of merit and methods of search for promising superlattice thermoelectric materials]. *Termoelektrichestvo - J.Thermoelectricity,* 3, 5 – 14 [in Russian].

Books

Anatychuk L.I. (2003). *Thermoelectricity. Vol.2. Thermoelectric power converters*. Kyiv, Chernivtsi: Institute of Thermoelectricity.

Patents

Patent of Ukraine № 85293. Anatychuk L. I., Luste O.Ya., Nitsovych O.V. Thermoelements [In Ukrainian].

Conference proceedings

Rifert V.G. Intensification of heat exchange at condensation and evaporation of liquid in 5 flowing-down films. In: *Proc. of the 9th International Conference Heat Transfer.* May 20-25, 1990, Israel.

Authors'abstracts

Mashukov A.O. *Efficiency hospital state of rehabilitation of patients with color carcer.* PhD (Med.) Odesa, 2011 [In Ukrainian].